JOURNAL
OF
GEOMAGNETISM
AND
GEOELECTRICITY

VOL. X NO. 3

SOCIETY
OF
TERRESTRIAL MAGNETISM AND ELECTRICITY
OF
JAPAN

1959
KYOTO

JOURNAL
OF
GEOMAGNETISM
AND
GEOELECTRICITY

VOL. X NO. 3

SOCIETY
OF
TERRESTRIAL MAGNETISM AND ELECTRICITY
OF
JAPAN

1959
KYOTO

JOURNAL OF GEOMAGNETISM AND GEOELECTRICITY

EDITORIAL COMMITTEE

Chairman: M. Kawasaki
(Kyoto University)

H. Hatakeyama
(Meteorological Agency)

T. Hatanaka
(Tohpe University)

Y. Kato
(Tohoku University)

A. Kimpara
(Nagoya University)

K. Maeda
(Kyoto University)

T. Nagata
(Tokyo University)

M. Ota
(Kyoto University)

Y. Rikitake
(Nagoya University)

Y. Tanaka
(Kyoto University)

H. Utada
(Kyoto University)

EDITORIAL OFFICER: M. Ota (Kyoto University)
EDITORIAL OFFICE: Society of Terrestrial Magnetism and Electricity of Japan,
Geophysical Institute, Kyoto University, Kyoto, Japan

The fields of interest of this quarterly Journal are as follows:

Terrestrial Magnetism	Aurora and Night Airglow
Atmospheric Electricity	The Ozone Layer
The Ionosphere	Physical States of the Upper Atmosphere
Radio Wave Propagation	Solar Phenomena relating to the Above Subjects
Cosmic Rays	Electricity within the Earth

The text should be written in English, German or French. The price is set at 1 dollar per number.

The Editors

JOURNAL OF GEOMAGNETISM AND GEOELECTRICITY

EDITORIAL COMMITTEE

Chairman: M. HASEGAWA (Fukui University)

H. HATAKEYAMA (Meteorological Agency)
T. HATANAKA (Tokyo University)
Y. KATO (Tohoku University)
A. KIMPARA (Nagoya University)
K. MAEDA (Kyoto University)
T. NAGATA (Tokyo University)
M. OTA (Kyoto University)
Y. SEKIDO (Nagoya University)
Y. TAMURA (Kyoto University)
H. UYEDA (Radio Research Laboratories)

EDITORIAL OFFICER: M. OTA (Kyoto University)
EDITORIAL OFFICE: Society of Terrestrial Magnetism and Electricity of Japan, Geophysical Institute, Kyoto University, Kyoto, Japan

The fields of interest of this quarterly Journal are as follows:

Terrestrial Magnetism	Aurora and Night Airglow
Atmospheric Electricity	The Ozone Layer
The Ionosphere	Physical States of the Upper Atmosphere
Radio Wave Propagation	Solar Phenomena relating to the Above Subjects
Cosmic Rays	Electricity within the Earth

The text should be written in English, German or French. The price is set as 1 dollar per number.

The Editors

JOURNAL OF GEOMAGNETISM AND GEOELECTRICITY

EDITORIAL COMMITTEE

Chairman: M. HARAGAWA
(Tokai University)

H. HATANEYAMA
(Meteorological Agency)

T. HATANAKA
(Tokyo University)

Y. KATO
(Tohoku University)

A. KIMPARA
(Nagoya University)

K. MAEDA
(Kyoto University)

T. NAGATA
(Tokyo University)

M. OTA
(Kyoto University)

Y. SHIMO
(Nagoya University)

Y. TAMURA
(Kyoto University)

H. UYEDA
(Radio Research Laboratories)

EDITORIAL OFFICER: M. OTA (Kyoto University)
EDITORIAL OFFICE: Society of Terrestrial Magnetism and Electricity of Japan,
Geophysical Institute, Kyoto University, Kyoto, Japan

The fields of interest of this quarterly Journal are as follows:

Terrestrial Magnetism	Aurora and Night Airglow
Atmospheric Electricity	The Ozone Layer
The Ionosphere	Physical States of the Upper Atmosphere
Radio Wave Propagation	Solar Phenomena relating to the Above Subjects
Cosmic Rays	Electricity within the Earth

The text should be written in English, German or French. The price is set as 1 dollar per number.

The Editors

also investigated the titanomagnetite in volcanic rocks and interpreted its magnetic property on the basis of the results of the synthetic experiments available at that time.

Chevallier and Girard (1950) have synthesized for the first time the solid solution between Fe_3O_4 and [illegible] in contrast to the $TiFe_2O_4$–Fe_3O_4 solid solution series (titanomagnetite I) (Pouillard, 1950). But their solid solution is still too limited (37 molecular [illegible] to interpret thoroughly the physical properties of the natural titanomagnetite [illegible] composition deviates from the $TiFe_2O_4$–Fe_3O_4 line. We have [illegible] in extending the spinel region to the more wide range in a FeO-Fe_2O_3-TiO_2 system by carrying out the oxidation experiments for a series of [illegible] over a whole range of the composition [illegible]. Generalized titanomagnetite having some vacant site in the metal ion positions of the spinel structure has also been postulated. In the present study this recent information concerning the synthetic [illegible] will be applied to an interpretation of the chemical, crystallographic and magnetic properties of the natural titanomagnetite contained in volcanic rocks.

In a recent paper, [illegible] (1957) have studied the heating experiments on some natural titanomagnetite having uniform lamellae of magnetite and ilmenite and the [illegible] heating experiments were followed [illegible] unit cell dimensions of the [illegible] their magnetic properties. [illegible] solid solution [illegible] compositional field [illegible] titanomagnetite in our [illegible] may persist without [illegible] in some rapidly cooled lavas. These considerations are quite accepted in general for the titanomagnetite in Japanese volcanic rocks, but it is also established that the chemical composition of some titanomagnetites in Japanese volcanic rocks enters into the magnetite-ilmenite-hematite compositional field beyond the magnetite-ilmenite join. They also pointed out that the fairly poor correlation between chemical, crystallographic and magnetic data in our previous study (Akimoto, 1954, 1955) arouse a suspicion that the specimens concerned might have [illegible] to varying extent and in different ways according to their composition.

Under the circumstances, we selected the [illegible] of titanomagnetite with spinel structure from the previous specimens, several new specimens being also added for the present study. Special care was paid for the [illegible] of the ilmenite-hematite series minerals in the specimens [illegible] titanomagnetite was used for the [illegible] vacancy in the spinel structure is [illegible].

2. Separation of Titanomagnetite and Its [illegible]

About 500 g of volcanic rock was crushed [illegible]

Magneto-Chemical Study of the Generalized Titanomagnetite in Volcanic Rocks*

By Syun-iti AKIMOTO

Geophysical Institute, Tokyo University

Takashi KATSURA

Laboratory of Analytical Chemistry and Geochemistry, Tokyo Institute of Technology

(Read May 19, 1958; Received February 28, 1959)

Abstract

Chemically analysed specimens of homogeneous titanomagnetites separated from various volcanic rocks were examined magnetically and crystallographically. Care was taken not to use the titanomagnetite carrying exsolved ilmenite-hematite series minerals. About 80 percent of the present specimens possesses the chemical composition situated in a magnetite-ulvöspinel-ilmenite compositional field in a FeO–Fe_2O_3–TiO_2 ternary system. Natural occurrence of the homogeneous titanomagnetite of which chemical composition enters into a magnetite-ilmenite-hematite compositional field was also found in some volcanic rocks. The concept of the generalized titanomagnetite, i.e. the spinel phase in the FeO–Fe_2O_3–TiO_2 system with varying vacancy in the metal ion site of the crystal structure, was applied for the magneto-chemical study of these natural titanomagnetites. The magnetic and crystallographic properties of the present specimens are interpreted successfully by making use of the equal lattice parameter diagram and equal Curie temperature diagram on the FeO–Fe_2O_3–TiO_2 system both of which have been determined from the synthetic experiments. A remarkable character that the titanomagnetite in some volcanic rocks is separable to an ensemble of the single phase grains of which chemical composition varies grain by grain nearly along the reduction-oxidation line was also found.

1. Introduction

An increasing amount of work recently carried out on the rock-forming ferromagnetic minerals has revealed that the great number of natural titanomagnetite with spinel structure possesses the chemical composition which deviates considerably from $TiFe_2O_4$–Fe_3O_4 join towards $TiFeO_3$–Fe_2O_3 join side. Since Iwasaki and Katsura (1950) have reported the chemical composition of the so-called "magnetite", i.e. ferromagnetic fraction separable by hand-magnet, in various Japanese volcanic rocks, the magneto-chemical studies of the natural titanomagnetite have been continued by one of the authors (Akimoto, 1951, 1954, 1955, 1957). Chevallier, Bolfa and Mathieu (1955) have

* Contribution from Division of Geomagnetism and Geoelectricity, Geophysical Institute, Tokyo University, Series II, No. 85.

also investigated the titanomagnetite in volcanic rocks and interpreted its magnetic property on the basis of the results of the synthetic experiments available at that time.

Chevallier and Girard (1950) have synthesized for the first time the solid solution between Fe_3O_4 and $TiFeO_3$ and named it titanomagnetite II in contrast to the $TiFe_2O_4$–Fe_3O_4 solid solution series (titanomagnetite I) (Pouillard, 1950). But their solid solution is still too limited (37 molecular percent of $TiFeO_3$) to interpret thoroughly the physical properties of the natural titanomagnetite of which chemical composition deviates from the $TiFe_2O_4$–Fe_3O_4 line. We have recently succeeded in extending the spinel region to the more wide range in a FeO–Fe_2O_3–TiO_2 system by carrying out the oxidation experiments for a series of solid solution $x TiFe_2O_4 \cdot (1-x)Fe_3O_4$ over a whole range of the composition $1 \geq x \geq 0$ (Akimoto, Katsura and Yoshida, 1957). Generalized titanomagnetite having some vacant site in the metal ion positions of the spinel structure has also been postulated. In the present study this recent information concerning the synthetic titanomagnetite will be applied to an interpretation of the chemical, crystallographic and magnetic properties of the natural titanomagnetite contained in volcanic rocks.

In a recent paper Vincent, Wright, Chevallier and Mathieu (1957) have studied the heating experiments on some natural titaniferous magnetite having unmixing lamellae of magnetite and ilmenite and the mineralogical changes occurring during the heating experiments were followed microscopically and by determining the change in unit cell dimensions of the various phases, and also by quantitative measurements of their magnetic properties. They have concluded that at high temperatures fairly extensive solid solution probably exists over much of the magnetite-ulvöspinel-ilmenite compositional field, and that homogeneous titanomagnetite (generalized titanomagnetite in our nomenclature) of widely varying composition and magnetic properties may persist without unmixing in some rapidly cooled lavas. These considerations are quite accepted in general for the titanomagnetite in Japanese volcanic rocks, but it is also established that the chemical composition of some titanomagnetites in Japanese volcanic rocks enters into the magnetite-ilmenite-hematite compositional field beyond the magnetite-ilmenite join. They also pointed out that the fairly poor correlation between chemical, crystallographic and magnetic data in our previous study (Akimoto, 1954, 1955) arouse a suspicion that the specimens concerned might have unmixed to varying extent and in different ways according to their composition.

Under the circumstances, we selected the excellent specimens of titanomagnetite with spinel structure from the previous specimens, several new specimens being also added for the present study. Special care was paid for the identification of the unmixing ilmenite-hematite series minerals in the specimen. In the present paper the name of titanomagnetite was used for the homogeneous titaniferous magnetite having some vacancy in the spinel structure in general.

2. Separation of Titanomagnetite and Its Identification

About 500 g of volcanic rock was crashed roughly by a gun-metal crasher, and the

also investigated the titanomagnetite in volcanic rocks and interpreted its magnetic property on the basis of the synthetic experiments available at that time.

Chevallier and Girard (1939) have synthesized for the first time the solid solution between Fe_3O_4 and $TiFeO_3$ and named it titanomagnetite. In contrast to the $TiFe_2O_4$–Fe_3O_4 solid solution series (titanomagnetite I) (Pouillard, 1950). But their solid solution is still too limited (37 molecular percent of $TiFeO_3$) to interpret thoroughly the physical properties of the natural titanomagnetite of which chemical composition deviates from the $TiFe_2O_4$–Fe_3O_4 line. We have recently succeeded in extending the spinel region to the more wide range in a FeO–Fe_2O_3–TiO_2 system by carrying out the oxidation experiments for a series of solid solution $xTiFe_2O_4$–$(1-x)Fe_3O_4$ over a whole range of the composition $1 \geq x \geq 0$ (Akimoto, Katsura and Yoshida, 1957). Generalized titanomagnetite having some vacant site in the metal ion positions of the spinel structure has also been postulated. In the present study this recent information concerning the synthetic titanomagnetite will be applied to an interpretation of the chemical, crystallographic and magnetic properties of the natural titanomagnetite contained in volcanic rocks.

In a recent paper Vincent, Wright, Chevallier and Matzieu (1957) have studied the heating experiments on some natural titaniferous magnetite having unmixing lamellae of magnetite and ilmenite and the mineralogical changes occurring during the heating experiments were followed microscopically and by determining the change in unit cell dimensions of the various phases and also by quantitative measurements of their magnetic properties. They have concluded that at high temperatures fairly extensive solid solution probably exists even much of the magnetite-ulvöspinel-ilmenite compositional field, and that homogeneous titanomagnetite (generalized titanomagnetite in our nomenclature) of widely varying composition and magnetic properties may persist without unmixing in some rapidly cooled lavas. These considerations are quite accepted in general for the titanomagnetite in Japanese volcanic rocks, but it is also established that the chemical composition of some titanomagnetites in Japanese volcanic rocks enters into the magnetite-ilmenite-hematite compositional field beyond the magnetite-ilmenite join. They also pointed out that the fairly poor correlation between chemical, crystallographic and magnetic data in our previous study (Akimoto, 1954, 1955) arouse a suspicion that the specimens concerned might have unmixed to varying extent and in different ways according to their composition.

Under the circumstances, we selected the excellent specimens of titanomagnetite with spinel structure from the previous specimens, several new specimens being also added for the present study. Special care was paid for the identification of the unmixing ilmenite-hematite series minerals in the specimen. In the present paper the name of titanomagnetite was used for the homogeneous titaniferous magnetite having some vacancy in the spinel structure in general.

2. Separation of Titanomagnetite and Its Identification

About 500 g of volcanic rock was crushed roughly by a pneumatic crusher, and the

ferromagnetic fraction was separated from silicate minerals by a hand-magnet. The fraction thus separated was then pulverized as finely as possible (below 200 mesh) in an agate-mortar in the presence of water. The fine powder thus prepared was suspended in 100 ml of water, and ferromagnetic deposits were attracted by a magnet through the beaker-glass, then the supernatant suspending materials were drawn off by decantation. These procedures were repeated several times until the total percent of iron oxide and titanium dioxide amounts to about 90 %. As already mentioned in a previous paper (Akimoto, 1955), the groundmass ferromagnetic minerals in basalt, are so finely grained that the small amounts of silicates such as olivine, pyroxene, etc. are still involved as impurities in spite of our effort. It is almost impossible to separate purely the groundmass ferromagnetic minerals from the small amounts of silicates, especially in the case of aphyric rocks, and when we try to separate them purely by means of a usual method, we had to eliminate the greater amounts of ferromagnetic fraction for their impurities. Although the ferromagnetic minerals thus separated, about 90 % purity mainly consist of titanomagnetite grains, a small quantity of ferromagnetic ilmenite, common ilmenite, and hematite may be sometimes involed either as an exsolution lamellae or as an impurity. The identification of them was carried out by an X-ray diffractometric method. X-ray diffraction patterns of the specimens were recorded by means of a wide range X-ray diffractometer "Norelco" with Fe K radiation in a fairly large scanning speed for 2θ angle range from 90° to 20°. From this general survey, we could identify an impurity involved in the specimen and estimate its quantity roughly. If there exist non-ferromagnetic common ilmenite and/or hematite in the form of exsolution lamellae, these samples are omitted from the present study, because it is hardly possible in present technique to separate them from titanomagnetite. If there exists ferromagnetic ilmenite, we can separate it from titanomagnetite by the thermomagnetic separation method by Nagata, Akimoto and Uyeda (1953), in making use of the difference of Curie temperature between titanomagnetite and ferromagnetic ilmenites. The Curie temperature of the ferromagnetic ilmenites in volcanic rocks is generally lower than about 250°C and differs by 100°C or more from that of the co-existing titanomagnetite.

It was verified from a careful investigation of the diffraction chart of the specimen which was prepared artificially by mixing ilmenite and magnetite in a definite ratio, that we could identify at least five percent of ilmenite in magnetite on the diffraction chart. When the content of ilmenite exceeds ten percent we could very easily identify it from magnetite. Therefore, the amount of the ilmenite-hematite series minerals contained in the specimens used in the present study must be less than five percent even if they exist as an exsolution lamellae.

3. Specimens and Their Chemical Composition

All the titanomagnetite specimens examined here are thirty-five in total number and each of them was separated from the host volcanic rocks with the aid of the separation method described in § 2. A part of these has already been reported in a

Table I. Chemical composition and crystallographic and magnetic properties of titanomagnetites contained in volcanic rocks.

No.	Localities	Rocks	Purity* (in wt.%)	FeO	Fe_2O_3 (in mol. %)	TiO_2	Fe+Ti O ×32
1.	Semi, Yamagata	dolerite	95.88	59.50	14.86	25.64	23.66
2.	Hamada, Simane	nepheline-basalt	86.16	57.74	22.81	19.45	23.81
3.	Zyôbosi, Sizuoka	olivine-basalt	85.32	56.96	26.05	16.96	23.86
4.	Imazu, Hukuoka	olivine-basalt	86.87	59.57	16.87	23.55	23.78
5.	Gembudô, Hyôgo	olivine-basalt	72.57	56.89	17.70	25.41	23.42
6.	Kakuda, Niigata	olivine-basalt	83.26	59.05	24.47	16.48	24.08
7.	Sidara, Aiti	basalt	93.37	59.96	17.73	22.31	23.88
8.	Sidara, Aiti	basalt	89.31	49.14	23.24	27.62	22.65
9.	Simohutago, Hakone	hy-aug-andesite	87.14	53.40	31.01	15.59	23.60
10.	Karataki, Hakone	aug-hy-andesite	88.23	57.63	25.81	16.56	23.94
11.	Taga Volcano	ol-aug-hy-andesite	86.92	56.77	28.12	15.05	23.93
12.	Sarusawa, Hakone	aphyric andesite	86.41	56.92	23.30	19.78	23.71
13.	Himesima, Ooita	horn-mica-andesite	95.52	45.36	44.79	9.85	23.23
14.	Minamihasi, Ooita	horn-andesite	95.63	44.91	42.50	12.59	23.08
15.	Garandake, Ooita,	horn-andesite	93.77	41.74	48.85	9.41	23.00
16.	Simohutago, Hakone	two-pyr-andesite	87.14	53.32	31.07	15.65	23.59
17.	Asoozawa, Totigi	pig-aug-hy-andesite	89.04	58.36	17.78	23.86	23.64
18.	Kakuda Niigata	aug-andesite	91.80	49.91	35.41	14.68	23.36
19.	Aso, Kumamoto	two-pyr-andesite	89.41	38.98	42.32	18.70	22.40
20.	Aso, Kumamoto	two-pyr-andesite	91.58	54.74	27.21	18.05	23.60
21.	Aso, Kumamoto	two-pyr-andesite	93.27	50.38	37.75	11.87	23.53
22.	Aso, Kumamoto	two-pyr-andesite	85.33	38.93	55.04	6.03	22.96
23.	Hutatudake, Haruna	hy-horn-dacite	91.90	51.52	38.58	9.90	23.71
24.	Haruna Volcano	hy-horn-dacite, pumice	91.90	51.59	38.55	9.86	23.71
25.	South of Hata, Hakone	horn-dacite	94.61	50.01	37.38	12.61	23.46
26.	Towada Volcano	hy-horn-dacite	90.63	53.00	34.59	12.41	23.72
27.	Kutukake, Asama	dacite pumice	87.59	52.48	36.49	11.03	23.74
28.	Sinkamibasi, Kagosima	dacite pumice	90.81	55.12	31.98	12.90	23.88
29.	Nikko, Totigi	pumice flow deposite	96.44	52.90	36.91	10.19	23.81
30.	Manazuru, Kanagawa	dacite pumice	88.39	55.96	28.51	15.53	23.83
31.	Northern Slope of Amagi Volc.	dacite pumice	85.68	52.38	36.72	10.90	23.73
32.	Asio, Totigi	eulite-fayalite-dacite	90.38	50.58	38.67	10.74	23.59
33.	Mukooyama, Niisima	biot-rhyolite	91.79	51.80	39.36	8.84	23.78
34.	Mukooyama, Niisima	biot-rhyolite	92.15	52.24	39.52	8.24	23.84
35.	Atumi, Yamagata	magnetite vein in dolerite	98.95	48.05	51.95	0.00	23.85

* Total % of $FeO+Fe_2O_3+TiO_2$ (by weight)

** As for the specimens showing the thermal hysteresis phenomena in their thermomagnetic curve, the Curie temperature in both heating and cooling processes is given. H and C represent heating and cooling process respectively.

$\frac{Fe}{Fe+Ti}$	Lattice parameter		Curie temperature		Saturation moment (at room temp.)
			H**	C**	
0.777	8.475 Å		400°C	260°C	27 u.m.u./gr.
			220	130	
0.842	8.462		235		32
0.865	8.444		440	300	36
0.798	8.458		120		20
0.784	8.490		120		14
0.868					
0.810	8.467		200		
0.776	8.439		310		
0.881	8.422	8.426***	505	505	66
				410	
0.868	8.426	8.432***	380	435	59
				360	
0.883	8.424	8.432***	500	410	61
0.840	8.454		480	450	44
	(8.405)				
0.932	8.400		510	500	69
0.912	8.405		495		70
0.937	8.399		495		78
0.881					
0.797	8.461	8.477***	400	170	
0.892					
0.869	8.387		565		
0.858	8.442		360		
			(520)		
0.914	8.408		540		
0.961	8.397		565		
0.929	8.410				
0.929	8.414		480	455	79
0.908	8.371		490		73
0.908	8.412		390		65
0.919	8.414		500	410	64
0.902	8.412	8.428***	515	370	51
0.926	8.408		445		
0.879	8.431		350		
0.920	8.415		460	445	67
0.923	8.418		470		
0.937					
0.941	8.408		470		87
1.000	8.385		580		

*** These values were determined after the thermomagnetic curve was measured.

previous paper (Akimoto, 1955) and some specimens which contained a fairly large amount of impurities were purified again and reanalysed for the present study, and the others are new specimens.

The localities where these host rocks were sampled and the rock species are shown in Table I. The petrological character of these host rocks represents that of the various kinds of typical volcanic rocks, since the chemical composition of magmas and the physical conditions under which solidification has taken place vary through these rocks over a wide range. That is, there will be seen, from basic to acidic, basalt, dolerite, andesite, dacite, rhyolite.

The titanomagnetite specimens have been analysed chemically by the simultaneous determination method, devised by Iwasaki et al. (1957), most suitable for the rapid analysis of three main components FeO, Fe_2O_3 and TiO_2 of the ferromagnetic oxide minerals. The results of the chemical analysis are also given in Table I and represented on the diagram of the FeO-Fe_2O_3-TiO_2 ternary system shown in Fig. 1.

In addition to these main components, the ferromagnetic oxide minerals usually contain a small amount of magnesium, aluminum, manganese, vanadium, silicium, calcium and alkali metals as essential components or as impurities (Iwasaki and Katsura, 1950). It is the most interesting problem from the geochemical viewpoint to

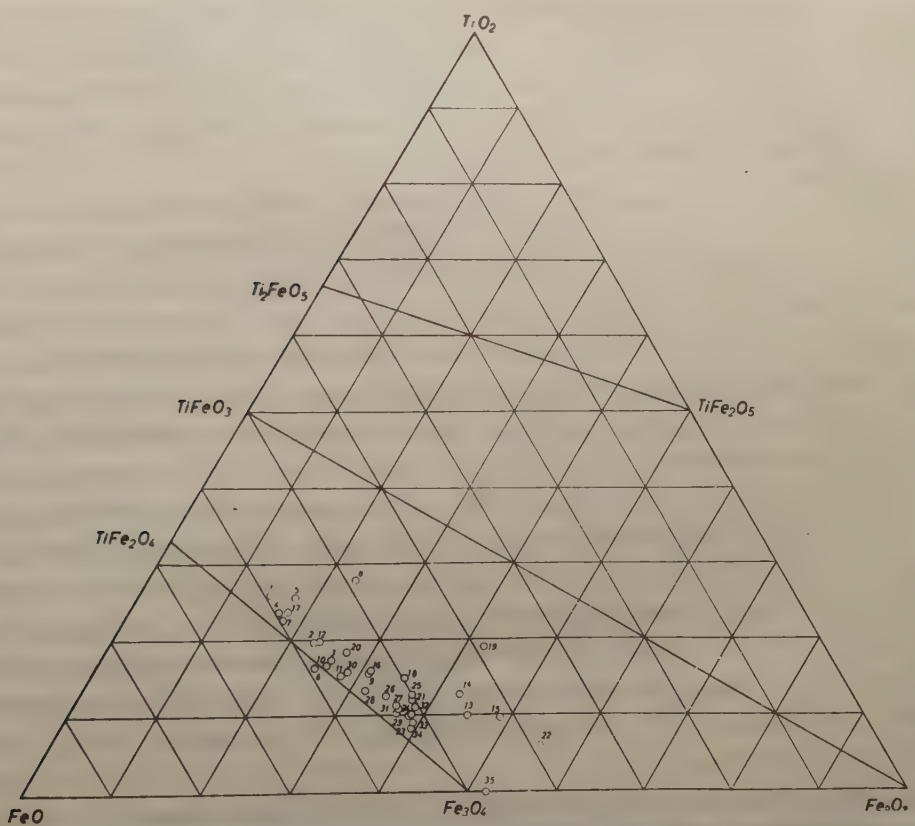

Fig. 1 Molecular composition of analysed natural titanomagnetites, represented on a FeO-Fe_2O_3-TiO_2 ternary system. The numbers refer to those in Table I.

As will be seen in Fig. 1, it is clear that the chemical composition of titanomagnetites does not always accord with $TiFe_2O_4$–Fe_3O_4 solid solution line but in most cases deviates from this join towards $TiFeO_3$–Fe_2O_3 join side. In the previous paper (Akimoto, [illegible]), we have suggested that the spinel phase of titanomagnetite existence as a single phase in a fairly broad region between the $TiFe_2O_4$–Fe_3O_4 join and the $TiFeO_3$–Fe_2O_3 join, according to the data on chemical conditions under which solidification of the volcanic rocks has taken place, i.e. the temperature of lava, the rate of cooling, partial pressure of oxygen, the chemical composition of

study the behaviour of distribution of these minor elements in various titanomagnetite as already reported by Iwasaki and Katsura (1950), Wager and Mitchell (1954) and Buddington, Fahey and Vlisidis (1955). Geochemical study on the minor elements of the present titanomagnetite specimens will be written later in a separate paper. Vincent and Phillips (1954) and Vincent, Wright, Chevallier and Mathieu (1957) have practised a complete chemical analysis and plotted the overall chemical composition on the conventional Fe-Ti oxide triangular diagram. The samples which contain a large amount of SiO_2 are omitted from their study. Since the variance of the molecular proportion of MO, R_2O_3 and TO_2 calculated by them with the actual molecular proportion of FeO, Fe_2O_3 and TiO_2 is fairly small, the difference in such an expression of the triangular diagram is not deemed conclusive in the interpretation of the chemical and magnetic properties of the titanomagnetite. Hence, in the present study, the effect of all these minor elements on the magnetic properties of titanomagnetites was ignored.

As will be seen in Fig. 1, it is clear that the chemical composition of titanomagnetites does not always accord with $TiFe_2O_4$–Fe_3O_4 solid solution line but in most cases deviates from this join towards $TiFeO_3$–Fe_2O_3 join side. In the previous paper (Akimoto, Katsura, Yoshida, 1957), we have suggested that the spinel phase of titanomagnetite can be in existence as a single phase in a fairly broad region between the $TiFe_2O_4$–Fe_3O_4 join and the $TiFeO_3$–Fe_2O_3 join, according to the physico-chemical conditions under which solidification of the volcanic rocks has taken place, i. e. the temperature of lava, the rate of cooling, partial pressure of oxygen, the chemical composition of the lava, the presence of the volatile constituents etc.

Recently, Chevallier and Girard (1950), Chevallier, Bolfa and Mathieu (1955), and Vincent, Wright, Chevallier and Mathieu (1957) have regarded the natural titanomagnetites as the Fe_3O_4–$TiFe_2O_4$ series (Titanomagnetite I), Fe_3O_4–$TiFeO_3$ (γ-ilmenite) series (Titanomagnetite II) or the intermediates between these two. The chemical composition of about 80 % of samples in the present paper are, indeed, distributed between these two principal lines, but eight samples, especially six samples (No. 8, 13, 14, 15, 19 and 22 in Table I) deviate greatly from these two principal lines and enter into the Fe_3O_4–Fe_2O_3–$TiFeO_3$ compositional field. We call, for the present, these six titanomagnetites the very abnormal titanomagnetite, and the intermediate titanomagnetites assumed by Vincent et al. the abnormal titanomagnetite, and the titanomagnetites on the line or near the line of Fe_3O_4–$TiFe_2O_4$ join the normal titanomagnetite. We by no means claim that these classifications have a certain strict sense, but they are adopted only as conventional ones. These abnormal series of titanomagnetites (generalized titanomagnetite in our previous paper) will be consistently interpreted as the resultant products obtained by oxidation of normal titanomagnetite as reported in our previous paper (1957).

In Table I the atomic ratio of Fe/Fe+Ti and the atomic proportion of metals to oxygen calculated on the basis of 32 oxygen atoms, (Fe+Ti)/O×32, are shown. The values of Fe/Fe+Ti vary in the range between 0.776 and 0.941, and that of

(Fe+Ti)/O×32 is in the range between 22.40 and 24.08. Itmust be noticed here that the normal titanomagnetite, $TiFe_2O_4$–Fe_3O_4 system, contains 32 oxygen ions and 24 metal ions in its unit cell. In Fig. 2, the relation between these two quantities of all the specimens is shown, where the lines EF and ABD represent the course of oxidation of magnetite (Fe_3O_4) and ulvöspinel ($TiFe_2O_4$) respectively, and the points C and F

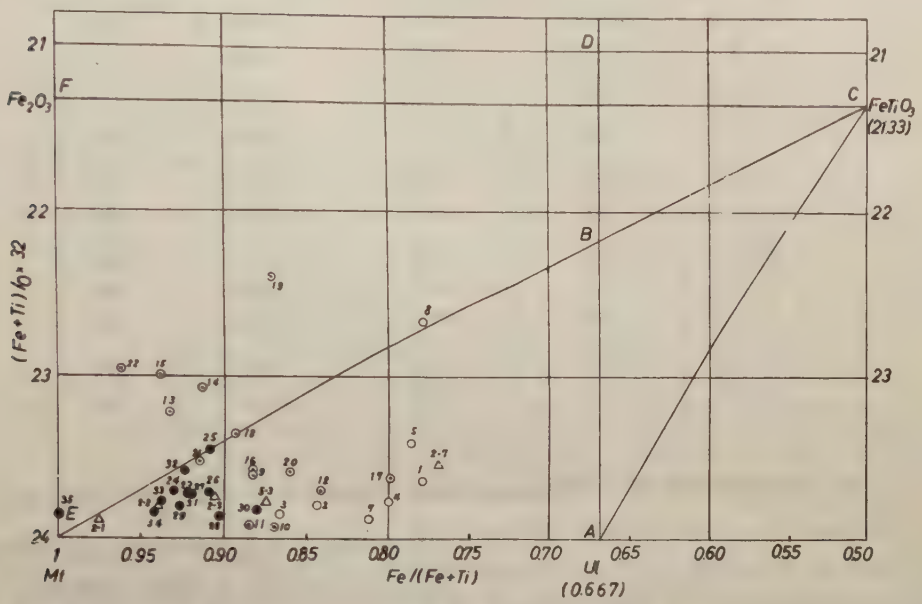

Fig. 2 Chemical composition of natural titanomagnetites, represented on Fe/(Fe+Ti) vs. (Fe+Ti)/O×32 diagram.

○ : titanomagnetites in basalt and dolerite.
⊙ : titanomagnetites in andesite
● : titanomagnetites in dacite and rhyolite
△ : synthetic titanomagnetites.

stand for $TiFeO_3$ and Fe_2O_3 respectively. The lines AE and EBC represent the magnetite-ulvöspinel solid solution and magnetite-ilmenite (γ-$TiFeO_3$) solid solution assumed by Chevallier and Girard (1950) respectively, and the compositional region ECA represent the intermediate titanomagnetite called by Vincent, Chevallier et al. It may also be clearly understood that the titanomagnetite of which chemical composition enters into the region ABC forming a part of intermediate region can not be prepared by the oxidation of magnetite-ulvöspinel solid solution. There will be seen a general tendency that the titanomagnetite contained in basic volcanic rocks is rich in titanium in comparison with that in acidic rocks. The atomic ratio Fe/Fe+Ti of the titanomagnetite decreases gradually in general sequence of rhyolite, dacite, andesite, basalt. The very abnormal character of the chemical composition of the six specimens mentioned before were again manifested in the figure in a more distinct manner than in Fig. 1. The very abnormal titanomagnetite No. 8, No. 19, No. 14 and No. 22 in Table I corresponds nearly to the case when synthetic titanomagnetite (normal) S2–7, S5–3, S2–3 and S2–1 in our previous paper (1957) is oxidized in appropriate conditions

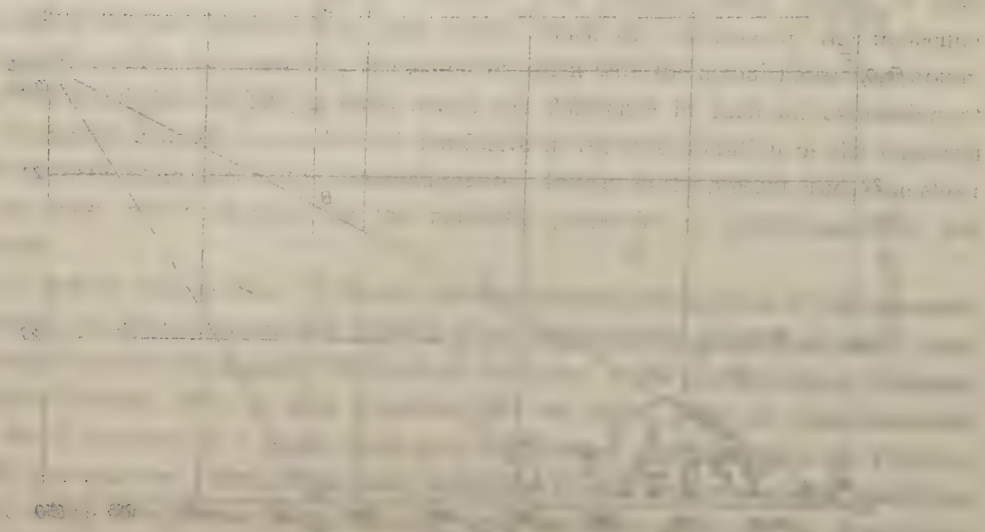

respectively, and No. 13 and No. 15 are nearly the case of oxidation of S2–2. Table II shows the relations mentioned here.

Table II

Specimen	$\frac{Fe}{Fe+Ti}$	$\frac{Fe+Ti}{O}\times 32$	Lattice parameter	Curie temperature
No. 8	0.776	22.65	8.439 Å	310°C
S 2–7	0.768	23.55	8.486	110
No. 19	0.869	22.40	8.387	565
S 5–3	0.874	23.78	8.442	350
No. 14	0.912	23.08	8.405	495
S 2–3	0.905	23.73	8.427	420
No. 13	0.932	23.23	8.400	500
No. 15	0.937	23.00	8.399	495
S 2–2	0.940	23.82	8.416	480
No. 22	0.961	22.96	8.397	565
S 2–1	0.975	23.87	8.402	550

4. Fractionation of a Titanomagnetite Separated from a Rock Specimen

As already reported (Nagata, Akimoto and Uyeda, 1953) an ensemble of ferromagnetic minerals separated from the original volcanic rocks by a usual magnetic method generally consists of a large number of grains of different chemical composition, having different Curie temperature, with the result that the magnetic properties of a rock specimen represent those of the average composition of the ensemble. Therefore, in order to obtain an accurate relation between magnetic properties and chemical composition of ferromagnetic minerals, it is required to fractionate the ferromagnetic mineral grains as uniquely as possible with respect to their chemical composition.

As for ferromagnetic ilmenites this has already been practised with the help of thermo-magnetic separation method (Nagata and Akimoto, 1956, Uyeda, 1957, 1958). In the present study, some amount of titanomagnetite grains separated from the rock specimen was further classified with respect to their Curie-temperature through the magnetic separation at various high temperatures. Titanomagnetites examined accurately here are the following three specimens: (1) titanomagnetite in olivine basalt, Imazu (No. 4 in Table I), (2) titanomagnetite in dacite, Manazuru (No. 30) and (3) titanomagnetite in rhyolite, Niisima (No. 33). Other specimens in Table I could not be fractionated in sufficient quantity for carrying out the accurate chemical analysis.

The results of thermomagnetic separation are illustrated in Fig. 3. In these diagrams, the area of each rectangle represents $M\int_{T_i}^{T_j} f(T_s)\,dT = Mf(T_s)\Delta T$, where M, T_s denote the total mass of the whole ensemble of grains and the separation temperature respectively, and $\Delta T = T_j - T_i$ is 20°C in the present cases. The ensembles thus fractionated for every 20°C range of T_s are used as specimens for the detailed study.

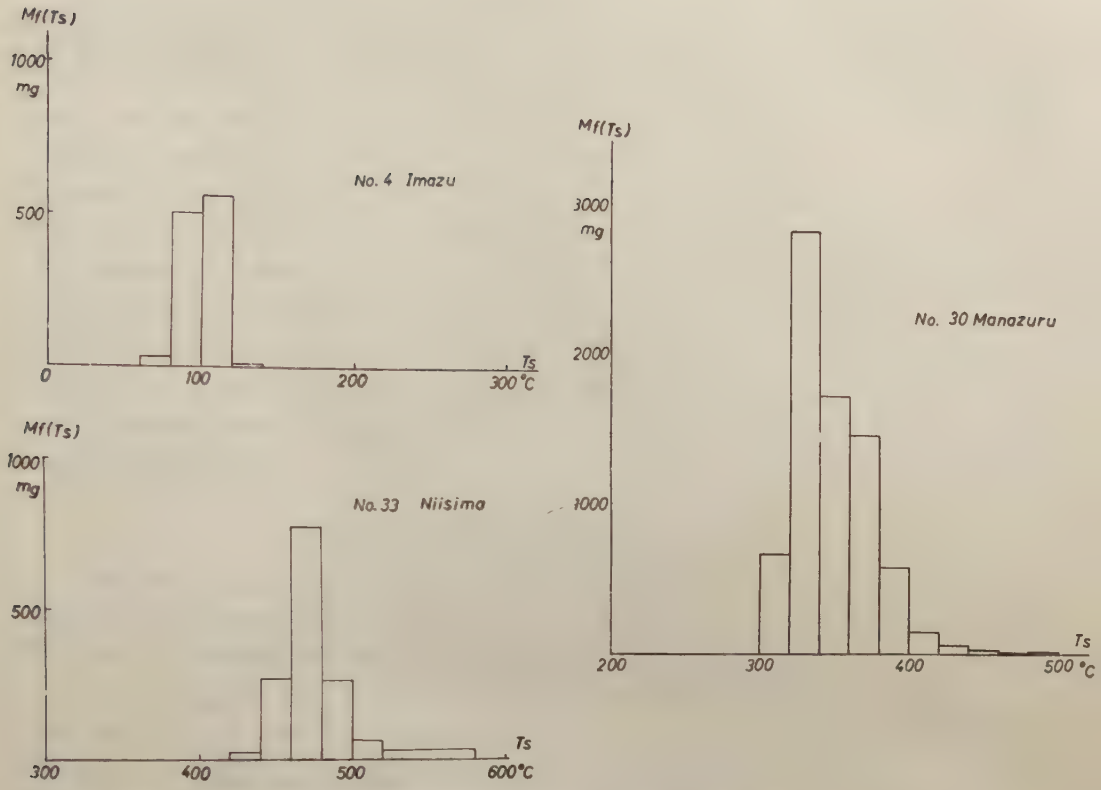

Fig. 3 Thermomagnetic separation spectra of titanomagnetites in volcanic rocks.

Table III Chemical composition and crystallographic and magnetic properties of the thermomagnetically separated titanomagnetites.

Rocks	Separation temperature	Purity in wt. %	FeO	Fe_2O_3	TiO_2 in mol. %	Fe/(Fe+Ti)	Fe+Ti O ×32	Lattice parameter	Curie temperature
Imazuyama olivine basalt	80>Ts>60°C								90°C
	100>Ts>80	73.21	56.53	19.09	24.38	0.795	23.44	8.456±0.003Å	115
	120>Ts>100	76.72	56.53	19.94	23.53	0.804	23.48	8.452±0.001	130
Manazuru dacite pumice	300>Ts>280								310
	320>Ts>300	85.58	56.96	27.51	15.53	0.878	23.92	8.433±0.002	330
	340>Ts>320	89.90	56.01	28.38	15.61	0.878	23.83	8.430±0.001	350
	360>Ts>340	91.73	54.98	29.48	15.55	0.880	23.74	8.429±0.001	365
	380>Ts>360	89.22	54.40	29.92	15.68	0.879	23.69	8.430±0.001	375
	400>Ts>380	89.69	54.99	29.45	15.56	0.880	23.74	8.427±0.001	400
	420>Ts>400	91.03	52.18	32.35	15.47	0.883	23.51		415
	440>Ts>420	94.24	50.58	34.76	14.66	0.891	23.41		
Niisima biotite rhyolite	460>Ts>440	91.80	52.12	39.50	8.38	0.940	23.82	8.415±0.001	450
	480>Ts>460	94.38	52.16	39.36	8.48	0.939	23.82	8.408±0.002	460
	500>Ts>480	93.37	50.39	41.75	7.86	0.945	23.70	8.407±0.002	480
	520>Ts>500	98.08	45.37	46.34	8.29	0.943	23.30	8.397±0.003	520
	Ts>520	94.84	41.85	49.01	9.14	0.939	23.02	8.403±0.002	550

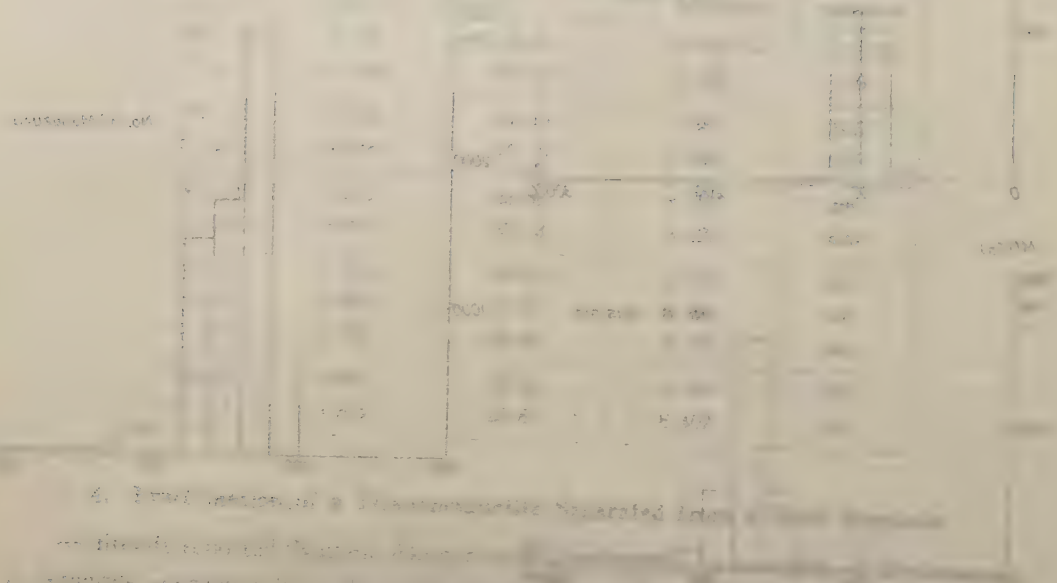

Chemical composition of each fractionated specimen is given in Table III together with the atomic ratios of Fe/Fe+Ti and (Fe+Ti)/O×32, and represented on the FeO–Fe_2O_3–TiO_2 diagram in molecular percent (Fig. 4).

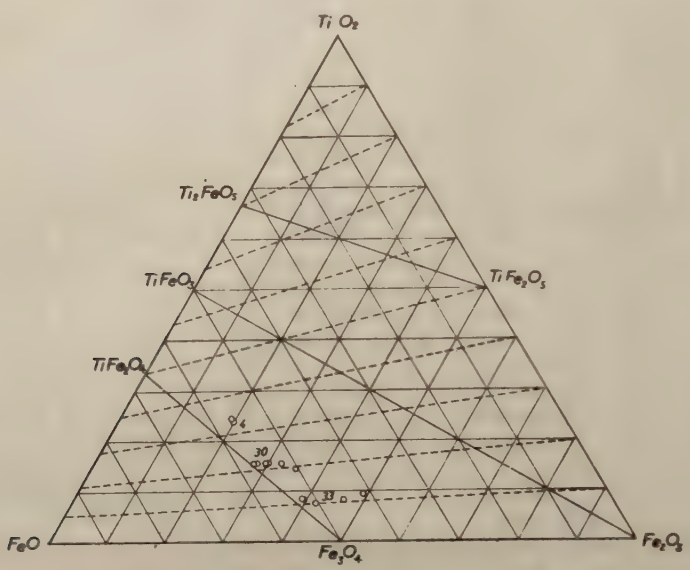

Fig. 4 Chemical composition of thermomagnetically separated titanomagnetites, represented on a FeO-Fe_2O_3-TiO_2 diagram in mol. percent. Broken lines indicate theoretical reduction-oxidation lines.

The fractions separated below 80°C and above 120°C in Imazu olivine basalt, separated below 300°C and above 440°C in Manazuru dacite pumice and separated below 440°C in Niisima rhyolite are so scanty that we could not analyse them chemically.

As will be seen in Table III and Fig. 4, the titanomagnetite in Imazu olivine-basalt, Manazuru dacite and Niisima rhyolite consists of several kinds of grains of different chemical composition having different separation temperature. It must be noticed here that the chemical composition of the thermomagnetically separated specimens changes continuously along the reduction-oxidation line of the FeO–Fe_2O_3–TiO_2 ternary system, which is also shown in Fig. 4 by a broken line. It is a remarkable character common to all the present titanomagnetite specimens from different locality that the atomic ratio of Fe/Fe+Ti distributes in fairly small ranges, while the ratio of (Fe+Ti)/O×32 indicating the degree of vacancy of metal positions in a spinel structure decreases with the increase of the separation temperature. This situation forms a marked contrast to the case of the rhombohedral ilmenite-hematite series minerals in volcanic rocks, where the chemical composition of the thermomagnetically separated specimens changes continuously along the $TiFeO_3$–Fe_2O_3 line according to variation in the separation temperature (Nagata and Akimoto, 1956).

It may be the most important problem for volcanic petrology that titanomagnetites

in some volcanic rocks consist undoubtedly of a large number of grains with different chemical composition which are easily separated as the individual homogeneous phases without any unmixing lamellae. We know by experience that this is the case for every volcanic rocks even if there may be a significant difference in the form of the chemical composition spectrum, peculiar to each rock sample. Hence, this fact may suggest that the formation of titanomagnetite is very much complicated even in the volcanic rocks which were considered to be the most simple form of igneous rocks. The titanomagnetite in the volcanic rocks which was presumed to be quenched from a high temperature state at the time of their outflow over the earth's surface may be affected not only by the physical and chemical conditions of magma but also by its total history during solidification. Simple equilibrium state in chemical reaction or stoichiometric relation to solid reaction among magnetite, ulvöspinel and ilmenite may not be expectable.

5. Lattice Parameters of Titanomagnetites

The lattice parameters of all the titanomagnetite specimens were determined by the precise measurement of the diffraction angles of the specified crystal plane. Practically we measured the diffraction angles, 2θ of (220), (311), (400), (422), (511 ; 333) and (440) planes by the "Norelco" with Fe Kα radiation in a slow scanning speed such as 1/2 per minute. Instrumental errors were calibrated by measuring the diffraction angles of the standard specimen of silicon. We determined the lattice parameter of the specimen as a mean value of the ones calculated from the 2θ angle for each plane.

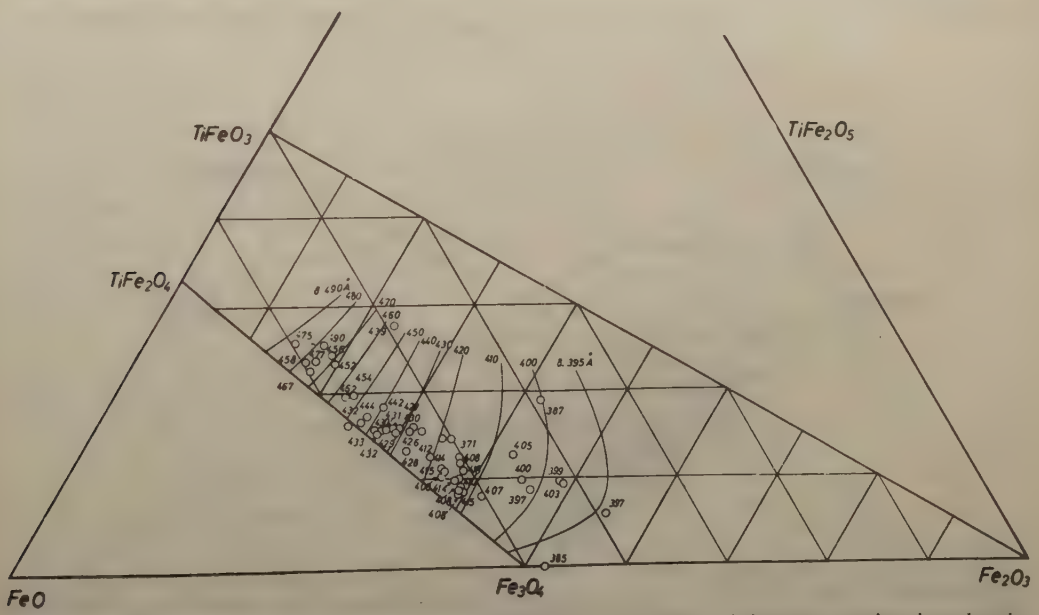

Fig. 5 Relation between lattice parameter and chemical composition of titanomagnetites in volcanic rocks. The equal lattice parameter diagam of the spinel region obtained from the synthetic titanomagnetites is also reproduced in the figure.

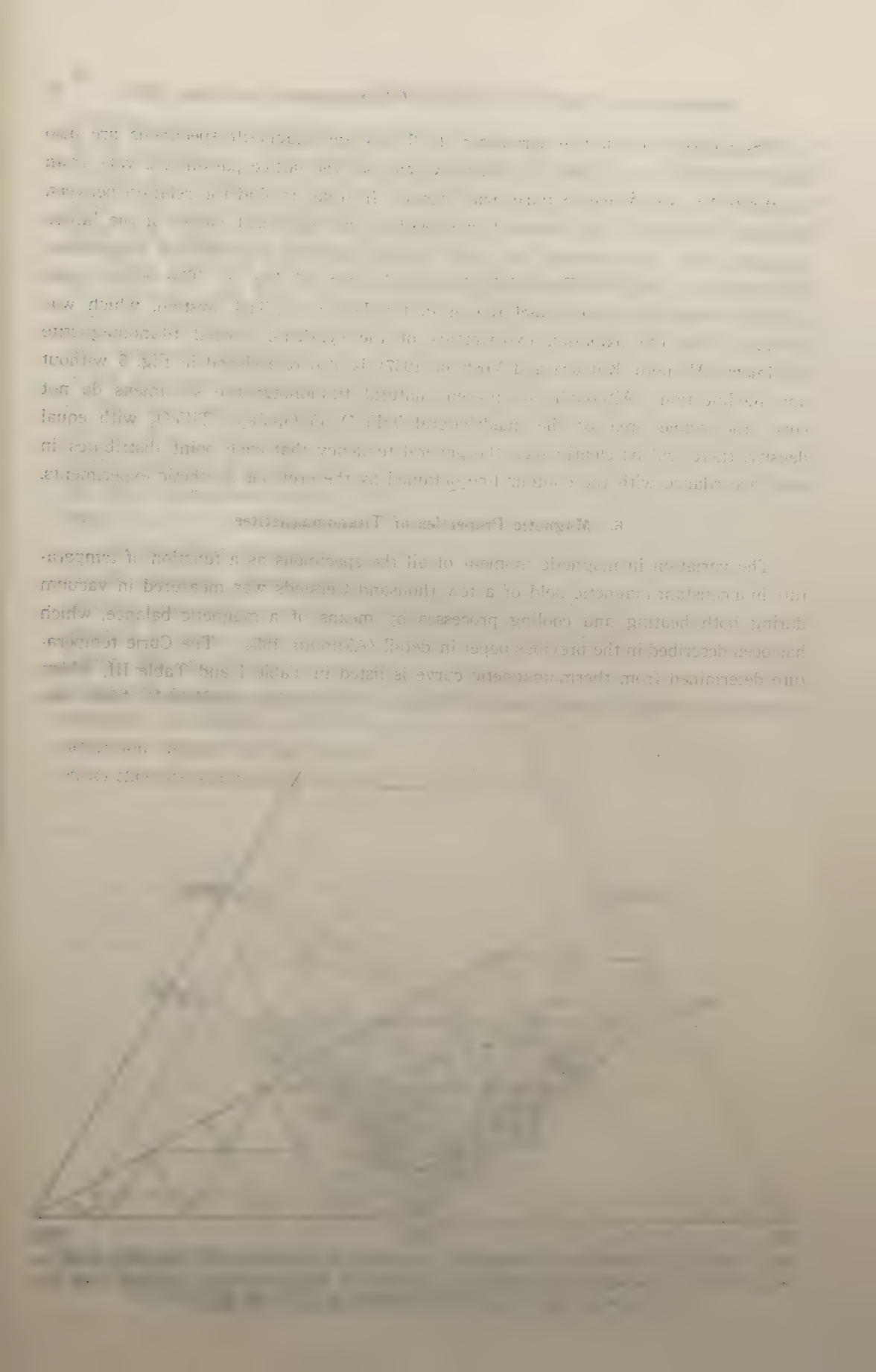

The values of the lattice parameter of all the titanomagnetite specimens are also listed in Table I and Table III, where we can see the lattice parameters vary from about 8.38 Å to 8.49 Å over a fairly wide range. In order to find the relation between the lattice parameter and chemical composition, the numerical values of the lattice parameter were also indicated for each point representing the chemical composition of specimen on the FeO–Fe_2O_3–TiO_2 ternary diagram of Fig. 5. The equal lattice parameter diagram of the spinel region in the FeO–Fe_2O_3–TiO_2 system, which was obtained from the oxidation experiments of the synthetic normal titanomagnetite specimens (Akimoto, Katsura and Yoshida, 1957), is also reproduced in Fig. 5 without any modification. Although the present natural titanomagnetite specimens do not cover the whole area of the quadrilateral $TiFe_2O_4$–Fe_3O_4–Fe_2O_3–$TiFeO_3$ with equal density, there will be clearly seen the general tendency that each point distributes in good accordance with the contour line obtained by the previous synthetic experiments.

6. Magnetic Properties of Titanomagnetites

The variation in magnetic moment of all the specimens as a function of temperature in a constant magnetic field of a few thousand Oersteds was measured in vacuum during both heating and cooling processes by means of a magnetic balance, which has been described in the previous paper in detail (Akimoto, 1954). The Curie temperature determined from thermomagnetic curve is listed in Table I and Table III, where a part of the results already reported (Akimoto, 1955) is also reproduced. As for the

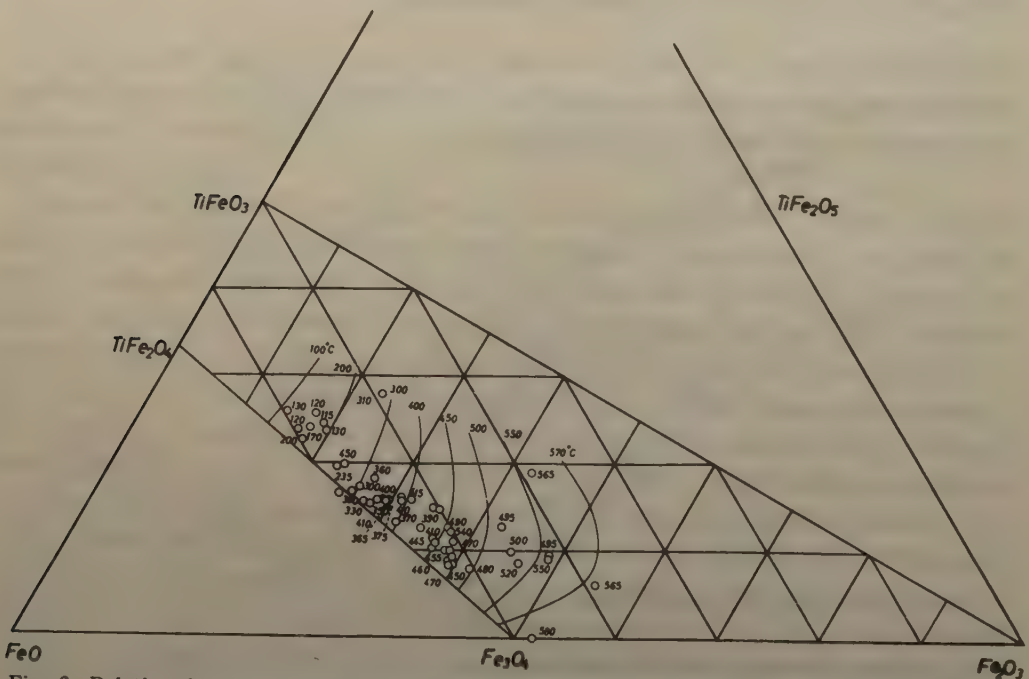

Fig. 6 Relation between Curie temperature and chemical composition of titanomagnetites in volcanic rocks. The equal Curie temperature diagram of the spinel region obtained from the synthetic titanomagnetites is also reproduced in the figure.

specimens having the thermal hysteresis character in their thermomagnetic curve, that is the specimens of which magnetic moment changes irreversibly with temperature in heating and cooling process, the Curie temperature of both processes are given in the table. The values of the Curie temperature of the present specimens spread over the fairly wide range from about 100°C to 570°C.

These numerical values of the Curie temperature of the natural titanomagnetites are compared with those of the synthetic titanomagnetite in Fig. 6, where the equal Curie temperature diagram of the spinel region in the FeO–Fe_2O_3–TiO_2 system, which was empirically determined from the previous study on the synthetic titanomagnetites, is also superposed. From the figure it is found in general that the Curie temperature of the present natural titanomagnetite specimens distributes in conformity with the contour line. Concerning the specimen with thermal hysteresis phenomenon in its thermomagnetic curve, the Curie temperature in the cooling process was adopted in the above discussion, because it seems likely to be in a more stable state (Akimoto, 1955).

The saturation moment of the specimens is also measured at a room temperature by the magnetic balance method. The details have already been reported in the previous paper (Akimoto, 1955). The results are also given in Table I. As already reported by many investigators (Chevallier et al., 1955, Néel, 1955, Nicholls, 1955, Gorter, 1957 and Akimoto et al., 1957), the saturation moment of the titanomagnetite is expected to be greatly affected by the cation configuration in both sites of the spinel structure, i. e. octahedral and tetrahedral site. Consequently it seems likely that the saturation moment of the natural titanomagnetite in volcanic rock depends not only on its chemical composition but on its total history experienced since the outflow over

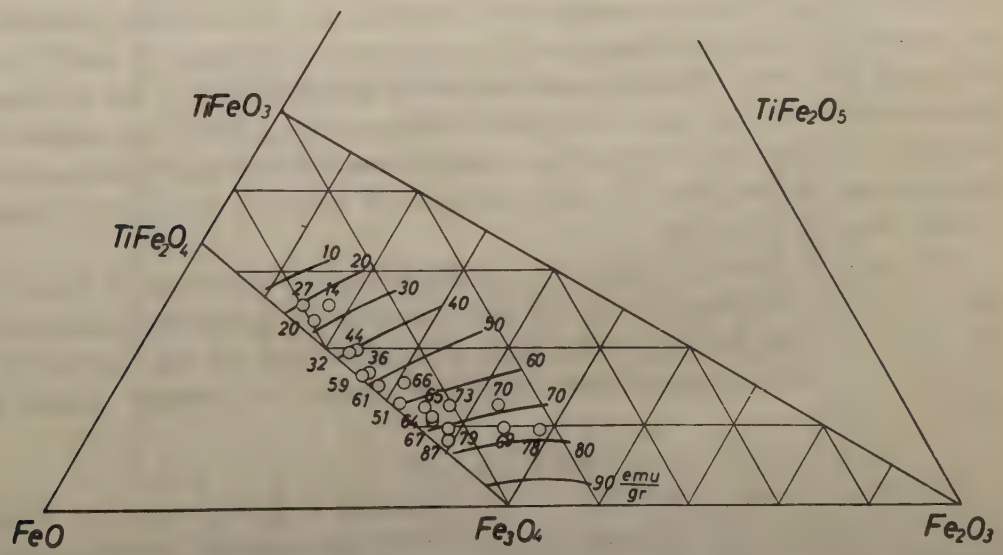

Fig. 7 Relation between saturation moment at room temperature and chemical composition of titanomagnetites in volcanic rocks. The equal saturation moment diagram of the spinel region obtained from the synthetic titanomagnetites is also reproduced in the figure.

saturation moment of the natural titanomagnetite in volcanic rock depends not only on its chemical composition but on its total history experienced since the outflow over

5. Oxidation of Ti$_2$O$_3$ to TiO$_2$

Ti$_2$O$_3$ was prepared by the reduction of TiO$_2$ (Degussa P25) with titanium metal powder (Koch-Light, 99.5%) at 1000°C for 24 hours in a sealed evacuated silica tube. The resulting Ti$_2$O$_3$ was found to be single-phase by X-ray powder diffraction and had a lattice parameter $a = 5.1678(1)$ Å, $c = 13.604(2)$ Å, in agreement with literature values (Swanson and Fuyat, 1953). Before oxidation, the Ti$_2$O$_3$ was ground to a fine powder (< 10 μm) in an agate mortar under acetone.

Thermogravimetric oxidation was carried out in a Stanton-Redcroft TG750 thermobalance. The sample, typically 50–80 mg, was heated in a platinum crucible in a flowing stream of dry air (flow rate 100 cm^3 min^{-1}) at a heating rate of 5°C min^{-1} from room temperature to 1000°C, followed by an isothermal hold of 2 hours. The mass gain was recorded continuously as a function of temperature and time. The oxidation is formally represented by

$$2\,Ti_2O_3 + O_2 \rightarrow 4\,TiO_2 \qquad (1)$$

The observed mass gain corresponded to 99.8 ± 0.3% of the theoretical value for complete conversion to TiO$_2$, confirming the stoichiometry of the reaction.

the earth's surface. This may be a reason why the numerical values of the saturation moment for each specimen on the FeO–Fe_2O_3–TiO_2 system shown in Fig. 7 do not always accord well with the contour line, which was determined from the oxidation experiments of the normal titanomagnetite synthesized under a definite physico-chemical conditions.

7. Oxidation-Reduction Experiments on Natural Titanomagnetite

As already quoted in the present paper, we showed from the oxidation experiments on the synthetic titanomagnetite that the normal titanomagnetite on Fe_3O_4–$TiFe_2O_4$ system can be shifted discretionally to fairly broad range within a quadrilateral $TiFe_2O_4$–Fe_3O_4–Fe_2O_3–$TiFeO_3$ in conserving its spinel structure if appropriate conditions were selected. (Akimoto, Katsura and Yoshida 1957). Since the preparation of the homogeneous titanomagnetite having some vacant site in the spinel structure was the impending purpose in the previous study, the chemical reaction between normal titanomagnetite and oxygen was carried out in atmospheric partial pressure of oxygen and the rate of this reaction was left out of consideration. The reaction is formulated qualitatively as below;

(normal titanomagnetite) $+O \rightarrow$ (abnormal titanomagnetite). (1)

The stoichiometric reaction suggested by Ramdohr ($3TiFe_2O_4+O=3TiFeO_3+Fe_3O_4$; Ramdohr, 1953) will be expected to be realized in an equilibrium state under a certain temperature and partial pressure of oxygen. In this section, we attempted not only to oxidize but to reduce the natural titanomagnetite. The reduction process regarded as a reverse reaction of the oxidation is formulated as follows.

(abnormal titanomagnetite) $-O \rightarrow$ normal titanomagnetite. (2)

To obtain the normal titanomagnetite from abnormal one, the following procedures are carried out. Abnormal titanomagnetite was heated in vacuum up to 1200°C in a transparent silica tube. The free oxygen caused by the dissociation of the specimens were subtracted with the aid of an oil diffusion vacuum pump. After the pressure in the silica tube reached to 1×10^{-4} mmHg at 1200°C, the natural abnormal titanomagnetite samples in the vacuum silica tube were quenched by removing the electric furnace laterally along the silica tube.

The results of the oxidation and reduction experiments are summarized in Table IV. In Fig. 8 and Fig. 9 the change of the chemical composition with these heat treatments was shown in the FeO–Fe_2O_3–TiO_2 ternary diagram and in the $Fe/Fe+Ti\sim Fe-Ti\ O\times32$ diagram respectively, where the direction of chemical change is indicated by arrows.

(1) Change of chemical composition

Comparing the results of oxidation by heat treatment with each other (see Table IV), it is likely that the titanomagnetite containing larger quantity of TiO_2 (titanomagnetite in Hamada nepheline basalt) is more easily oxidized than that containing smaller quantity of TiO_2 (titanomagnetite in Niisima rhyolite). The heat treatment temperature in the case of Niisima rhyolite is lower by 50°C than that of Hamada

Table IV Change in chemical composition, lattice parameter and Curie temperature of natural titanomagnetites with oxidation or reduction.

Specimen	Heat treatment	FeO	Fe_2O_3	TiO_2 in mol. %	$\frac{Fe}{Fe+Ti}$	$\frac{Fe+Ti}{O}\times 32$	Lattice parameter	Curie temperature
Titanomagnetite in Hamada nepheline basalt*	Original	57.79	23.21	19.00	0.846	23.83	8.460±0.001Å	240 C
	500°C, air, 2 hrs.	44.05	35.11	20.84	0.846	22.63	8.427±0.004	350–550
Titanomagnetite in Niisima rhyolite**	Original	52.24	39.52	8.24	0.941	23.84	8.408±0.001	470
	650°C, air, 12 hrs.	43.89	47.40	8.71	0.941	23.18	8.394	540
Titanomagnetite in Niisima rhyolite, 520>Ts>500°C	Original	45.37	46.34	8.29	0.943	23.30	8.397±0.003	520
	1200°C, vac, 30 min.	53.05	38.83	8.11	0.942	23.91	8.410	470
Titanomagnetite in Manazuru dacite pumice, 380>Ts>360°C	Original	54.40	29.92	15.68	0.879	23.69	8.430±0.001	375
	1200°C, vac, 30 min.	56.68	27.88	15.44	0.879	23.90	8.424±0.002	335
Titanomagnetite in Himesima andesite	Original	45.36	44.79	9.86	0.932	23.23	8.400±0.003	500
	1200°C, vac, 30 min.	54.65	35.94	9.41	0.931	24.00	8.409	450
Titanomagnetite in Gokurakuzi iron sand	Original	51.50	36.78	11.72	0.914	23.62	8.401±0.002	420
	1200°C, vac, 30 min.	53.49	34.37	12.14	0.910	23.77	8.402±0.001	415
Titanomagnetite in Semi dolerite*	Original	59.61	14.97	25.42	0.779	23.68	8.475±0.001	
	1200°C, vac, 30 min.	60.96	14.15	24.89	0.782	23.84	8.472±0.002	100

* These titanomagnetites are newly separated for the present purpose from the same rocks as listed in Table I.

** These data are cited from the report by Nagata and Ozima (1955).

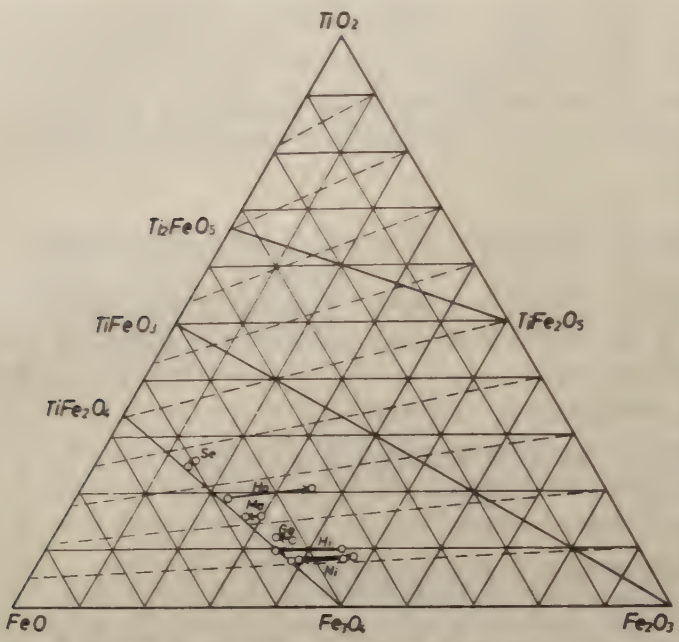

Fig. 8 Change in chemical composition of titanomagnetites in volcanic rocks with oxidation or reduction, represented on a FeO-Fe_2O_3-TiO_2 diagram (see Table IV).

Se: titanomagnetite in Semi dolerite
Ha: titanomagnetite in Hamada basalt
Ma: titanomagnetite in Manazuru dacite pumice
Go: titanomagnetite in Gokurakuzi iron sand
Hi: titanomagnetite in Himesima andesite
Ni: titanomagnetite in Niisima rhyolite.

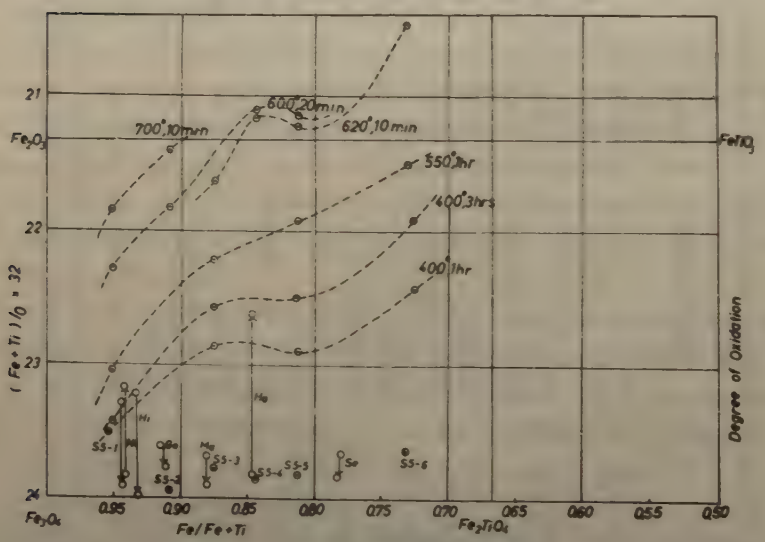

Fig. 9 Change in chemical composition of titanomagnetites with oxidation or reduction, represented on $Fe/(Fe+Ti)$ vs. $(Fe+Ti)/O \times 32$ diagram (see Table IV and V).

○: titanomagnetite in volcanic rocks. Abbreviation of the specimens is the same as in Fig. 8.
⊙: synthetic titanomagnetites.

and moreover the duration of heating is much larger in Niisima rhyolite compared with that of Hamada nepheline basalt. In spite of these experimental conditions favourable to the oxidation of the titanomagnetite in the Niisima rhyolite, the rate of decrease in the value of $(Fe+Ti)/O\times32$, which represents the degree of oxidation, is much larger in the case of the titanomagnetite in nepheline basalt. The feasibility of this situation may also be expected by our previous study (Akimoto, Katsura and Yoshida 1957). The results of the heating experiments in the open air of the synthetic titanomagnetite (normal series) are reproduced in Table V. The degree of oxidation of the synthetic titanomagnetite is also shown in Fig. 9, where we can clearly see the

Table V Change in chemical composition, lattice parameter and Curie temperature of synthetic titanomagnetites with oxidation.

Specimen	Heat treatment	$\frac{Fe}{Fe+Ti}$	$\frac{Fe+Ti}{O}\times32$	Lattice parameter	Curie temperature	Existing mineral phases
S 5-1	Original	0.950	24.15	8.416±0.002Å	490°C	TiMt*
	400°C, air, 1 hr.	0.952	23.51			〃
	400°C, air, 3 hrs.	0.950	23.43	8.400±0.002	550	〃
	550°C, air, 1 hr.	0.950	23.05	8.391±0.001	570	〃
	600°C, air, 20 min.	0.950	22.29			Il-Hm,** TiMt
	700°C, air, 10 min.	0.951	21.86			Il-Hm,** TiMt PB***
S 5-2	Original	0.908	23.95	8.428±0.001	420	TiMt
	600°C, air, 20 min.	0.908	21.84			TiMt, Il-Hm, PB
	700°C, air, 10 min.	0.908	21.42			Il-Hm, PB, TiMt
S 5-3	Original	0.874	23.78	8.442±0.001	350	TiMt
	400°C, air, 1 hr.	0.874	22.87			〃
	400°C, air, 3 hrs.	0.874	22.58	8.405±0.002	550	〃
	550°C, air, 1 hr.	0.874	22.23	8.399±0.000	565	〃
	620°C, air, 10 min.	0.874	21.65			TiMt, Il-Hm, PB
S 5-4	Original	0.843	23.86	8.456±0.000	265	TiMt
	600°C, air, 20 min.	0.843	21.12			TiMt, Il-Hm, PB
	620°C, air, 10 min.	0.843	21.18			〃
S 5-5	Original	0.812	23.83	8.474±0.000	190	TiMt
	400°C, air, 1 hr.	0.812	22.91			〃
	400°C, air, 3 hrs.	0.812	22.50	8.414±0.001	540	〃
	550°C, air, 1 hr.	0.812	21.94	8.414±0.002 (8.358)	540 (585)	〃
	600°C, air, 20 min.	0.812	21.16			TiMt, Il-Hm, PB
	620°C, air, 10 min.	0.812	21.24			〃
S 5-6	Original	0.731	23.65	8.507±0.002	15	TiMt
	400°C, air, 1 hr.	0.725	22.44			〃
	400°C, air, 3 hrs.	0.725	21.92	8.423±0.002 (8.474)	505 (140)	〃
	550°C, air, 1 hr.	0.730	21.51	8.424±0.001	530 (585)	TiMt, Il-Hm (trace)
	620°C, air, 10 min.	0.730	20.48			TiMt, Il-Hm, PB

* TiMt: titanomagnetite having spinel structure
** Il-Hm: ilmenite-hematite series solid solution having rhombohedral structure.
*** PB: pseudobrookite series solid solution having orthorhombic structure.
(Akimoto, Nagata, Katsura, 1957)

general tendency that the oxidation proceeds more easily in the specimens having higher content of TiO_2. When we examine the figure more carefully, however, it may be noticed that the titanomagnetite having the Fe/Fe+Ti ratio between 0.80 and 0.90 shows the almost similar character for the oxidation under the present experimental conditions. The details of these phenomena will be reported in a further paper in taking the reaction velocity into consideration.

Through the heating experiments carried out at high temperature (1200°C) and in high vacuum state (10^{-4}mm Hg), the metastable natural titanomagnetite having a vacant site in the metal position of the spinel structure shows a trend to approach to a more stable and complete spinel structure (Table IV and Fig. 8). Since the duration of the present treatment may be too short to attain a true dissociation equilibrium at that temperature and pressure, the reduction process may probably proceed until the spinel structure of the concerned titanomagnetite becomes complete if the sufficiently long heat treatment was taken into practice.

(2) Change in lattice parameter and Curie temperature

The general tendency that the crystal parameter becomes smaller and the Curie temperature becomes higher according as the oxidation proceeds has already been reported in the previous paper (Akimoto, Katsura and Yoshida, 1957). This was again confirmed in more definite manner by the present oxidation or reduction experiments on the natural titanomagnetite specimens, the results being given in Tables IV and V. We have previously pointed out in § 4 that the chemical composition of the thermomagnetically separated specimens changes continuously along the reduction-oxidation line of the FeO–Fe_2O_3–TiO_2 system. These data are also available for examining the effect of oxidation or reduction on the lattice parameter and Curie temperature.

In Fig. 10 the lattice parameter of the titanomagnetite specimens having a definite atomic ratio of Fe/Fe+Ti is plotted as a function of the number of the metal ions in a unit cell, which indicates the degree of oxidation. Two groups of titanomagnetites of which atomic ratio Fe/(Fe+Ti) is of a fairly narrow range of 0.87～0.88 and 0.94～0.95 are selected for the present purpose from Tables I, II, III, IV and V. Fractionated specimens of Manazuru dacite are involved in the former group and Niisima rhyolite

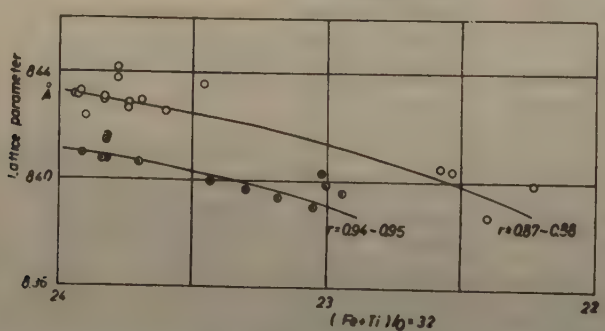

Fig. 10 Variation in lattice parameter of titanomagnetites with oxidation or reduction. Ordinate; lattice parameter, Abscissa; (Fe+Ti)/O×32, r=Fe/(Fe+Ti).

in the latter group. Continuous change of the lattice parameter with the (Fe+Ti)/O ×32 value is found in each group. The dependence of the Curie temperature of the specimens upon the numbers of metal ions in a unit cell is shown in Fig. 11, where continuous increase of the Curie temperature is also found with increase of the (Fe+Ti)/O×32 value in each group.

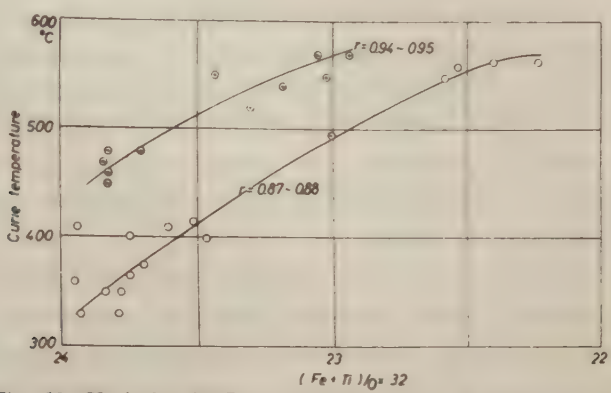

Fig. 11 Variation in Curie temperature of titanomagnetites with oxidation or reduction. Ordinate; Curie temperature, Abscissa; (Fe+Ti)/O×32, r=Fe/(Fe+Ti).

8. Conclusions

The concept of the generalized titanomagnetite which has been derived from the oxidation experiments for the $TiFe_2O_4$–Fe_3O_4 solid solution series was applied for the magneto-chemical study of the natural titanomagnetite in volcanic rocks. About 80 % of specimens in the present study possesses the chemical composition distributing in the magnetite-ulvöspinel-ilmenite compositional field. However, natural occurrence of the single phase titanomagnetite, of which chemical composition is situated in the magnetite-hematite-ilmenite compositional field far beyond the $TiFeO_3$–Fe_3O_4 line in the FeO–Fe_2O_3–TiO_2 diagram, was also confirmed in some volcanic rocks. These very abnormal titanomagnetites can probably be understood thoroughly only by assuming that the spinel phase with the varying vacancy in the metal ion site of the crystal structure can be in existence successively according as the oxidation process proceeds on the $TiFe_2O_4$–Fe_3O_4 solid solution series. The $TiFeO_3$–Fe_3O_4 solid solution series postulated by Chevallier and Girard (1950) should be regarded as a special series of the generalized titanomagnetite standing in the line concerned. It remains still unsolved, however, to fix ultimately the boundaries over which the spinel phase can not exist as a single phase under any circumstance. Since we can not find any special reason for considering that the oxidation of the $TiFe_2O_4$–Fe_3O_4 series should terminate at the $TiFeO_3$–Fe_2O_3 line, the very abnormal titanomagnetite having the chemical composition situated in the ilmenite-hematite-rutile compositional field may probably exist in some rocks which underwent a severe oxidation by alteration or weathering. The presence of a titanomaghemite reported by Nicholls (1955) in quotation from Basta's data (1953) may support the above consideration.

[illegible]

[illegible] is discussed in connection with the [illegible] of chemical [illegible] magnetic [illegible]

[illegible] and magnetic properties of [illegible] previous study, are [illegible] explained by [illegible] the equal lattice parameter [illegible] $(H_2O)_3$-TiO_2 ternary system which have been [illegible] experiments. The [illegible] that a [illegible] decrease in lattice parameter and increase in Curie temperature of titano-[illegible] take place according as the [illegible] is also established from the [illegible] by [illegible] the value of [illegible]

In concluding, the authors should like to express their sincere thanks to Prof. T. Nagata for his [illegible] guidance since the very beginning of the authors' study of [illegible]

[illegible]

New findings that the titanomagnetite in some volcanic rocks is separable to an ensemble of the single phase grains of which chemical composition varies grain by grain nearly along the reduction-oxidation line may be of great petrogenetic interest. This suggests that the formation of titanomagnetite in volcanic rocks is more complicated than expected.

The presence of the very abnormal titanomagnetite is also of great significance on the study of palaeomagnetism. Since the remanent magnetization of rocks may be greatly influenced by the chemical reaction throughout geological age, a systematic study of the variation in both intensity and direction of the natural remanent magnetization of rocks with oxidation is required, in connection with the generation of chemical remanent magnetization or the physical explanation of the unstable remanent magnetization observed in some kind of rocks.

It must be emphasized here that the crystallographic and magnetic properties of the natural titanomagnetite, which have been considered complicated apparently in the previous study, are successfully explained by utilizing the equal lattice parameter diagram and equal Curie temperature diagram on the FeO–Fe_2O_3–TiO_2 ternary system which have been determined from the synthetic experiments. The situation that a continuous decrease in lattice parameter and increase in Curie temperature of titanomagnetite take place according as the oxidation proceeds is also established from the oxidation or reduction experiments of natural titanomagnetite by adopting the value of $(Fe+Ti)/O\times32$ for an oxidation parameter.

In concluding the authors should like to express their sincere thanks to Prof. T. Nagata for his constant guidance since the very beginning of the authors' study of rock magnetism. They also wish to thank Prof. I. Iwasaki for his kind encouragement and interest throughout the study. They thank cordially Prof. H. Kuno, who kindly allowed the authors to use various ferromagnetic minerals separated by him and gave much valuable suggestions and discussions from the petrological point of view. Their hearty thanks are also due to Messrs. S. Aramaki and H. Matsumoto for their kindness in putting the specimens at the authors' disposal. The authors are also indebted to Mr. M. Yoshida for his fruitful discussion throughout the study.

References

Akimoto S. (1951) Journ. Geomag. Geoelectr. **3**, 47.
Akimoto S. (1954) Journ. Geomag. Geoelectr. **6**, 1.
Akimoto S. (1955) Jap. Journ. Geophys. **1**, No. 2, 1.
Akimoto S. (1957) Advanc. Phys. **6**, 288.
Akimoto S., Nagata T. and Katsura T. (1957) Nature **179**, 37.
Akimoto S., Katsura T. and Yoshida M. (1957) Journ. Geomag. Geoelectr. **9**, 165.
Basta E.Z. (1953) Thesis, Bristol.
Buddington A.F., Fahey J. and Vlisidis A. (1955) Amer. Journ. Sci. **253**, 497.
Chevallier R. and Girard J. (1950) Bull. Soc. Chim. France **5 17**, 576.
Chevallier R. Bolfa J. and Mathieu S. (1955) Bull. Soc. Franc. Miner. Crist. **78**, 307, 365.
Gorter E.W. (1957) Advanc. Phys. **6**, 336.
Iwasaki I. and Katsura T. (1950) Kyûsyû Kôzan Gakkai-si **18**, 197, 256, 291 (in Japanese).
Iwasaki I., Katsura T., Yoshida M. and Tarutani T. (1957) Japan Analyst **6**, 211 (in Japanese).

Nagata T., Akimoto S. and Uyeda S. (1953) Journ. Geomag. Geoelectr. **5**, 168.
Nagata T. and Ozima M. (1955) Journ. Geomag. Geoelectr. **7**, 105.
Nagata T. and Akimoto S. (1956) Geofisica pura e applic. **34**, 36.
Néel L. (1955) Advanc. Phys. **4**, 191.
Nicholls G.D. (1955) Advanc. Phys. **4**, 113.
Pouillard E. (1950) Ann. Chimie **5**, 164.
Ramdohr P. (1953) Econ. Geol. **48**, 677.
Uyeda S. (1957) Journ. Geomag. Geoelectr. **9**, 61.
Uyeda S. (1958) Jap. Journ. Geophys. **2**, No. 1, 1.
Vincent E.A. and Phillips R. (1954) Geochim. Cosmochim. Acta **6**, 1.
Vincent E.A., Wright J.B., Chevallier R. and Mathieu S. (1957) Miner. Mag. London **31**, 624.
Wager L.R. and Mitchell R.L. (1951) Geochim. Cosmochim. Acta **1**, 129.

A Theory of Ionospheric Radio Wave Scattering Under the Influences of Ion Production and Recombination

By Ken-ichi MAEDA, Susumu KATO and Takao TSUDA

Department of Electronics, Kyoto University

(Read May 17, 1958; Received March 1, 1959)

Abstract

For the daytime E-layer ionospheric scatter propagation, the controlling solar influences cannot be neglected. To account for the experimental results obtained by D.K. Bailey *et al.*, showing solar influences, a new theory is proposed which introduces the effects of ion production and recombination to Villars-Weisskopf's pressure theory. The electrons are assumed to be compressed or dilated at the same rate as the air itself, the latter being subject to adiabatic change of pressure, while the electrons and ions moving with the air molecules are produced by solar radiation and then recombined. The results obtained are quite satisfactory to account for the dependence of received scattered signal intensity on both frequency and scattering angle, at least concerning the daytime solar controlled scatter propagation in the E-region.

1. Introduction

Among the results of scatter experiments made by Bailey *et al.* (1955), one of the most interesting is that of diurnal variation of received scattered electric field.

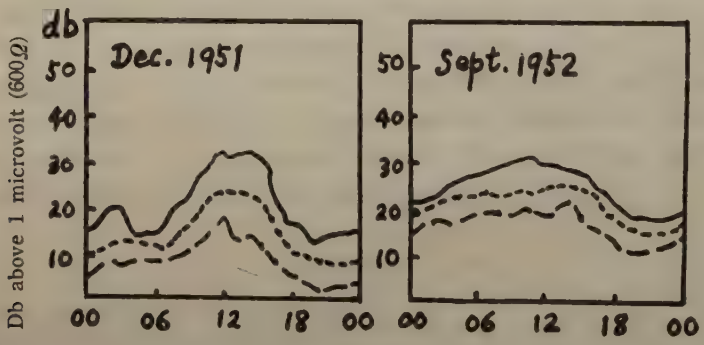

Fig. 1 Diurnal variation of signal intensity (at medium latitude) (after D.K. Bailey *et al.*)
f=49.80 Mc/s; D=1243 km; Pt=30 kw
—— level equalled or exceeded by 10% of days
····· level equalled or exceeded by 50% of days
– – – level equalled or exceeded by 90% of days

Above figures show that the received scattered field has its remarkable maxima at noon for the path mid-point located in the middle latitude. The fact is quite significant because those maxima occur when the solar radiation is great enough and

the ionization is enhanced through ion production by the sun. In this paper we will try a theory assuming that the air is subject to adiabatic change of pressure and the electric charges, frozen amid the tremendous number of air molecules, are constrained to move with them and at the same time undergo the processes of both being produced by solar radiation and being neutralized through recombination between electrons and ions. We assume small perturbations on the air and electron densities. This treatment is equivalent to the so-called pressure theory proposed by Villars and Weisskopf (1954) except where special attention is paid to the above-mentioned chemical reactions. The scope of our discussions will necessarily be limited to E-region scattering, since there is at least some experimental data for it.

2. Assumptions and Formulation

The existence of the geomagnetic field should be taken into considerations; but, roughly speaking, only by such an existence of the geomagnetic field, a single charged particle is not influenced in its movement except in the deflection transverse to the magnetic field and the kinetic energy of the charged particle remains constant as was given initially. We want to see the multi-phased scattering phenomena only in energy relation and the effect of the geomagnetic field will be ignored. This amounts to the treatment of the turbulent motion as isotropic. Further, by the relation, which is valid throughout the ionosphere, $\nu \ll \lambda$ (ν: kinematic viscosity ; λ: magnetic diffusivity), all the spontaneous electromagnetic fields will be neglected (Batchelor, 1951). Those assumptions make us possible to treat the electron density fluctuations hydrodynamically: in other words, the electrons embedded amid the air molecules are compressed or dilated in the same way and at the same rate as the air itself, but only suffer ion production and recombination during these processes. Besides, the air is supposed to be subject to adiabatic changes: the only point that distinguishes our theory from that made by Villars and Weisskopf (1954) is the effects of ion production and recombination.

The ionosphere is made up of free electrons and the same number of ions and far more numerous air molecules. Concerning the quantities of these three constituents, subscripts e, i and n will be used. For the electrons and ions, the following equations are respectively valid:

$$\rho_e \frac{D}{Dt} v_{ej} = -\frac{\partial p_e}{\partial x_j} - \eta_{en} (v_{ej} - v_{nj}), \quad (j=1, 2, 3) \tag{1}$$

$$\frac{\partial \rho_e}{\partial t} + \sum_{j=1}^{3} \frac{\partial}{\partial x_j} (\rho_e v_{ej}) = m_e (q\rho_n - \beta \rho_e \rho_i) ; \tag{2}$$

Similar equations for ions,

where $\eta_{en}[=\rho_e \nu_{en}(\mathrm{gr.\,cm^{-3}\,sec^{-1}})]$ represents the effect of electron-*versus*-neutral particles collisions, $q(\mathrm{gr^{-1}\cdot sec^{-1}})$ and $\beta(\mathrm{gr^{-2}\cdot sec^{-1}\cdot cm^3})$ ion production and effective recombination respectively. For other quantities, the use of notations is conventional.

In view of the rapidly oscillating radio waves, we assume that the state of turbulence remains stationary; the above equations (1) and (2) yield the following complicated equation:

In the above identity equation, several terms containing 2nd, 3rd and 4th order correlations appear. As in the case of multiple normal distribution, all the 3rd order correlations give very slight effects when compared with the contribution by the 2nd

$$0=\frac{\partial^2}{\partial t^2}\overline{\rho_e\rho_e'}=\overline{\rho_e\frac{\partial^2\rho_e'}{\partial t^2}}+2\overline{\frac{\partial\rho_e}{\partial t}\frac{\partial\rho_e'}{\partial t}}+\overline{\rho_e'\frac{\partial^2\rho_e}{\partial t^2}}=2m_eq\left(\overline{\rho_e'\frac{\partial\rho_n}{\partial t}}-\overline{\beta\rho_e'\frac{\partial}{\partial t}(\rho_e\rho_i)}\right)$$
$$+\sum_j\sum_k\frac{\partial^2}{\partial\xi_j\partial\xi_k}\left\{\overline{\rho_e\rho_e'v_{ek}v_{ej}}+\overline{\rho_e\rho_e'v_{ek}'v_{ej}'}\right\}+m_eq\sum_j\left\{\overline{\rho_e'\rho_nv_{ej}}-\overline{\rho_e\rho_n'v_{ej}'}\right\}$$
$$-m_e\beta\sum_j\frac{\partial}{\partial\xi_j}\left\{\overline{\rho_e\rho_e'\rho_iv_{ej}}-\overline{\rho_e\rho_e'\rho_i'v_{ej}'}\right\}+2p^2\overline{p_e\rho_e'}$$
$$+\gamma_{en}\sum_j\frac{\partial}{\partial\xi_j}\left\{(\overline{v_{ej}'\rho_e}-\overline{v_{ej}\rho_e'})-(\overline{v_{nj}'\rho_e}-\overline{v_{nj}\rho_e'})\right\}$$
$$+2m_e^2\left[q^2\overline{\rho_n\rho_n'}-q\beta(\overline{\rho_n\rho_e'\rho_i'}+\overline{\rho_n'\rho_e\rho_i})+\beta^2\overline{\rho_e\rho_e'\rho_i\rho_i'}\right]$$
$$-2m_e\beta\sum_j\frac{\partial}{\partial\xi_j}\left\{\overline{\rho_e\rho_e'\rho_i'v_{ej}}-\overline{\rho_e\rho_e'\rho_iv_{ej}'}\right\}+2m_eq\sum_j\frac{\partial}{\partial\xi_j}\left\{\overline{\rho_n'\rho_ev_{ej}}-\overline{\rho_e'\rho_nv_{ej}'}\right\}$$
$$-2\sum_j\sum_k\frac{\partial^2}{\partial\xi_j\partial\xi_k}\overline{\rho_e\rho_e'v_{ek}'v_{ej}'}, \qquad (3)$$

where the over-bars represent taking the average for a sufficiently long time and $\xi_j=x_j'-x_j$ $(j=1, 2, 3)$.

We define

$$\delta\rho_e=\rho_e-\overline{\rho_e},$$
$$\delta p_e=p_e-\overline{p_e}, \text{ etc.}$$

In the above lengthy equation, several terms containing 2nd, 3rd and 4th order correlations appear. As in the case of multiple normal distribution, all the 3rd order correlations give very slight effects when compared with the contribution by the 2nd and 4th order correlation terms. And the 4th order terms can be expressed by summation of combinations of 2nd order terms with a good approximation (Chandrasekhar, 1951; Tatsumi, 1957).

As mentioned above, the electrons are supposed to flow without deviating from the flow of tremendously numerous air molecules, so that

$$v_{ej}\cong v_{nj} \quad (j=1, 2, 3). \qquad (4)$$

And we assume solenoidal property on the air velocity. Regarding both time and space

$$n_e\cong n_i, \qquad (5)$$
$$q\overline{\rho_n}\cong\beta\overline{\rho_e}\overline{\rho_i}. \qquad (6)$$

Let us give special attention to the following (in the E-region):

Recombination

Time rate: about 1000 sec≅16 minutes,

Ion production

This takes place almost as quickly as neutral density fluctuation.

Now suppose that a neutral density fluctuation occurs at one place or another. Ion production follows the concentration so quickly that the electron density will be on the increase then and there. Effects of recombination will show up to counterbalance this electron density increase, but it takes too long a time to work as a complete off-set reaction. So we would rather regard the electron density fluctuations

as being completely dissipated before they suffer due counterbalancing effect through recombination. Therefore, during several stages in the decay of turbulence, electron-ion encounters for recombination will have less direct influence on any correlation than quick ion production. Hence

$$\frac{\partial n_e}{\partial t}+\sum_{j=1}^{3}\frac{\partial}{\partial x_j}(n_e v_{ej})=q\cdot\delta\rho_n+\text{higher order terms.} \qquad (7)$$

Thus, as the first step, we ignore the slow fluctuation by recombination except for the mean value $\beta\rho_e\rho_i$ ($\cong q\bar{\rho}_n$), and utilizing all the assumptions so far mentioned and taking into account only the 2nd and 4th order correlations we have, from the equation (3), the following equation:

$$\left\{F(o)-F(r)\right\}\omega_e''+\left\{\frac{2}{r}\left(F(o)-F(r)\right)-F'(r)\right\}\omega_e'+m_e^2q^2\omega_n=0, \qquad (8)$$

where

$$r=\sqrt{\xi_1^2+\xi_2^2+\xi_3^2},$$

$$F(r)=\frac{1}{3}\overline{v_e^2}f(r),$$

$f(r)$: the only defining scalar function (p. 46, Batchelor, 1953; Chandrasekhar, 1951) of electronic velocity correlation (now, equivalent to that of the air velocity),

$$\omega_e=\omega_e(r)=\overline{\delta\rho_e\delta\rho_e'},$$

$$\omega_n=\omega_n(r)=\overline{\delta\rho_n\delta\rho_n'},$$

$$\omega_e'=\frac{d}{dr}\omega_e, \text{ etc.}$$

In the above derivation, we have assumed small perturbations on density fluctuations. Moreover,

$$\nabla^2\overline{p_e\rho_e'}=\nabla^2\overline{\delta p_e\delta\rho_e'}\sim\nabla^2\overline{v_e^2\delta\rho_e'},$$

therefore the pressure term forms a 3rd order correlation and so is small enough in magnitude when compared with other 2nd order or 4th order terms. Further, the loss terms in the equation (1) do not affect the correlations as far as we assume solenoidal property on the velocity.

The above differential equation (8) is deduced from a rough approximation of the actual phenomena. We may naturally assume that the functions $F(r)$, ω_e and ω_n are analytic in the neighborhood of the origin $r=0$. Then when $r\longrightarrow 0$, the first two terms on the left side vanish while the last does not, i.e.

$$m_e^2q^2\omega_n\longrightarrow m_e^2q^2\overline{\delta\rho_n^2}.$$

Let us turn our attentions to the effects of recombination, so far neglected (except in the mean effect). The effect of slow recombination appears quite at random being well-mixed by the stirring action of smaller energetic neutral eddies. Therefore, if we could introduce another term to counterbalance ion production term, it must take the form $-\beta_e^2\tilde{\omega}_e$, where β_e is a kind of effective recombination coefficient and $\tilde{\omega}_e$ is a

of electronic velocity correlation now, equivalent to that of the air velocity.

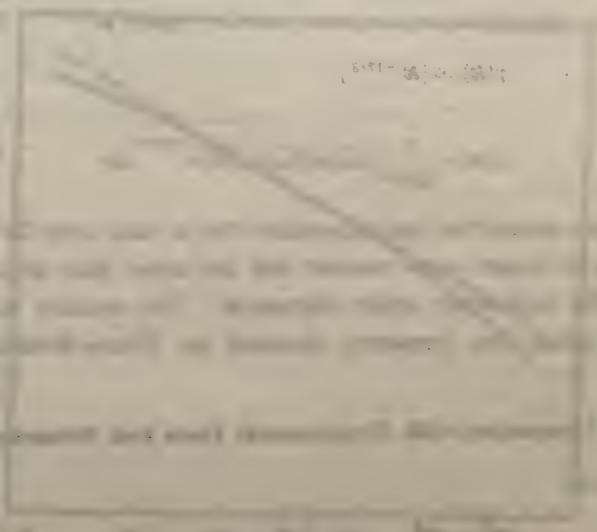

function like ω_n, only the scale factor being such as to make $\tilde{\omega}_e$ contribute near $r=0$.

$$\left\{F(o)-F(r)\right\}\omega_e''+\left\{\frac{2}{r}\left(F(o)-F(r)\right)-F'(r)\right\}\omega_e' + m_e^2q^2\omega_n-\beta_e^2\tilde{\omega}_e=0\,. \tag{9}$$

As the air is subject to adiabatic change,

$$\left.\begin{aligned}&\omega_n=\omega_n(o)\ (1-x^{4/3}),\\ &x=r/r_o\ \text{(normalized distance)},\end{aligned}\right\} \tag{10}$$

so that

$$\tilde{\omega}_e=\tilde{\omega}_e(o)\ (1-cx^{4/3}),\ c>1. \tag{11}$$

And

$$F(r)=\frac{1}{3}\overline{v_e^2}\ (1-x^{2/3}). \tag{12}$$

Equations (10) and (12) are well-known in the case of hydrodynamic turbulence with adiabatic change of pressure (p. 183, Batchelor, 1953). $\tilde{\omega}_e$ in the equation (11) vanishes, when x becomes larger, far sooner than ω_n in the equation (10).

Equations (9)~(12) result in $\alpha=8/3$, for the type of solution

$$\omega_e=\omega_e(o)\ (1-ax^a)\,; \tag{13}$$

i. e.

$$\omega_e(x)=\omega_e(o)\ (1-ax^{8/3}),\ a>0\,. \tag{14}$$

The result corresponds to, in wave number space $\boldsymbol{\kappa}$,

$$\gamma(\boldsymbol{\kappa})\propto|\boldsymbol{\kappa}|^{-17/3}, \tag{15}$$

where

$$\gamma(\boldsymbol{\kappa})=\frac{1}{(2\pi)^3}\int\delta\rho_e(\boldsymbol{x})\delta\rho_e(\boldsymbol{x}+\boldsymbol{r})e^{-i\boldsymbol{\kappa}\cdot\boldsymbol{r}}\,d\boldsymbol{r} \tag{16}$$

We should take notice that the expression (15) is valid only for the wave number far smaller than the largest wave number and far larger than the smallest wave number relevant to the turbulence under discussion. The solution (15) corresponds to the solution for rather low frequency obtained by Villars-Weisskopf's pressure theory (1954).

3. Comparison with Experimental Facts and Numerical Examples

If we denote

$$\frac{P_r}{P_t}\propto\frac{A}{f^2}\cdot\frac{1}{r^2\left(\sin\dfrac{\theta}{2}\right)^n}, \tag{17}$$

where θ: the scattering angle,

A: the aperture of the receiving antenna,

P_r: the received available power,

P_t: the power radiated by the transmitting antenna,

then our theory gives

$$\begin{cases} s=\dfrac{17}{3}=5.7 & \text{for frequency dependence,} \\ n=\dfrac{20}{3}=6.7 & \text{for scattering-angle dependence.} \end{cases}$$

These values of s and n are quite satisfactory to explain the experimental fact for rather low frequency at noon or in the afternoon when the ion production is very pronounced. In Fig. 2 and Fig. 3, our theoretical results are compared with the experimental results obtained by D.K. Bailey *et al.* for the solar controlled E-layer scatter propagation (pp. 1196 and 1199, Bailey, 1955). The results (15) may not be a good approximation for very high frequency scattering whose radio wave length is nearly equal to or less than the dimension of the smallest eddy, which is believed to be of meter order. This is because the correlation function (14) or the spectrum function (15) cannot be expressed by such a simple power-law for the range near the smallest wave number.

The scatter cross section is directly proportional to $\delta\rho_e^2=\omega_e(o)$.
Suppose

$$\delta\rho_n^2/\rho_n=10^{-2}$$

for the daytime and from the equation (7) on putting the divergence term zero, we have

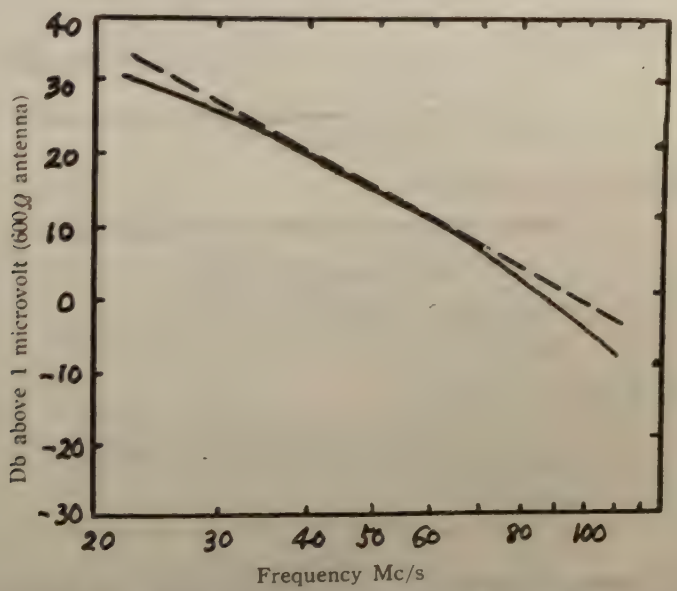

Fig 2 Dependence of signal intensity on frequency.
--- our theoretical result; —— based on selected comparisons for constant aperture in the midday and early afternoon periods when the signal intensity shows a controlling solar influence. For the effective frequency exponent expressed as $A+Bf$, Bailey *et al.* obtained, from the selected comparisons of 107.8 and 27.775 Mc/s respectively with 49.8 Mc/s, $A=5.3$, $B=0.0066$ (f expressed in Mc/s). Allowance was made for the effect of non-deviating absorption.

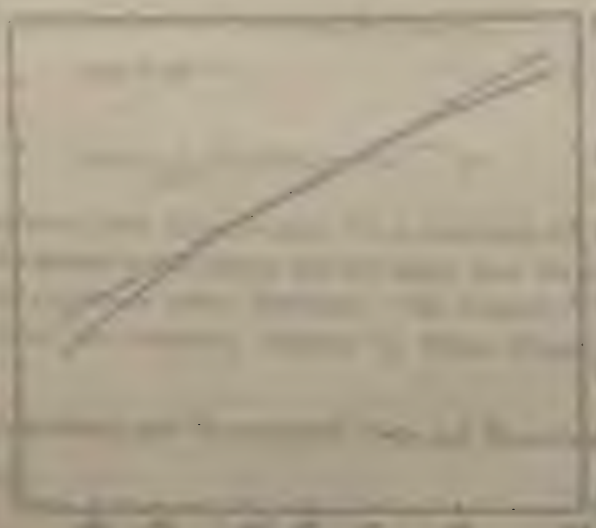

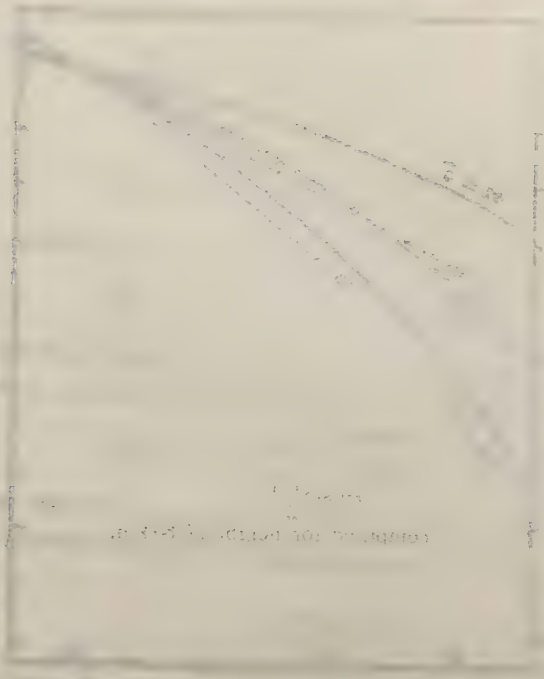

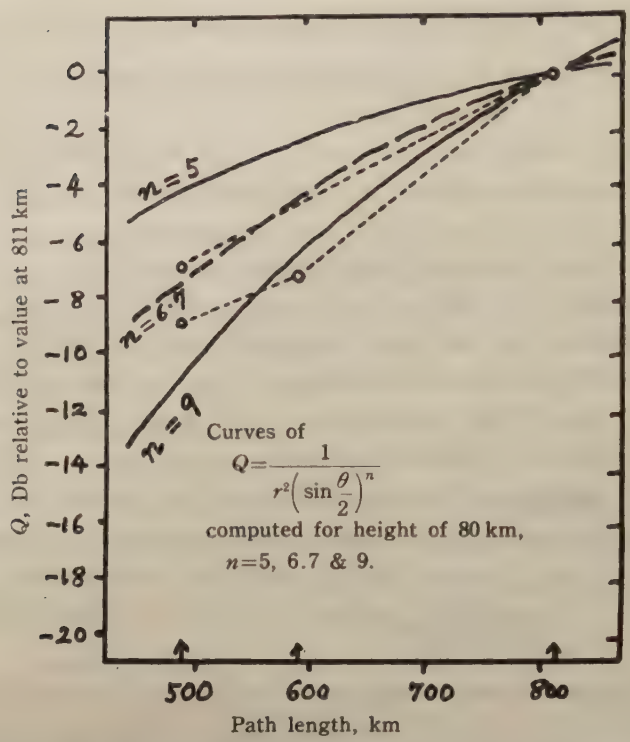

Fig. 3 Angle dependence. All the comparisons are for daytime (Jul., 1953), when the signal intensity was high. (after D.K. Bailey *et al.*)

---- our theoretical result, ····· experimental comparison

θ : the scattering angle

r: the ray distance from the path midpoint in the scattering stratum to the receiver

I) In daytime: $|\delta n_e| \sim q \cdot |\delta \rho_n| \cdot |\delta t|$,

δt being the time constant of an irregularity.

In the E-layer $\begin{cases} \delta t \sim 10^2 \text{ sec} \quad \text{(after H.G. Booker).} \\ q \sim 0.8 \times 10^{24} \text{ gr} \cdot \text{sec}^{-1} \\ m_n/m_e \sim 5 \times 10^4 \end{cases}$

II) At night (no ion production)

$$\frac{\partial n_e}{\partial t} = q\rho_n - \beta m_e m_i \cdot n_e^2, \quad q=0, \quad \beta m_e m_i \cong 10^{-8},$$

i.e.
$$\frac{\partial (\bar{n}_e + \delta n_e)}{\partial t} = -\beta m_e m_i (\bar{n}_e + \delta n_e)^2 .$$

Multiplying the above equation with $(\bar{n}_e + \delta n_e)$ and taking the average, we have

$$\frac{1}{2}\frac{\partial}{\partial t}(\bar{n}_e^2 + \overline{\delta n_e^2}) = -\beta m_e m_i (\bar{n}_e^3 + 3\overline{\bar{n}_e \cdot \delta n_e^2}) .$$

On the other hand, for the mean electron density

$$\frac{1}{2}\frac{\partial}{\partial t}\bar{n}_e^2 = -\beta m_e m_i \bar{n}_e^3 ,$$

so that

$$\frac{1}{2}\frac{\partial}{\partial t}\delta n_e^2 = -3\beta m_i m_e \overline{n_e}\cdot\overline{\delta n_e^2},$$

hence

$$\overline{\delta n_e^2} = \overline{\delta n_{e0}^2}\cdot e^{-6\beta m_e m_i n_e t}$$

$\overline{\delta n_e^2}$ for $t=0$ coincides with that given in I), *viz.*,

$$\overline{\delta n_e^2} = 4\times 10^2 e^{-6\times 10^{-5}t} \quad (\overline{n_e}=10^3\text{cm}^{-3} \text{ at night}).$$

Thus, if we set the origin $t=0$ at 1600 hours, then at 2000 hours, $\overline{\delta n_e^2}$ diminishes by 3.5*db* below $\overline{\delta n_{e0}^2}$, thus continues decreasing by 3.5*db* every 4 hours. Similarly, when

$$\overline{\delta n_e^2} = 4\times 10^2 e^{-3\times 10^{-4}t} \quad (\overline{n_e}=5\times 10^3\text{cm}^{-3} \text{ at night}),$$

$\overline{\delta n_e^2}$ diminishes 18*db* every 4 hours. Thus we can explain the difference of 10~20*db* between the received scattered power at noon and midnight.

References

Bailey D.K. et al. (1955) Proc. I.R.E. **43**, 1181.
Batchelor G.K. (1951) Proc. Roy. Soc. A **201**, 405.
Batchelor G.K. (1953) "The Theory of Homogeneous Turbulence" Cambridge University Press.
Booker H.G. (1956) Jour. Geophys. Res. **61**, 673.
Chandrasekhar S. (1951) Proc. Roy. Soc. A **201**, 18.
Tatsumi T. (1957) Proc. Roy. Soc. A **239**, 16.
Villars F. and Weisskopf V.F. (1954) Phys. Rev. **94**, 232.

Chemical Remanent Magnetization of Ferromagnetic Minerals and Its Application to Rock Magnetism

By Kazuo KOBAYASHI

Geophysical Institute, Tokyo University

(Read October 9, 1957, May 17, 1958 and October 26, 1958; Received March 10, 1959)

Abstract

Experimental studies have been carried out on the remanent magnetization generated by chemical reactions (which may properly be called *chemical remanent magnetization* or C.R.M. in abbreviation) for both natural and synthetic specimens. Remanent magnetization generated during two kinds of reaction processes, that is, reduction of α-Fe_2O_3 to Fe_3O_4 and oxidation of Fe_3O_4 to maghemite is firstly examined (Part I). It may be safely concluded that the remanent magnetization thus generated has an intensity which is intermediate between isothermal remanent magnetization and thermo-remanent magnetization, and that its magnetic and thermal stability is similar to that of thermo-remanent magnetization, much higher than that of isothermal remanent magnetization.

In Part II, magnetic properties of several natural rocks and ore deposits containing maghemite are systematically examined. These natural specimens can be classified into two groups with respect to the magnitude of *Qn*-ratio; the one has large magnitude of remanence and large *Qn*-value amounting to 100, while *Qn* of the other is quite small. Greatest parts of natural remanent magnetization of the specimens having large *Qn*-value are attributable to the chemical remanent magnetization of maghemite, which is considered to result from oxidation of magnetite probably by weathering at nearly atmospheric temperature. On the other hand, the natural remanent magnetization of the specimens belonging to the second group with low *Qn* are found to be merely isothermal remanent magnetization. These two groups are also compared with each other from the petrological point of view.

The results of these investigations suggest that various magnitude of remanence can be generated by chemical processes possibly according to the mode of precipitation of ferromagnetic minerals.

Introduction

In recent years, there has been much progress in understanding of magnetic characteristics of rocks and ore deposits as well as in its applications to various geophysical problems. Above all, palaeomagnetic researches based upon the rock magnetism have remarkably been developed by a number of investigators almost all

* Contribution from Division of Geomagnetism and Geoelectricity, Geophysical Institute, Tokyo University. Series II. No. 86.

over the world in recent several years. It is needless to say that, if we want to use the natural remanent magnetization of rocks in palaeomagnetism as a kind of fossil of geomagnetic field at the time of formation of the rocks, we must carefully examine the origin of the remanence and its change induced by some disturbing or modifying factors.

Through the comprehensive studies by many investigators, it is well known that igneous rocks acquire their magnetic polarization during cooling from a temperature above the Curie temperature (T.R.M.) and sedimentary rocks become magnetized during deposition by statistical alignment of detrital ferromagnetic minerals along geomagnetic force. However, we have little knowledge about the origin of remanent magnetization of metamorphic rocks as well as some igneous and sedimentary rocks and ores, which were altered or weathered after their solidification from magma or deposition in lakes, rivers and the sea. Not a small number of examples seem to suggest that there would be some other mechanisms of production or appreciable modification of remanent magnetization in addition to the above-mentioned two processes. Therefore, complete studies of all possible origins of rock magnetism are highly necessary for the purpose of full interpretation of magnetization of rocks *in situ*.

For example, Graham (1956) proposed to take the role of magnetostriction into consideration. Dômen (1958) reported the existence of piezo-remanent magnetization from his high pressure experiments. It seems that the effect of pressure on remanent magnetization is very important in rock magnetism, as suggested by several investigators (Nagata 1943, Kawai 1957).

Another important factor in rock magnetism is chemical change or recrystallization of ferromagnetic constituents during or after the formation of mother rocks. It may be supposed that such chemical processes may generate remanent magnetization under the influence of a magnetic field even at a temperature much below the Curie point, and that they may have some effects upon already existing remanence, if any. Koenigsberger (1938) and Nicholls (1955) pointed out such possibility mainly in sedimentary rocks, and occurrence of this type of remanent magnetization in nature was suggested by Nagata and Watanabe (1950) (cf. Part II of this article) for weathered gabbro in Japan, by Blackett for red sandstones in Great Britain (1956), by Doell for folded blue sandstones in U.S.A. (1956) and Martinez and Howell for chemical sediments in U.S.A. (1956). Since very little is known about the chemical change effect mentioned here, detailed examinations are highly desirable for the more precise understanding of rock magnetism.

In recent years, the writer has engaged in this sort of research by using not only natural specimens but also artificially made samples. Quite independently of the writer, Haigh (1958) reported his experiments and discussion on this topics. Since his experiments are very similar to the writer's experiments described in Part I of this article, his results will be discussed in comparing with the writer's.

In the present case, therefore, two kinds of reactions, that is, reduction of α-Fe_2O_3 to FeO, and oxidation of Fe_3O_4 are used. In the former case, a Fe_2O_3 powder is

Part I.

Experimental Studies of Generation of Remanent Magnetization by Chemical Changes.

1–1. *General Remarks.*

As a first step of an attempt to confirm the existence of chemical remanent magnetization and to make clear the physical mechanism of its formation, laboratory experiments were so planned that the remanent magnetization is generated by chemical changes under the known physico-chemical conditions. In these experiments careful attention was paid to obtain remanent magnetization of purely chemical origin, which does not include thermal influences and other confusing phenomena.

Although it is desirable for chemical reaction to proceed at a temperature as low as possible compared with the Curie point of the specimen in order to avoid an influence of thermo-remanent magnetization, reaction rate is generally very slow at low temperature especially in solid phase. On the other hand, it seems that liquid phase reaction is more suitable for producing ferromagnetic deposition from the viewpoint of reaction rate. It was found, however, in the results of some trial experiments that the identification of reaction products with the aid of *X*-ray analysis is very difficult in this case, and that statistical alignment of magnetized particles under the effect of magnetic field during deposition is inevitable.

In the present case, therefore, two kinds of reactions, that is, reduction of α-Fe_2O_3 to Fe_3O_4 and oxidation of Fe_3O_4 are used. In the former case, α-Fe_2O_3 powder is reduced to Fe_3O_4 in hydrogen gas atmosphere at 340°C or so for about twenty hours and, in the latter, Fe_3O_4 is oxidized to maghemite at 270°C in oxygen gas flow. Non-chemical component of remanent magnetization is subtracted from the total remanence by assuming that chemical remanence and the other kinds of remanence are linearly superposed to each other.

1–2. *Generation of Remanent Magnetization by Change of α-Fe_2O_3 to Fe_3O_4.*

About two grams of α-Fe_2O_3 powder of mean diameter of less than one micron are packed in a porcelain boat and are reduced at 340°C for 20 hours, sometimes at 300°C for 28 hours and 270°C at 170 hours in hydrogen gas flow of about 300cc/hr supplied by Kipp's apparatus, under the influence of a weak magnetic field. In case of experiments by Haigh (ibid.), it is reported that the transformation is completed within 1 hour at about 300°C. This rapid completion of reaction is possibly owing to the higher reduction power of the atmosphere or the finer size of hematite grains which he used.

In the present, X-ray analyses with Norelco X-ray diffractometer were performed before and after the chemical reaction to confirm the completion of reaction. Crystallographic data thus obtained, grain size determined by an Akashi electron-microscope and magnetic constants of α-Fe_2O_3 and Fe_3O_4 are shown in Table I. Grain size of the specimens seems to be unchangeable in spite of the change of chemical composition in this case.

The mode of growth of magnetization of the specimen during the chemical reaction

Table I. Magnetic and Crystallographic Properties of Ferromagnetic Minerals used in This Experiment.

Material	Crystal Parameters	Coercive Force H_c (oersted)	Ir for 700 Oe $\left(\frac{\text{emu}}{\text{gr}}\right)$	Grain Size
α-Fe_2O_3	$a_{rh}=5.433$Å $\alpha=55°14'$	>2000 Oe	0.13	0.1μ~0.6μ
Fe_3O_4	$a=8.400$Å	218 Oe	35.5	0.1μ~0.6μ

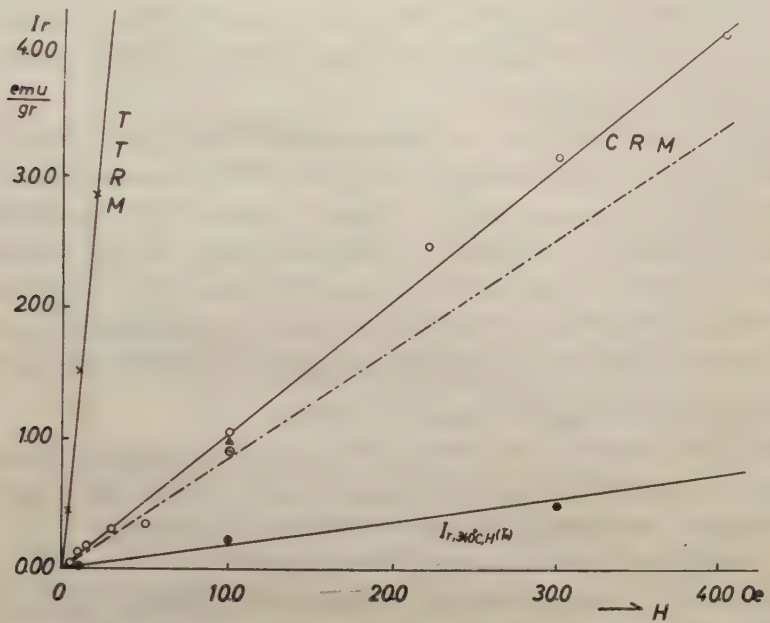

Fig. 1. Intensity of various kinds of remanent magnetization of Fe_3O_4 as dependent on applied magnetic field.

—○— $I_{cr,340°C,H}(T_0)$
C.R.M. (Chemical remanent magnetization) generated at 340°C

△ $I_{cr,300°C,H}(T_0)$, C.R.M. generated at 300°C

◉ $I_{cr,270°C,H}(T_0)$, C.R.M. generated at 270°C

·····• $I'_{cr,340°C,H}(T_0)$, $=I_{cr,340°C,H}(T_0)-I_{r,340°C,H}(T_0)$
Real chemical remanent magnetization

—×— $I^{T_0}_{T_c,H}(T_0)$ Total thermo-remanent magnetization

—●— $I_{r,340°C,H}(T_0)$

process could not be followed in the present experiments. The remanent magnetization, being denoted by $I_{cr,T,H}(T_0)$, could only be measured by an astatic magnetometer at room temperature after the suppression of the magnetic field and cooling in field-free space. Fig. 1 indicated the field dependence of chemical remanent magnetization thus generated, which is linear up to 40 Oe.

Haigh (ibid.) followed the variation of magnetization during the change, but the growing process of chemical remanent magnetization could not be detected distinctly, as being covered by the increase of quantity of Fe_3O_4. The detailed investigations of this growth, however, seem to be important for the discussion of the mechanism of generation of chemical remanent magnetization.

After these measurements, this synthetic Fe_3O_4 powder, sealed in a quartz tube evacuated to 10^{-3} mm Hg in order to prevent oxidation, was kept at 340°C for 20 hours in magnetic field of intensity H, and then cooled to the room temperature in field-free space. Remanent Magnetization thus generated, denoted by $I_{r,340°C,H}(T_0)$, is also shown in Fig. 1, together with total thermo-remanent magnetization $I_{T_c,H}^{T_0}(T_0)$ of the same specimen, where T_c denotes the Curie temperature. Strictly speaking, $I'_{cr,T,H}(T_0) = I_{cr,T,H}(T_0) - I_{r,T,H}(T_0)$ must be used as a real chemical remanent magnetization, as being shown in the figure by a chain line, since $I_{r,T,H}(T_0)$ is the same order of magnitude as $I_{cr,T,H}(T_0)$. As for the thermo-remanent magnetization $I_{T_c,H}^{T_0}(T_0)$, $I_{r,T_c,H}(T_0)$ is ignored, because $I_{r,T_c,H}(T_0) \ll I_{T_c,H}^{T_0}(T_0)$.

As shown by a triangle and a double circle in Fig. 1, the intensity of chemical remanent magnetization generated at 300°C and 270°C, $I_{cr,300°C,100Oe}(T_0)$, $I_{cr,270°C,100Oe}(T_0)$ is nearly the same as $I_{cr,340°C,100Oe}(T_0)$. It may be expected that the difference of these remanence becomes much smaller by using the values of real chemical remanent magnetization, because $I_{r,340°C,H}(T_0) > I_{r,300°C,H}(T_0) > I_{r,270°C,H}(T_0)$. This fact seems to indicate that the intensity of real chemical remanent magnetization is only dependent on the chracter of the reaction, but not on temperature in which the reaction proceeds.

1–3. ***Thermo-chemical examination of the process.***

As the heat of reaction from Fe to α-Fe_2O_3, Fe to Fe_3O_4 and H_2 to H_2O *aq.* is 1740, 1580 and 34150 cal/gr respectively, the chemical change concerned here is exso-thermic reaction, the thermo-chemical equation being expressed by

$$Fe_2O_3 + H_2 = Fe_3O_4 + H_2O\ aq. + 2.440\ \text{Cal.}$$

Therefore, even if the heat of reaction remains in the specimen and can not so much transmitted to a porcelain boat (in fact, it will be not the case), temperature of the specimen would increase by only about 100°C at most, and would not cause noticeable influence.

In this experiment the temperature of specimen was measured with a thermo-junction which was covered with a thin quartz tube and was set almost in contact with the upper side of the specimen. It can not be considered to happen that the specimen would be so locally heated that the junction could not detect such local irregularities in temperature distribution, because thermal convection and conduction would be induced in the furnace.

1–4. ***Magnetic and Thermal Stability***

Fig. 2 shows the behavior of various kinds of remanent magnetization in the demagnetization process by alternating magnetic field of $f=50$ c/s, 0~500 Oe, where ordinate gives the normalized intensity, i.e. $I'_{cr,340°C,100Oe}(H)/I'_{cr,340°C,100Oe}(H=0)$ etc. Although demagnetization curve of chemical remanent magnetization is shown in the figure only for $I'_{cr,340°C,100Oe}(T_0)$, it was shown from the same kinds of experiments that chemical remanent magnetization generated at 270°C~340°C in applied magnetic field of 0.5~10 Oe gives nearly the same demagnetization curve. It is remarkable in the figure that stability of chemical remanent magnetization against demagnetization by

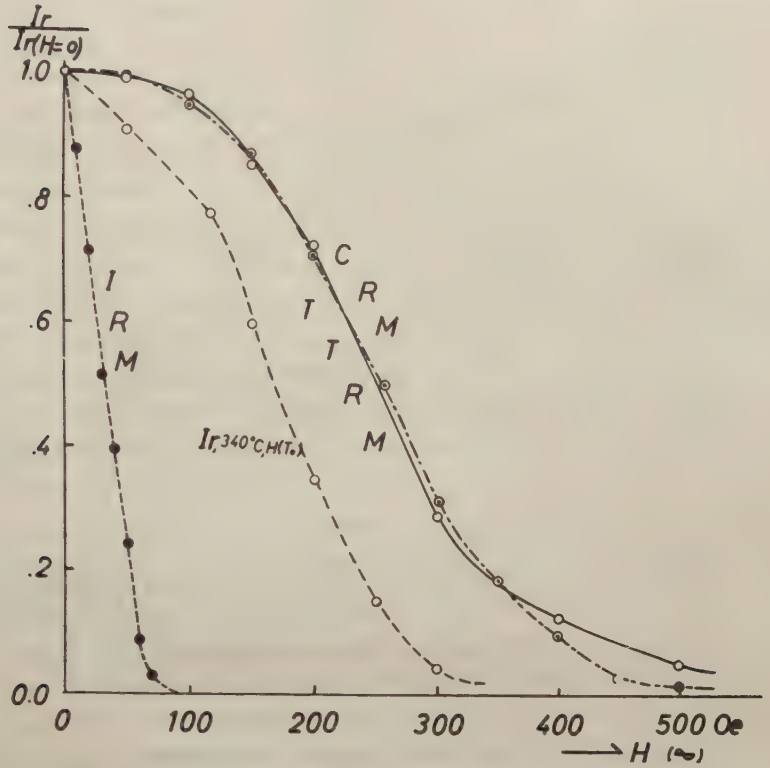

Fig. 2. Demagnetization curves of remanent magnetization of Fe_3O_4 by alternating magnetic field.
—○— $I'_{cr,340°C,H}(T_0)$, Real chemical remanent magnetization
--◉-- $I^{T_0}_{T_c,0.5Oe}(T_0)$, Total thermo-remanent magetization
···●··· $I_{r,20°C,30Oe}(T_0)$ Isothermal remanent magnetization
····○···· $I_{r,340°C,10Oe}(T_0)$

alternating magnetic field is quite similar to thermo-remanent magnetization $I^{T_0}_{T_c,0.5Oe}(T_0)$ and is much higher than isothermal remanent magnetization $I_{r,20°C,300e}(T_0)$ and $I_{r,340°C,100e}(T_0)$.

In Fig. 3 thermal demagnetization curve of chemical remanent magnetization $I'_{cr,340°C,30e}(T_0)$ is shown together with that of total thermo-remanent magnetization $I^{T_0}_{T_c,30e}(T_0)$, isothermal remanent magnetization $I_{r,20°C,2000e}(T_0)$ and $I_{r,340°C,200e}(T_0)$. Remanence $I_{r,340°C,H}(T)$ has TRM character below the heat treatment temperature 340°C and has IRM nature between 340°C and the Curie point. This may be understood by considering the physical meaning of $I_{r,340°C,H}(T_0)$; the specimen is magnetized isothermally at temperature 340°C in the same manner as generation of the ordinary isothermal remanent magnetization and then is frozen by cooling to room temperature in field-free space. It is also confirmed from the figure that chemical remanent magnetization is extremely stable compared with isothermal remanent magnetization and changes with temperature in almost the same manner as thermo-remanent magnetization.

In recent years systematic studies of stability of thermo-remanent magnetization,

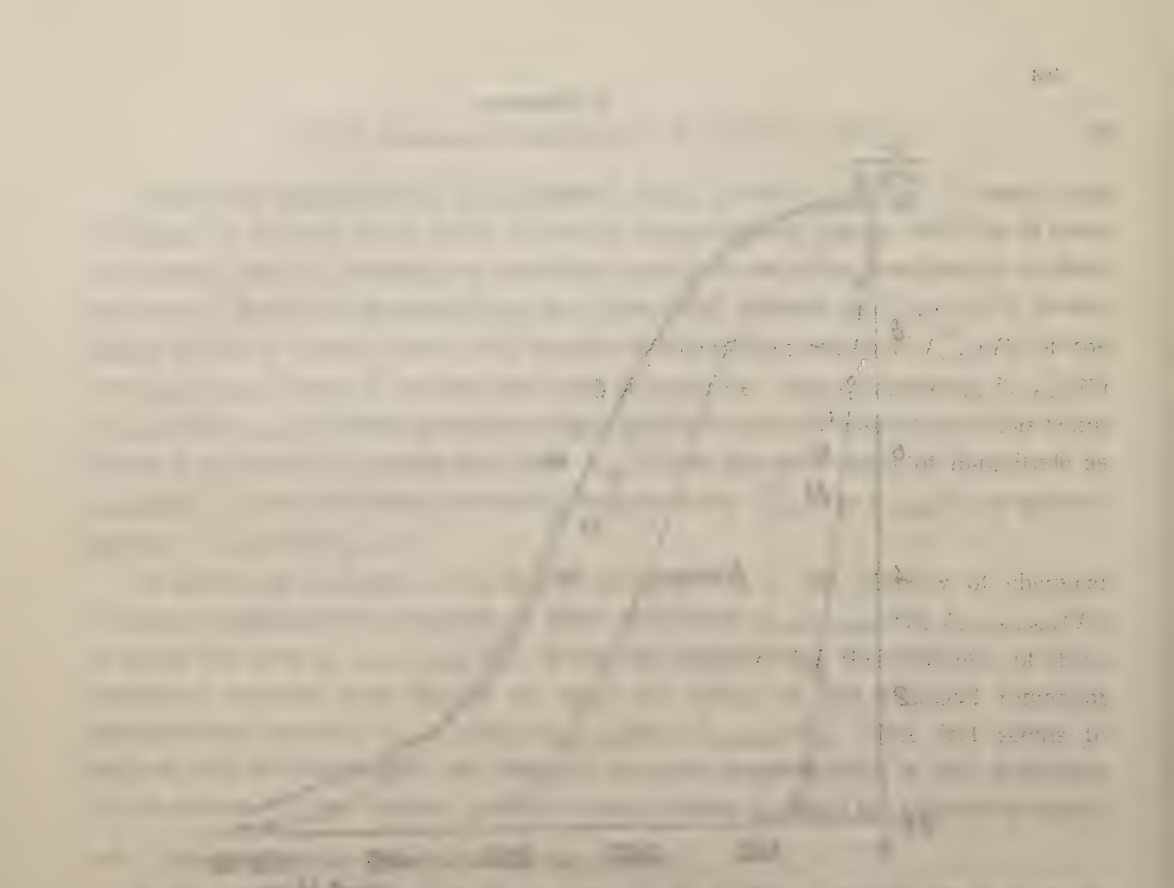

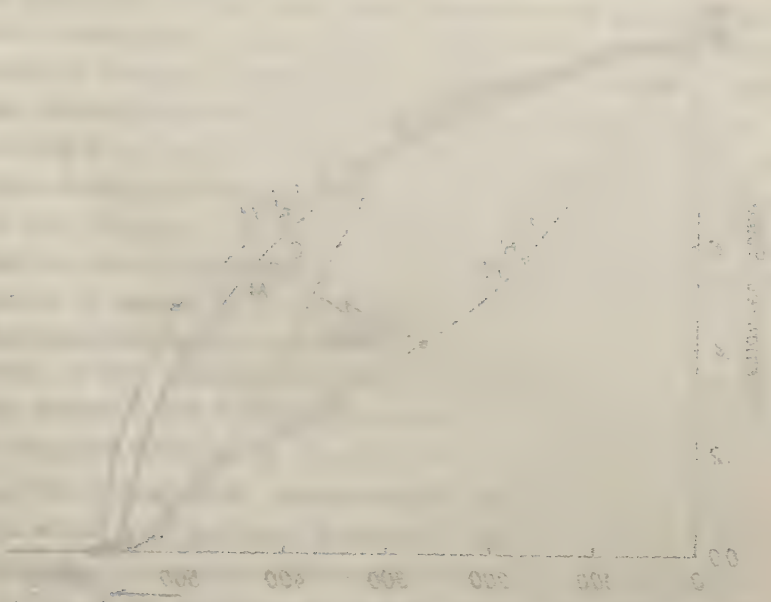

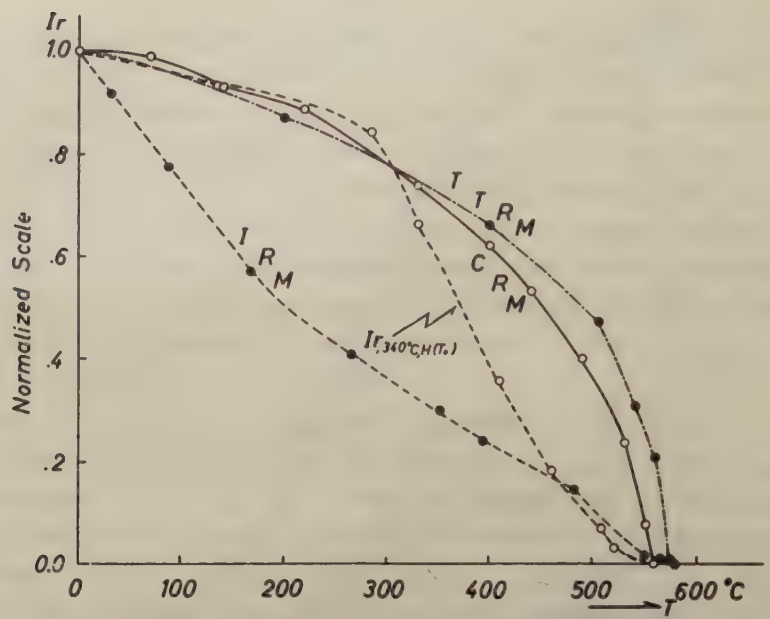

Fig. 3. Thermal variation of remanent magnetization of Fe_3O_4
—○— $I'_{cr,340°C,3Oe}(T_0)$, Real chemical remanent magnetization
···◉— $I^{T_0}_{T_c,3Oe}(T_0)$, Total thermo-remanent magnetization
···●··· $I_{r,20°C,200Oe}(T_0)$, Isothermal remanent magnetization
···○··· $I_{r,340°C,20Oe}(T_0)$,

isothermol remanent magnetization and ideal or anhysteretic magnetization was reported by Thellier and Rimbert (1954, 1955), Rimbert (1956 a, b, 1958), Petrova (1957) and Petrova and Pospelova (1957). It was shown in their investigation that isothermal remanent magnetization becomes more stable according as the magnitude of I_r increases, while stability of thermo-remanent magnetization becomes a little lower or remains almost constant according to the increase of I_r, and that thermo-remanent magnetization is much more stable than isothermal remanent magnetization for small magnitude of I_r far from saturation one. Comparison of stability of various kinds of remanence against heating was examined with similar results by Petrova (ibid.) and Petrova and Pospelova (ibid.).

Since such difference of stability is considered to depend essentially on the mechanism of generation of the remanence, as suggested by the above authors, it may be concluded in the present experiments that chemical remanent magnetization is generated through the mechanism which resembles that of thermo-remanent magnetization.

1-5. *Oxidation of Fe_3O_4 and Chemical Remanent Magnetization*

Synthetic Fe_3O_4, being packed in a porcelain or quartz boat, is heated at about 270°C in space of about 10^{-2}mm Hg in air pressure and then oxygen gas is poured into the furnace, being kept at the temperature within fluctuation of about 20°C in a magnetic field. Chemical reaction seems to be completed within several minutes in this case. X-ray analyses for the oxidation products were carried out with Norelco X-ray diffractometer. It is shown from the examinations that nearly 10 percent of

α-Fe_2O_3 is generally contained in the oxidation products. The lattice constant of ferrimagnetic component having cubic spinel structure in the specimens is altered to $a=8.34\sim8.35$Å, corresponding to that of solid solution between Fe_3O_4 and γ-Fe_2O_3.

Intensity of remanent magnetization is measured by means of ballistic method, increasing proportionally with the applied magnetic field up to 40 Oe. The gradient $I_{cr,270°C,H}(T_0)/H$ is calculated to be about 0.18 per unit mass of total products, being nearly twice as the magnitude of $I_{cr,340°C,H}(T_0)/H=0.10$ for chemical remanent magnetization by the reduction from α-Fe_2O_3 to Fe_3O_4. Intensity of total thermo-remanent magnetization can not be determined in the present case, because it is inevitable that large quantity of maghemite in the specimen is oxidized further and inverts to α-Fe_2O_3 at the neighbourhood of the Curie point.

Stability of the chemical remanent magnetization against demagnetization by alternating magnetic field is examined in the same manner as mentioned in section 1–4, and compared with that of $I^{T}_{T_c,100e}(T_0)$ and $I_{r,270°C,300Oe}(T_0)$ of the specimen (Fig. 4). For $I^{T}_{T_c,100e}(T_0)$ of maghemite, thermo-remanent magnetization of remaining parts of maghemite which were free from inversion is used, the dispersion effect by α–Fe_2O_3 being neglected in the process of demagnetization. General tendency that the demagnetization curves of the specimen are a little steeper than those of the specimen in Fig. 2 seems to be due to the smaller magnitude of coercive force ($H_c=90$ Oe) of this maghemite. (cf. Table 1, $H_c=218$ Oe for synthetic Fe_3O_4). It may be also concluded, therefore, that chemical remanent magnetization generated by change from Fe_3O_4 to maghemite is really stable one.

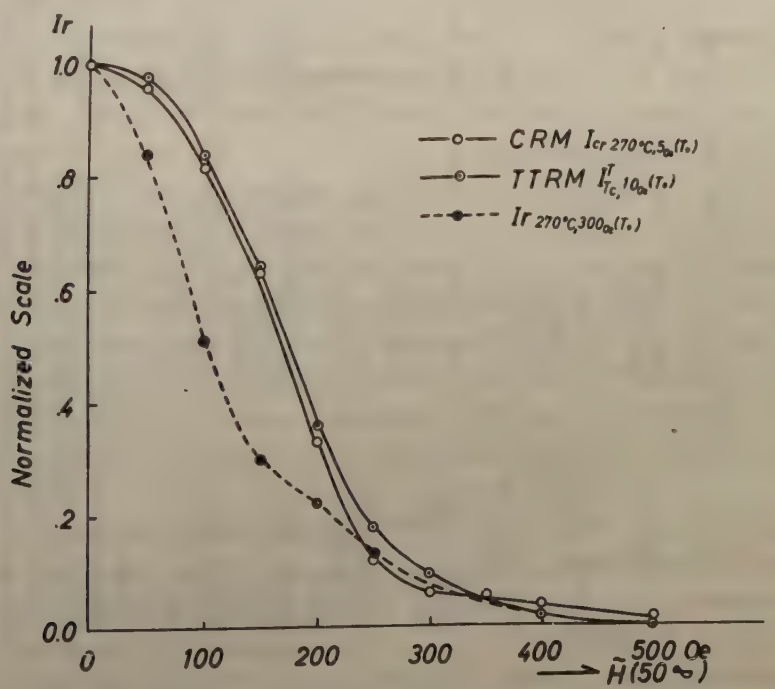

Fig. 4. Demagnetization curves of remanent magnetization of synthetic maghemite by alternating magnetic field.

Table II. Magnetic and Crystallographic Properties of Maghemite-containing Specimens.

Specimens. No.	Locality	Petrological Description	$In\left(\frac{\text{emu}}{\text{gr}}\right)$ (NRM)	$\chi_0\left(\frac{\text{emu}}{\text{gr}}\right)$	Qn	s*1) (%)	Qn^{Mh}	Q_T	Lattice Paramater (Å)	Curie Point of Mt, T_c(°C)	Inversion Point of Mh (°C)*4)
1.	Manget Cove Arkansas, U.S.A.	Iron Ore Deposit (Lodestone)	2.53	6.23×10^{-2}	93.7	22	400		$a_1=8.389$	585	260
2.	Kamaishi, Iwate Pref., Japan	Gabbro (magnetic)	0.055	2.94×10^{-3}	38.7	13	280	2.3	$a_1=8.398$	570	240
3.	Taishi Mine Hiroshima Pref., Japan	Skarn Type Iron Ore Deposit (Lodestone)	0.58	3.27×10^{-2}	39.5	6	360	6.1	$a_1=8.402$	580	$\sim T_c$
4.	Kurosawa Mine Yamagata Pref. Japan	Quartz Porphyrite	1.09×10^{-4}	6.85×10^{-4}	0.354	40*2)			$a_1=8.386$ $a_2=8.353$	540	320
5.	Kumano Mine (I) Yamaguchi Pref. Japan	Skarn Type Iron Ore Deposit	0.97	2.18×10^{-2}	98.9	34	270		$\tilde{a}=8.361$*3)	585	340
6.	Kumano Mine (II) Yamaguchi Pref. Japan	Skarn Type Iron Ore Deposit	0.63×10^{-2}	2.18×10^{-2}	0.648	42			$a_1=8.389$ $a_2=8.352$	590	360

Remarks;

*1) s denotes the weight percentage of maghemite to total ferromagnetic minerals determined from thermo-maginetic analysis.

*2) This value is determined from X-ray analysis.

*3) $\tilde{a}$ denotes the mean value of a determined from the broad peaks in diffraction chart.

*4) Inversion point of maghemite is determined as a point where the inversion is almost finished from thermo-magnetic curves.

With respect to the meaning of Qn, Qn^{Mh} and Q_T, see p. 108, p. 115, and p. 111 respectively.

Part II.

Natural Remanent Magnetization of Some Rocks and Ore Deposits as Typical Examples of Chemical Remanent Magnetization.

2-1. *Natural Occurrences of Maghemite and Its Remanent Magnetization.*

Possibility of causation of chemical remanent magnetization in case of weathered gabbro has been suggested by Nagata (1953) with some reasonable evidences that their remanent magnetization is mostly due to chemical process. This is the only case in which practical evidences were shown, though many authors have pointed out possibility of production of chemical remanence in sedimentary rocks.

In order to examine such a case in more detail, the specimens shown in table II were collected with the aid of H. Imai of Department of Mining Engineering, Tokyo University (No. 1, 2, 3), T. Saitô of Geological Survey of Japan (No. 4) and G. Shibuya of Yamaguchi University (No. 5,6). Specific intensity of natural remanent magnetization In, Initial susceptibility χ_0 and the value of Qn of these specimens are listed in this table, where Qn denotes the ratio of In to the intensity of induced magnetization by earth's magnetic field F_0 (F_0 is about 0.45 Oe in Japan), *i.e.*

$$Qn=\frac{In}{\chi_0 F_0}=\frac{In}{0.45\chi_0}.$$

It is the most interesting character that these specimens can be distinctly classified into two groups according to their magnitudes of Qn, in spite of the variety in their intensity of remanence. The magnitude of Qn of the one group (No. 1,2,3,5) is nearly 100. This value is remarkably large, considering that Qn amounts to 2~10 in general eruptive rocks except in some basaltic eruptive rocks and that it takes the smaller value in ordinary ores and other types of rocks. On the other hand, the magnitude of Qn of the other group (No. 4,6) is in order of magnitude of 10^{-1}, being nearly one thousandth of that of the first group.

Plate 1~6 show photo-micrographs of the polished surfaces of these specimens. In each photograph, magnetite and maghemite can be clearly identified. Under reflection microscope maghemite appears white to grey-blue with oil immersion lens like hematite and also may show red internal reflection. Maghemite has generally higher reflectivity than magnetite and lower than hematite. Its polish hardness is less than hematite (Newhouse and Glass, 1936). Maghemite belongs to cubic spinel system and, therefore, can be easily distinguished from hematite under polarized light (Nicholls, ibid.).

It is quite remarkable that the occurrence of maghemite in two groups differs greatly from each other. In the specimens having large magnitude of Qn, fine veinlets of maghemite irregularly penetrating into magnetite are always observed, while maghemite occurs as regional transition from a part of magnetite in the specimens of low Qn. The size of the former is 0.1μ to 5μ, and that of the latter sometimes amounts to 80μ, as is clearly shown in the plates.

Occurrences of maghemite in natural rocks and ore deposits have been reported

as Typical Examples of Chemical Remanent Magnetization

2-1. Natural Occurrence of Chemically Deposited Magnetite

Possibility of formation of magnetite by chemical reaction has been suggested by Nagata (1953) with some rock samples. Chemical remanent magnetization is mostly due to chemical process. This is the only case in which practical evidences were shown, though many authors have pointed out possibility of production of chemical remanence in sedimentary rocks.

In order to examine such a case in more detail, the specimens as shown in table II were collected with the aid of H. Imai of Department of Mining Engineering, Tokyo University (No. 1, 2, 3), T. Saito of Geological Survey of Japan (No. 4) and G. Shibuya of Yamaguchi University (No. 5,6). Specific intensity of natural remanent magnetization I_n, initial susceptibility χ_0 and the value of Q_n of these specimens are

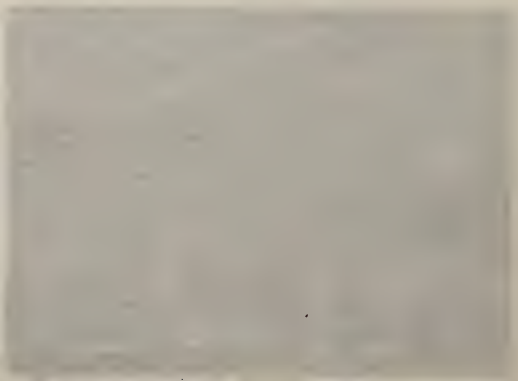

Plate. Photo-micrographs of polished surfaces of maghemite-containing specimens (*cf.* Table II) white ; maghemite, grey ; magnetite, dark ; limonite

Plate 1. Specimen No. 1, Lodestone, Magnet Cove, under oil immersion. ×2200

Plate 2. Specimen No. 2, Gabbro, Kamaishi, under oil immersion. *Il* ; ilmenite. ×1800

Plate 3. Specimen No. 3, Skarn Type Iron Ore Deposit, Taishi Mine, under oil immersion. ×1600

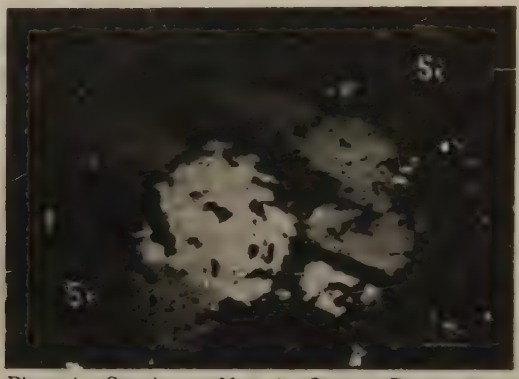

Plate 4. Specimen No. 4, Quartz Porphyrite, Kurosawa. *Si* ; silicate minerals. ×140

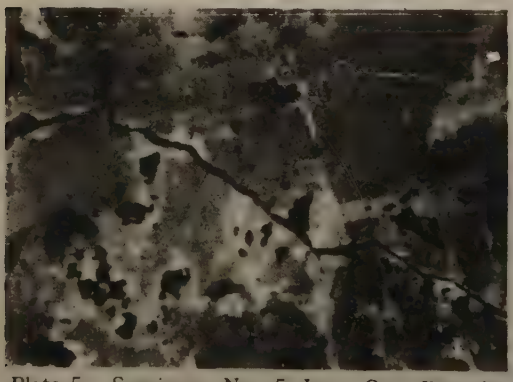

Plate 5. Specimen No. 5, Iron Ore Deposit, Kumano Mine (I), under oil immersion. ×1400

Plate 6. Specimen No. 6, Iron Ore Deposit, Kumano Mine (II), under oil immersion, brightest ; hematite. ×1250

by some authors in several localities in the world. The veinlets of maghemite closely related to the strong magnetization were found by Newhouse and Glass (ibid.) and Imai (1951).

Imai pointed out that such veinlets of maghemite are found at the surface of the

outcrops of deposits and rocks containing magnetite. The intensity of natural remanent magnetization of such specimens is not uniform and generally differs from place to place

Fig. 5. Thermal variation of natural remanent magnetization and thermo-remanent magnetization formed after geomagnetic field cooling of maghemite-containing specimens. Rate of heating≒200°C/hr. Heated in air.

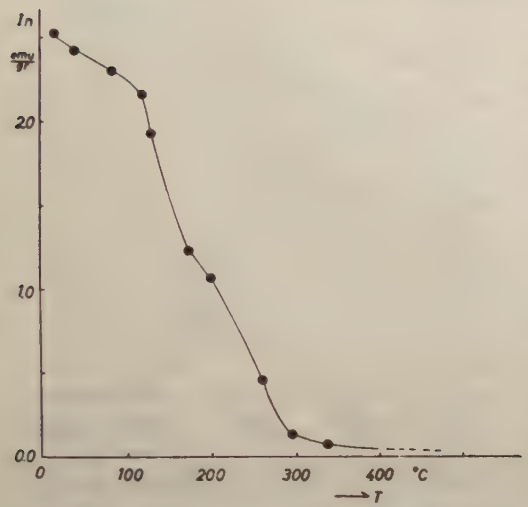

Fig. 5, (1). Specimen No. 1, Magnet Cove.

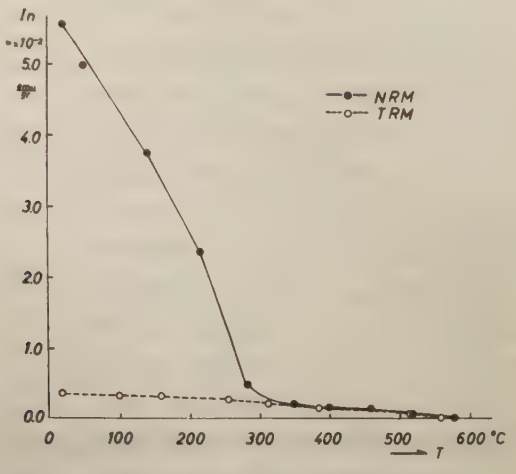

Fig. 5, (2). Specimen No. 2, Kamaishi,

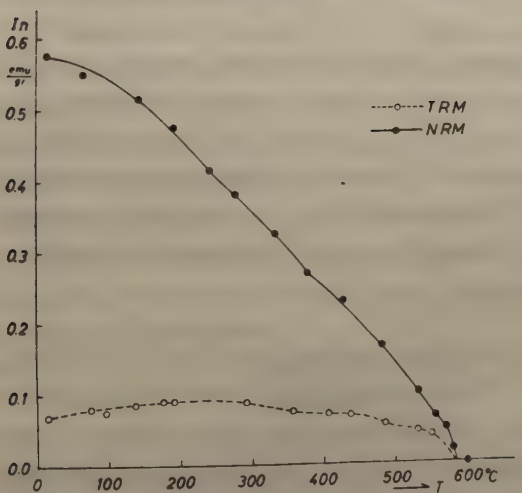

Fig. 5, (3.) Specimen No. 3, Taishi Mine,

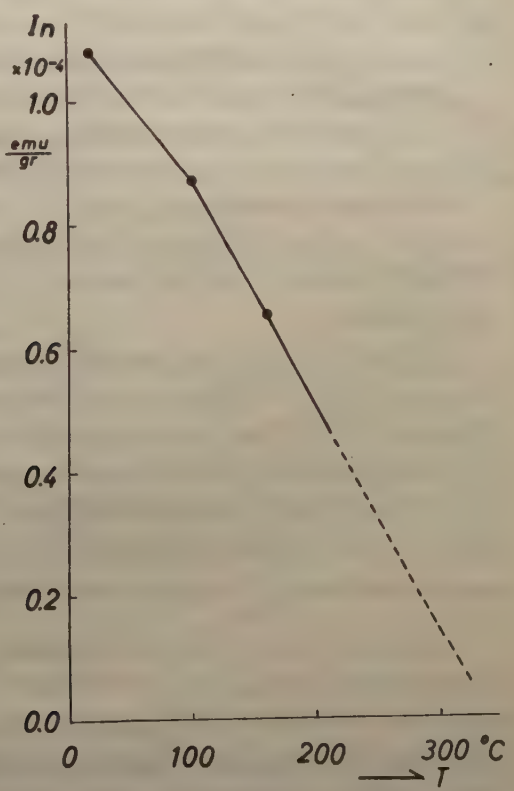

Fig. 5, (4). Specimen No. 4, Kurosawa,

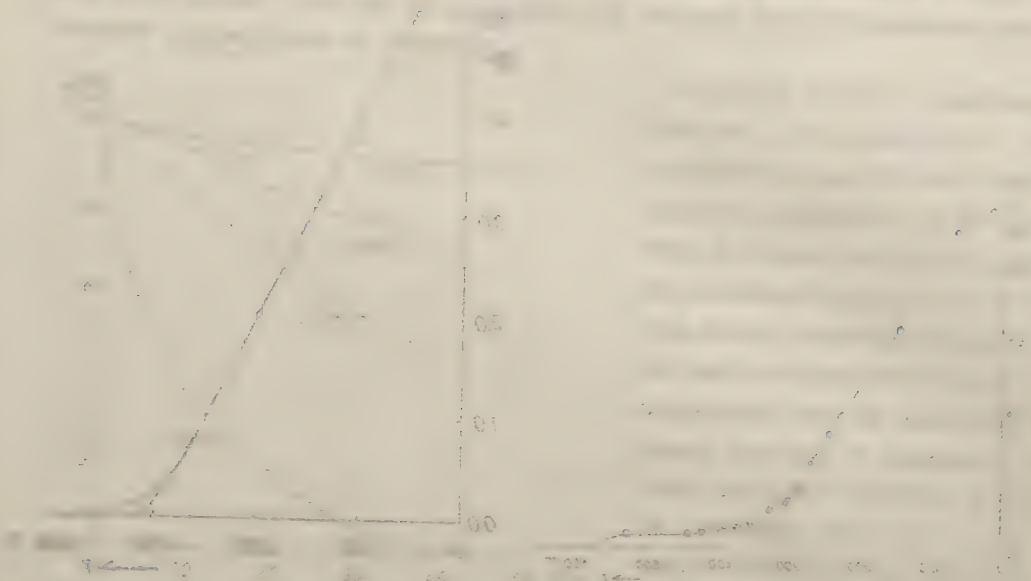

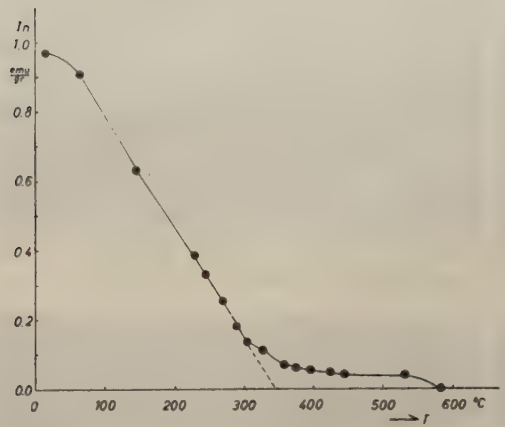

Fig. 5, (5). Specimen No. 5, Kumano Mine (1),

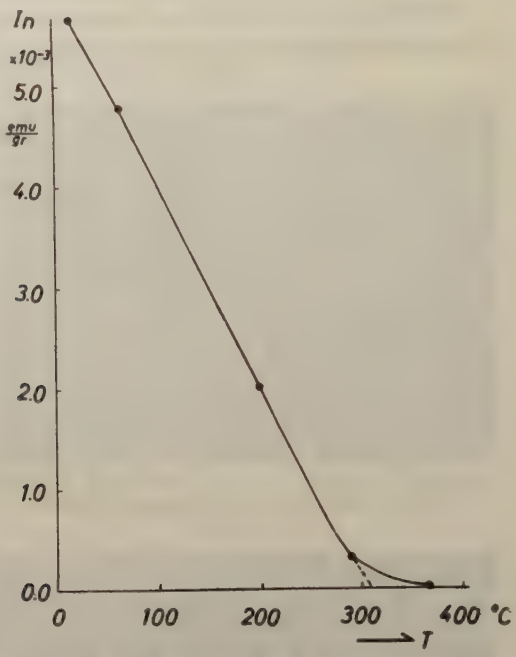

Fig. 5, (6). Specimen No. 6, Kumano Mine (2),

even in one hand-block, as Nagata classified the gabbro at Kamaishi (No. 2 in table II) into the magnetic gabbro and ordinary one. This non-uniformity was also considered to be due to heterogeneous distribution of this type of maghemite.

Maghemite ore occurring at Kumano Mine in Western Japan was studied by Shibuya (1958). He suggested that the specimens having intense remanence occurs chiefly in the outer layer of the ore mass or along faulting plane. These facts seem to show that maghemite belonging to group I is formed by weathering, while the oxidation of minerals in group II is due to the influence of hydrothermal solution. At least, it may be surely concluded that the process of generation of maghemite of two groups is much different.

The situation that the maghemite component has an important bearing upon the natural remanent magnetization of the specimens is directly shown by the thermal decay curves of In and I_{Tc} of each specimens (Fig. 5, (1)(2)(3)(4)(5)(6)), where I_{Tc} indicates intensity of thermo-remanent magnetization formed after geomagnetic field cooling from the temperature of nearly 700°C. The magnitude of I_{Tc} is very small compared with that of In nearly at the atmospheric temperature, as also shown in Table II in the term of $Q_T=\frac{I_{Tc}}{\chi_0 F_0}$.

As shown in the figures, the natural remanent magnetization of the specimens decreases abruptly to a very small value at various temperatures generally much below the Curie temperature of magnetite. It is remarkable in the decay curves of the specimen No. 2 that $In(T)$ is quite coincident with $I_{Tc}(T)$ at temperatures higher than about 300°C notwithstanding $In(T_0) \gg I_{Tc}(T_0)$. Since it is well-known that maghemite

is metastable and, on heating, it inverts monotropically to α-Fe_2O_3 at a temperature, variously quoted from 200 to 700°C (Nicholls, ibid.), it would be naturally deduced that most parts of $In(T_0)$ are due to maghemite and the small remaining parts are thermo-remanent magnetization of magnetite.

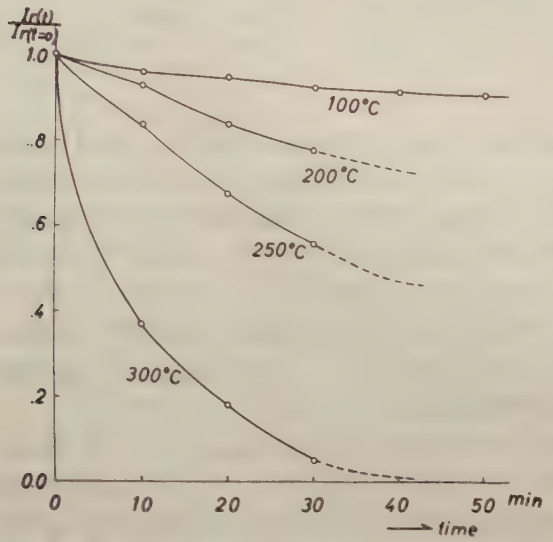

Fig. 6. Time decrease of natural remanent magnetization of specimen No. 2 at various temperature, showing the rate of inversion of maghemite contained. (after Akimoto and Suzuoki)

According to Akimoto and Suzuoki (Personal Communication), who examined the time decrease of natural remanent magnetization of No. 2 specimen at various temperatures, rate of the inversion of maghemite is so rapid (Fig. 6) that it would be impossible to heat such specimens above their Curie temperature without destroying the crystal structure of maghemite contained in them. Therefore, it would be concluded that most parts of natural remanent magnetization of these specimens are not the thermo-remanent magnetization.

These circumstances seem to show that natural remanent magnetization of veinlets of maghemite contained in the specimens with high Qn-value is due to chemical remanent magnetization generated at nearly atmospheric temperature. It seems likely, on the other hand, that the isothermal remanent magnetization plays an important role in the specimens of group II distinguished by the feeble and unstable remanence and low Qn-value.

2–2. *Interpretation of the results of microscopic, crystallographic, chemical and thermo-magnetic analyses.*

a). Volumetric investigation of maghemite

From the microscopic observation of polished surface, we may estimate the content of maghemite relative to other minerals contained in the specimen. A photo-micrograph of polished surface of the specimen No. 1, Lodestone of Magnet Cove, in which the distribution of maghemite is rather homogeneous, was divided by fine meshes into 153 $\times$108 squares so as to make each square correspond to any one of the three kinds of minerals, i.e. magnetite, maghemite and limonite. The relative content of each mineral was determined by counting the numbers of corresponding squares, the results being summarized as follows.

magnetite	50.7 %
maghemite	12.1 %
limonite	37.2 %

The maghemite percentage to the total ferromagnetic constituents (magnetite and maghemite in this case) is, therefore, calculated to be 19.3 %.

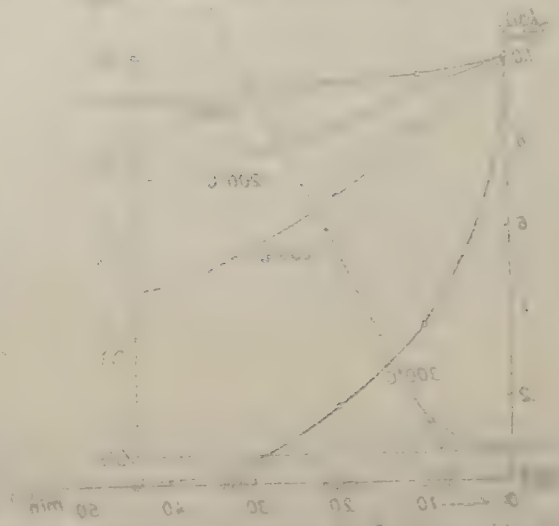

Table III. Chemical Composition of Ferromagnetic Minerals in Maghemite-containing Specimens.

Specimen No.		in weight %				in mol. %		
		$Fe_2O+FeO+TiO_2$	Fe_2O_3	FeO	TiO_2	Fe_2O_3	FeO	TiO_2
1.	Magnet Cove	97.93	73.47	24.46	trace	57.48	42.52	0.0
4.	Kurosawa Mine	86.39	62.34	14.78	9.27	54.82	28.89	16.29

b). Chemical Analysis

As to the specimens No. 1 (Magnet Cove) and No. 4 (Kurosawa), chemical analysis was carried out by T. Katsura of Tokyo Institute of Technology on the ferromagnetic constituents separated from the original ores and rocks. Limonite which occasionally contaminatesthe ferromagnetic constituents was washed out in dilute HCl solution before chemical analysis. The results are given in Table III. A relative content of maghemite in Magnet Cove specimen (No. 1) can be determined from the chemical analysis to be 19.53%, if the stoichiometric composition was assumed for magnetite (Fe_3O_4) and maghemite (γ-Fe_2O_3) in the specimen.

An average chemical composition of the specimen of Kurosawa (No. 4) is situated in the Fe_3O_4-Fe_2O_3-$FeTiO_3$ compositional field on the FeO-Fe_2O_3-TiO_2 ternary system. Since co-existence of the maghemite and magnetite in the specimen was found from the microscopic observation (Plate 4), the maghemite phase (strictly speaking titanomaghemite) in the specimen is expected to possess the chemical composition more close to the $FeTiO_3$-Fe_2O_3 join on the ternary system. It must be noted here, however, that the accurate chemical composition of both the titanomaghemite and the original titanomagnetite can not be determined until the precise knowledge on the crystallographic and magnetic properties of the specimen is obtained.

c). X-ray analysis

The lattice parameters of all the specimens were determined by means of the Norelco X-ray diffractometer. The results are also summarized in Table II. The diffraction charts of the specimens of group I except No. 5 (Kumano) do not show the peaks peculiar to maghemite but merely show the peaks corresponding to ordinary magnetite. This seems to be due to the bad crystallization of maghemite contained in the specimens. As to the specimens from Kumano mine (No. 5, 6), the co-existence of the maghemite with various degree of oxidation was inferred from the broad peaks in the diffraction chart. Shibuya (ibid.) reported the specimens with a unit cell dimension ranging from 8.344±0.003Å to 8.386±0.001Å. A pair of lattice parameters (a_1=8.386Å and a_2=8.353Å) was obtained in the present examination from the diffraction chart of the Kurosawa specimen belonging to the group II. The relative content of the a_2-component to a_1-component in the specimen was also estimated to be about 0.65 from the careful examination of the intensity of the diffraction peak.

d). Thermo-magnetic analysis

Fig. 7 ((1), (2), (3), (4), (5), (6)) shows the thermo-magnetic curves of the specimens measured in vacuum by means of a thermo-magnetic balance (Akimoto, 1954). Each curve shows a distinct irreversible change of magnetization corresponding to

Fig. 7. Thermo-magnetic curves of maghemite-containing specimens.
Heating rate≒200° C/hr

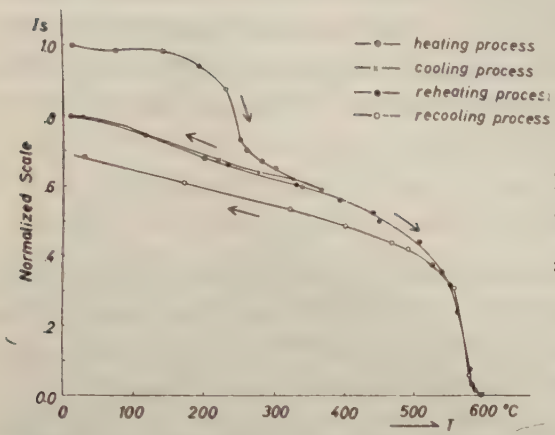

Fig. 7. (1). Specimen No. 1, Magnet Cove, $H=2200$ Oe, in vac. of 10^{-3}mm Hg

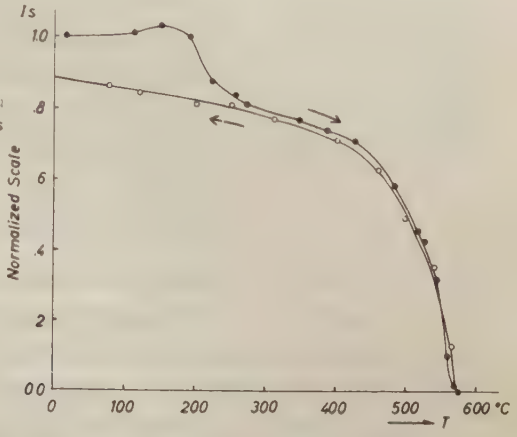

Fig. 7, (2). Specimen No. 2, Kamaishi, $H=2100$ Oe, in vac. of 10^{-3}mm Hg

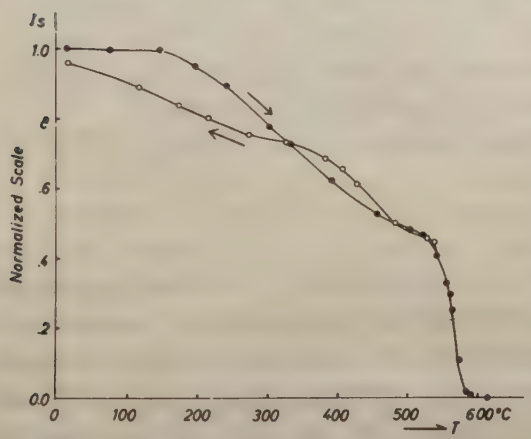

Fig. 7, (3). Specimen No. 3, Taishi, $H=1700$ Oe, in vac. of 10^{-3}mm Hg

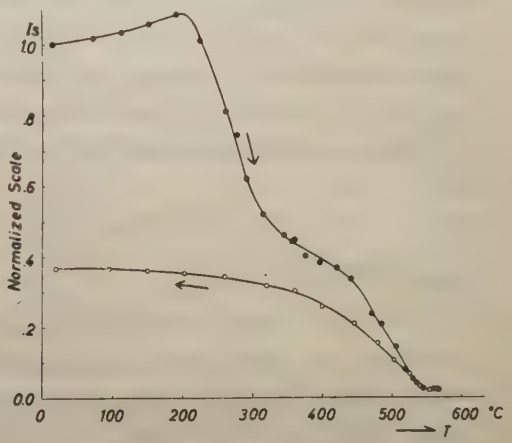

Fig. 7, (4). Specimen No. 4, Kurosawa, $H=1000$ Oe, in air (After Saitô)

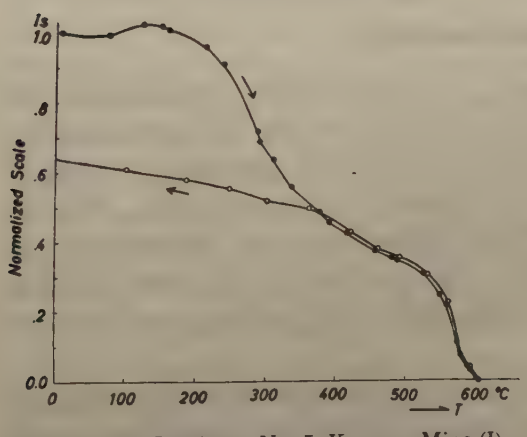

Fig. 7, (5). Specimen No. 5, Kumano Mine (I), $H=1900$ Oe, in vac. of 10^{-3}mm Hg

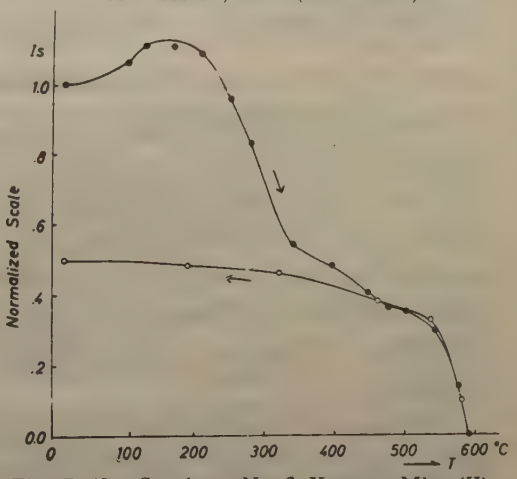

Fig. 7, (6). Specimen No. 6, Kumano Mine (II), $H=1200$ Oe, in vac. of 10^{-3}mm Hg

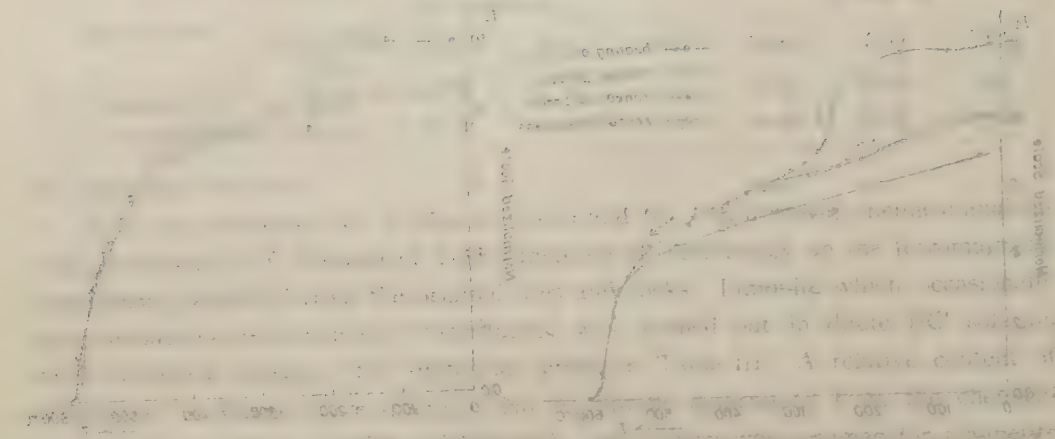

$$\chi''(T_0) = \frac{\left(\frac{C}{T}\right)^{\alpha}}{\chi'^{\alpha}(T_0)\cdot T_0^{\alpha}}$$

$\chi'^{\alpha}(T_0)$ is replaced by $s\cdot\chi(T_0)$ in the present case. The maximum of this

the inversion of maghemite. Inversion temperature of maghemite, also listed in Table II, is read from Fig. 7 as a point where the inversion is almost finished. Provided that the influence of oxidation or reduction of the minerals during the thermo-magnetic measurement is negligible, an irreversible part of the thermo-magnetic curve, $I_s^{irr}(T_0)$ can be regarded as a magnetization of maghemite phase. When the applied field is sufficiently strong to saturate the specimen, we may write

$$\frac{I_s^{irr}(T_0)}{I_s^{rev}(T_0)} = \frac{s \cdot \sigma_s^{Mh}}{(1-s)\sigma_s^{Mt}}$$

where s denotes the weight percentage of maghemite to total magnetic minerals, and σ_s^{Mt} and σ_s^{Mh} are the saturation magnetization of magnetite and maghemite at the room temperature, being given numerically as 92 e.m.u/gr. and 83.5 e.m.u/gr. respectively. The maghemite percentage s calculated from this formula is listed in Table II.

There will be seen that the maghemite content of the Magnet Cove specimen determined independently from three kinds of measurements, i.e. volumetry, chemical analysis, thermo-magnetic curve, agrees well with one another. From this evidence we may conclude that the veinlets observed in the Magnet Cove specimen should be described as γ-Fe_2O_3. This may also indicate that the thermo-magnetic analysis generally give a useful information on the constitution of ferromagnetic minerals.

By using the s-values we may calculate Qn^{Mh}-ratio relating to maghemite alone:

$$Qn^{Mh} = \frac{I_n^{Mh}(T_0)}{\chi^{Mh}(T_0) \cdot F_0}$$

where $\chi^{Mh}(T_0)$ is replaced by $s \cdot \chi(T_0)$ in the present case. The magnitude of this value listed in Table II shows that natural remanent magnetization of maghemite of the group I is considerably large compared with the magnitude of thermo-remanent magnetization, since the ordinary Q_T-value of the synthetic magnetite is 2~7 (Uyeda, 1958). This high Q_n^{Mh}-value is not attributable only to high coercive force of maghemite in very fine size. Some unknown mechanism producing such intense remanent magnetization must be considered for interpreting the above results.

Discussion and Conclusion

From the results described in this paper, it would be safely concluded that the remanent magnetization, of which stability is similar to that of thermo-remanent magnetization, is generated in nature as well as in synthetic specimens by chemical reaction below the Curie temperature under the influence of a magnetic field. This fact suggests that the mechanism of generation of chemical remanent magnetization and thermo-remanent magnetization is somewhat of the same nature. It seems, therefore, that Haigh's application of Néel's single-domain grain theory to this process would be successful.

The present investigations show, however, that the intensity of chemical remanent magnetization is much varied in different cases. Among the natural maghemite specimens there are two kinds of specimens having quite different magnitude of

remanence. Intense remanent magnetization of the first group characterized by the higher Qn-value is considered to be the most typical example of the chemical remanent magnetization in nature. But the specimens belonging to the second group of the lower Qn have really no chemical remanent magnetization, as is easily understood from the mode of the thermal variation of the remanence (see Fig. 5 (4)(6)), which indicates the typical mode of the thermal decrease of isothermal remanent magnetization. The thermo-remanent magnetization of the original magnetite seems to have been completely destroyed through the chemical reaction in this case. Systematic study of such a weak and unstable remanent magnetization of the chemically altered rocks was recently carried out by Akimoto and Kushiro (1959), with special reference to the scattered remanent magnetization of rocks.

The chemical remanent magnetization generated artificially in laboratory experiments is generally smaller than the thermo-remanent magnetization by one order of magnitude and greater than isothermal remanent magnetization, as has been described in Part I of this article. From the results described in Part II showing that the difference in the natural remanent magnetization of maghemite corresponds to the difference in the mechanism of generation of maghemite, it would be naturally expected that such a noticeable variety of magnitude of the chemical remanent magnetization of both synthetic and natural specimens is due to the difference in precipitation process of the reaction products, possibly results from the difference in the process of nucleation of the ferromagnetic products. For interpretation of these circumstances, detailed examinations of growing process of chemical remanent magnetization and systematic study of generation of remanence by various kinds of chemical changes are now undertaken.

Acknowledgement

All of the present work has been carried out under the supervision of Prof. T. Nagata. The author wishes to express his sincere thanks to Prof. T. Nagata for his kind guidance throughout the study. He also wishes to thank Dr. S. Akimoto for his continuous guidance and encouragement, and to thank Dr. S. Uyeda of Earthquake Research Institute of Tokyo University, Dr. Y. Ishikawa of Department of Applied Physics, Faculty of Engineering, Tokyo University and Mr. Y. Shimizu, Geophysical Institute, Tokyo University for their useful advice and discussion. The author's grateful thanks are due to Prof. H. Imai, Department of Mining Engineering, Tokyo University for his kindness of putting the ore specimens at the writer's disposal and for his kind guidance on the petrological side. The writer is also very grateful to Mr. G. Shibuya of Yamaguchi University and T. Saitô of Geological Survey of Japan for their kindness of putting the specimens at the writer's disposal and for their useful comments. Chemical analysis was conducted by Dr. T. Katsura of Tokyo Institute of Technology, to whom the author is very grateful. The writer is also indebted to Mr. I. Kushiro of Geological Institute, Tokyo University for his assistance on the microscopy. Finally, he would like to acknowledge fruitful discussion and suggestions rendered by Dr.

examinations of growing process of chemical remanence

study of generation of remanence by various kinds of chemical changes are now undertaken

Acknowledgement

Y. Tomono and Dr. S. Iida, Physical Institute, Tokyo University and Members of their laboratories.

References

Akimoto S. (1954) Journ. Geomag. Geoelect. **6**, 1.
Akimoto S. and Kushiro. I.; to be published.
Akimoto S. and Suzuoki. Z.; private communication.
Blackett P.M.S. (1956) Lectures on Rock Magnetism, Weizmann Science Press, Jerusalem.
Doell R.R. (1956) Trans. Amer. Geophys. Un. **37**, 156.
Dômen H. (1958) Bull. Fac. Educ. Yamaguchi Univ. **7**, Part II, 41.
Graham J.W. (1956) J. Geophys. Res. **61**, 735.
Haigh. G. (1958) Phil. Mag. **3**, 267.
Imai H. (1951) Journ. Geol. Soc. Japan **57**, 211.
Kawai N. (1957) Journ. Geomag. Geoelect. **9**, 140.
Koenigsberger J.G. (1938) Terr. Mag. **43**, 119, 299.
Martinez J.D. and Howell L.G. (1956) Nature **178**, 204.
Nagata T. (1943) "Hattorihôkôkai-kenkyûhôkoku" (in Japanese) **10**, 150.
Nagata T. and Watanabe T. (1950) Geophys. Notes, Tokyo Univ. **3**, No. 21.
Nagata T. (1953) Rock Magnetism, Maruzen Co. Ltd., Tokyo 115, 124.
Newhouse W.H. and Glass J.P. (1936) Econ. Geol. **31**, 699.
Nicholls G.D. (1955) Advanc. in Physics **4**, 113.
Petrova G.N. (1957) Izvest. Akad. Nauk, SSSR, ser. Geofiz. 52.
Petrova G.N. and Pospelova G.A. (1957) Izvest. Akad. Nauk, SSSR, ser. Geofiz. 728.
Rimbert F. (1956 a) Comptes Rendus **242**, 890.
Rimbert F. (1956 b) Comptes Rendus **242**, 2536.
Rimbert F. (1958) Thesis, Paris.
Saito T.; private communication.
Shibuya G. (1958) Journ. Miner. Soc. Japan (in Japanese) **57**, 211.
Thellier E. and Rimbert F. (1954) Comptes Rendus **239**, 1399.
Thellier E. and Rimbert F. (1955) Comptes Rendus **240**, 1404.
Uyeda S. (1958) Japan, Journ. Geophys. **2**, No. 1, 1.

A Method for Obtaining the Atmospheric Temperature and Wind from Sound Propagation in the Rocket Sounding

By Yoshio TAKEYA and Takaaki OKUMOTO

Faculty of Engineering, Osaka City University
(Read October 24, 1958; Received March 10, 1959)

Abstract

In this paper an attempt is made to determine the atmospheric temperature and wind velocity at high altitude from sound propagation.

The space to be measured is divided into several layers, in each of which the temperature and wind distributions are assumed to take the form of second order equation with height. In this assumption the formulae to deduce the temperature and the wind are given by use of Snell's law for sound propagation under the existence of wind.

As the results involve hyperelliptic integrals, it is difficult to get explicitly the quantities giving the distributions of temperature and wind velocity. But it will be possible to find the numerical values of the required quantities by numerical calculus of integral.

It is shown that the results are determined uniquely, in general, and that in the simple case, too, for explaning this theory and using practically.

1. Introdnction

The sound source is the explosion of grenade, which is ejected out from a high-altitude rocket at a pre-determined time. It is measured for the location and time of grenade explosion, and for the time of arrival of sound from it, at several receiving points by Sound Ranging Set on the ground. Temperature and wind velocity vector are deduced from these observations, by the present method described below which is a further developement of the path trace method first given by Gutenberg (1951).

2. Snell's law at receiving points

a) In case of receiving points laying on horizontal plane

Consider the coordinate O–$x'y'z'$ shown in Fig. 1, where O, A and B are the three points of receiving sound. And we define

$$\overline{OA}=S_{x'},$$
$$\overline{OB}=S_{y'}.$$

If the sound wave is plane, sound velocities $v_{x'}$ and $v_{y'}$ along the x'- and y'- axes are given by

and Wind from Sound Propagation in the Lower Troposphere

By Alva of Lexington, Ohio

Received October 20, 1950; Revised March 12, 1951

Abstract

In this paper an attempt is made to determine the simultaneous temperature and wind velocity at high altitudes from sound propagation data.

The temperature and wind distributions are assumed to be the first of several order equation with height. The assumption the formula to derive the temperature and the wind are given by use of Snell's law for sound propagation under the existence of wind.

the quantities giving the distributions of temperature and wind velocity. But it

Wave front
A

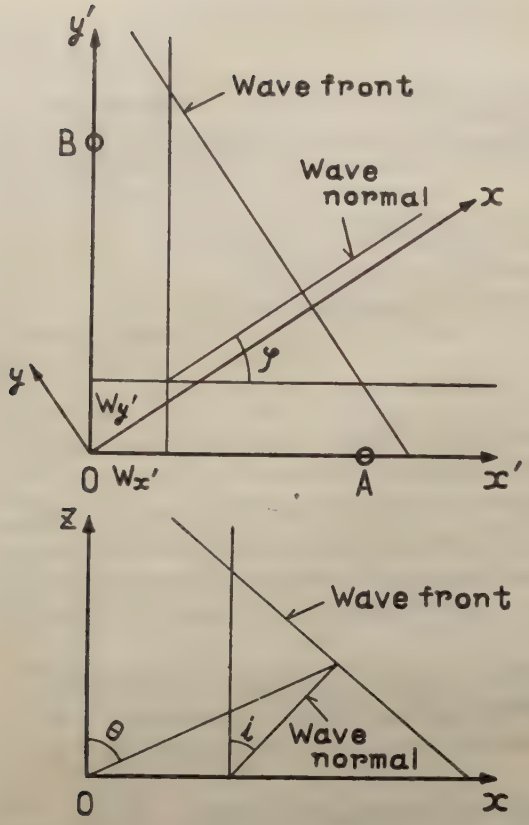

Fig. 1 Diagram showing the coordinates and wave in case 2-a.

$$\left.\begin{aligned} v_{x'} &= W_{x'} + W_y \tan\varphi + \frac{C}{\sin i \cos\varphi}, \\ v_{y'} &= W_{y'} + W_{x'} \cot\varphi + \frac{C}{\sin i \sin\varphi}, \end{aligned}\right\} \quad (1)$$

where $W_{x'}$ and $W_{y'}$ are the x'- and y'-components of the wind velocity at ground, i and φ are the incident angle and the azimuth of wave normal of sound respectively, and C is the sound velocity. And assume that the wind has no component with altitude, i.e. $W_z=0$. It is well-known that sound velocity C is

$$C=\sqrt{\frac{\gamma p}{\rho}}=\sqrt{\frac{\gamma R\theta}{m}}, \quad (2)$$

where;

γ=the ratio of the specific heats of air,

p=atmospheric pressure,

ρ=atmospheric dencity,

R=the gas constant,

and m=molecular weight.

Corresponding to dry air of ground level composition, Eq. (2) is

$$C^2=(20.06)^2\theta, \quad (3)$$

where θ is temperature in ^0K.

Under the existence of wind, Snell's law is expressed by

$$\frac{C}{\sin i}+W_c=k_0, \quad (4)$$

where k_0 is constant and W_c is the horizontal component in direction of sound wave normal. Change the coordinate O-$x'y'z'$ into in O-xyz in Fig. 1, in which x-axis is parallel to the horizontal projection of wave normal, and the xy-plane is horizontal. Hence, W_c is written

$$W_c=W_x=W_{x'}\cos\varphi+W_{y'}\sin\varphi. \quad (5)$$

Then, from Eqs. (1), (4) and (5),

$$k_0=v_{x'}\cos\varphi+v_{y'}\sin\varphi,$$

$$\tan\varphi=\frac{v_{x'}}{v_{y'}},$$

$$k_0=\frac{v_{x'}v_{y'}}{\sqrt{(v_{x'})^2+(v_{y'})^2}}. \qquad (6)$$

Denote the time differences of sound arriving at points O and A, and O and B with Δt_A and Δt_B. Eq. (6) rewrite

$$\left.\begin{aligned}\tan\varphi&=\frac{S_{x'}\cdot\Delta t_B}{S_{y'}\cdot\Delta t_A},\\ k_0&=\frac{S_{x'}\cdot S_{y'}}{\sqrt{(S_{x'}\cdot\Delta t_B)^2+(S_{y'}\cdot\Delta t_A)^2}},\end{aligned}\right\} \qquad (7)$$

The direction of x-axis (φ) and the constant k_0 are obtained from Eq. (7) with observations at ground.

b) In general case

The location of receiving point M_j is (x_j, y_j, z_j) in coordinate O–$x'y'z'$ and M_o is $O(o, o, o,)$

Now, the equation of wave front take the form as

$$lx+my+nz=p\Delta \qquad (8)$$

then, at each receiving points

$$\left.\begin{aligned}&lx_j+my_j+nz_j=p\Delta_j, \quad [j=1,2,3]\\ &l^2+m^2+n^2=1,\end{aligned}\right\} \qquad (9)$$

where Δ_j is the difference of time arrival of sound wave front between M_o and M_j as shown Fig. 2, (l,m,n) is direction cosine of wave normal, and p is

$$p=C+lW_{x'}+mW_{y'}. \qquad (10)$$

From Eq. (9), 1 is

$$l=p\frac{\begin{vmatrix}\Delta_1 & y_1 & z_1\\ \Delta_2 & y_2 & z_2\\ \Delta_3 & y_3 & z_3\end{vmatrix}}{\begin{vmatrix}x_1 & y_1 & z_1\\ x_2 & y_2 & z_2\\ x_3 & y_3 & z^3\end{vmatrix}}=\frac{|\Delta\ y\ z|}{|x\ y\ z|}p, \qquad (11)$$

and, m and n are similarly

$$\left.\begin{aligned}m&=\frac{|x\ \Delta\ z|}{|x\ y\ z|}p,\\ n&=\frac{|x\ y\ \Delta|}{|x\ y\ z|}p.\end{aligned}\right\} \qquad (12)$$

Then, as the necessary quantities are Snell's constant k_0 and the direction of x-axis φ, to calculate the path equations, from Eqs. (11), (12), φ is

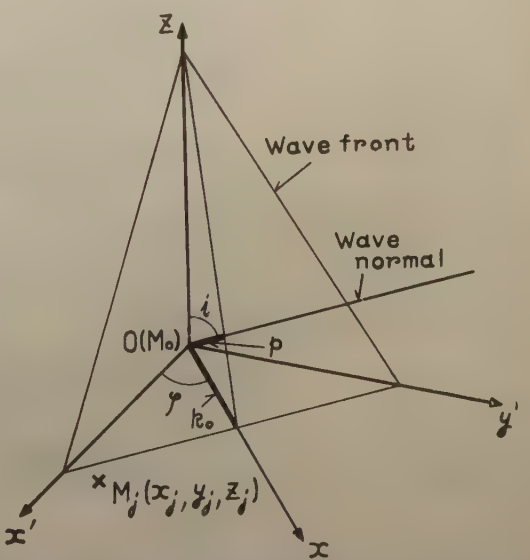

Fig. 2 Diagram showing the coordinates, receiving point and wave in case 2-b.

$$\tan\varphi=\frac{m}{l}=\frac{|x\ \Delta\ z|}{|\Delta\ y\ z|} \tag{13}$$

And k_0 is

$$k_0=\frac{C}{\sin i}+W_x=\frac{C+lW_{x'}+mW_{y'}}{\sqrt{1-n^2}}=\frac{p}{\sqrt{l^2+m^2}}, \tag{14}$$

From Eqs. (11), (12) and (14)

$$k_0^2=\frac{|x\ y\ z|^2}{|\Delta\ y\ z|^2+|x\ \Delta\ z|^2}. \tag{15}$$

c) In the case of having many receiving points

In case of (b), it is necessary for receiving points to have four, theoretically. But, as wave front is not plane owing to the local disturbance of air, it is seen that four receiving points are not sufficient.

Therefore, consider the case of j ($j\geqq 4$) receiving points. Using method of least square, Eq. (11) become

$$l=\frac{\begin{vmatrix}\Sigma x_j\Delta_j & \Sigma x_jy_j & \Sigma x_jz_j\\ \Sigma y_j\Delta_j & \Sigma y_j^2 & \Sigma y_jz_j\\ \Sigma z_j\Delta_j & \Sigma y_jz_j & \Sigma z_j^2\end{vmatrix}}{\begin{vmatrix}\Sigma x_j^2 & \Sigma x_jy_j & \Sigma x_jz_j\\ \Sigma x_jy_j & \Sigma y_j^2 & \Sigma y_jz_j\\ \Sigma x_jz_j & \Sigma y_jz_j & \Sigma z_j^2\end{vmatrix}}\cdot p=\frac{|\Sigma\Delta x\ \Sigma xy\ \Sigma xz|}{|\Sigma x^2\ \Sigma xy\ \Sigma xz|}\cdot p\ . \tag{16}$$

Then, φ and k_0^2 are, correspond to Eqs. (13) and (15) with expression of Eq. (16)

$$\left.\begin{aligned}\tan\varphi&=\frac{|\Sigma x^2\ \Sigma\Delta x\ \Sigma xz|}{|\Sigma x^2\ \Sigma xy\ \Sigma xz|},\\ k_0^2&=\frac{|\Sigma x^2\ \Sigma xy\ \Sigma xz|^2}{|\Sigma\Delta x\ \Sigma xy\ \Sigma xz|^2+|\Sigma x^2\ \Sigma\Delta x\ \Sigma xz|^2}.\end{aligned}\right\} \tag{17}$$

3. Path equation of sound wave

As described in the proceding section, the x-axis is the direction of sound wave normal and the z-axis is the direction of altitude. If the sound wave from the source $G(X, Y, Z)$ arrives at point M_0 i.e. $O(0, 0, 0,)$ the following relations hold generally, provided that W_z is equal to zero.

$$\left.\begin{aligned}X&=\int_0^z\tan\theta dz=\int_0^z\frac{C\sin i+W_x}{C\cos i}\,dz,\\ Y&=\int_0^T W_y dt=\int_0^z\frac{W_y}{C\cos i}dz,\\ Z&=\int_0^z dz,\end{aligned}\right\} \tag{18}$$

where θ is the angle shown in Fig. 1, W_y is y-component of wind and T is the time spent for sound travel from G to O, as follows

$$T=\int_0^T dt=\int_0^z \frac{1}{C\cos i}\cdot dz \tag{19}$$

a) In case of constant distributions of temperature and wind velocities

Assume the constant distributions of temperature and wind velocities. Or, for the calculation of roughly approximated solution, for example, the constants are mean values in a range of the altitude, which is under consideration now. As it is

$$\left.\begin{aligned} C^2&=\xi\,,\\ W_x&=\eta\,,\\ W_y&=\zeta\,, \end{aligned}\right\} \tag{20}$$

then, Eqs. (18) and (19) are as follows

$$\left.\begin{aligned} X&=\frac{\xi+k_0\eta-\eta^2}{\sqrt{\xi}\,\sqrt{(k_0-\eta)^2-\xi}}\cdot z\,,\\ Y&=\frac{(k_0-\eta)\zeta}{\sqrt{\xi}\,\sqrt{(k_0-\eta)^2-\xi}}\cdot z\,,\\ T&=\frac{(k_0-\eta)}{\sqrt{\xi}\,\sqrt{(k_0-\eta)^2-\xi}}\cdot z\,. \end{aligned}\right\} \tag{21}$$

b) In case of linear distributions

In case of temperature and wind velocities are linear with altitude as follows

$$\left.\begin{aligned} C^2&=a_0+\xi\cdot z\,,\\ W_x&=b_0+\eta\cdot z\,,\\ W_y&=c_0+\zeta\cdot z\,, \end{aligned}\right\} \tag{22}$$

where a_0, b_0, c_0 are the known constants and the values of C, W_x, W_y, which are described the next section. From Eqs. (22), Eqs, (18) are written as

$$\left.\begin{aligned} X&=\int_0^z \frac{(a_0+k_0b_0-b_0^2)+(\xi+k_0\eta-2b_0\eta)z+\eta^2z^2}{S}\,dz\,,\\ Y&=\int_0^z \frac{(k_0-b_0)c_0+[(k_0-b_0)\xi-c_0\eta]\,z-\eta\zeta z^2}{S}\,dz\,,\\ T&=\int_0^z \frac{(k_0-b_0)-\eta z}{S}\,dz\,, \end{aligned}\right\} \tag{23}$$

where

$$S=(a_0+\eta z)^{1/2}\left[(k_0-b_0)^2-a_0-\left\{2(k_0-b_0)\eta+\xi\right\}z-\eta^2z^2\right]^{1/2}.$$

Eqs. (23) are elliptic integrals. And if elliptic integral is easily able to calculate, it is more suitable approximation that temperature takes a second oder term of altitude, i.e.,

$$C^2=a_0+a_1z+\xi z^2\,,$$

then, Eq. (23) changes as follows

a) In case of constant density

values in a range of the altitude, which is under consideration, as well as

linear with altitude as follows

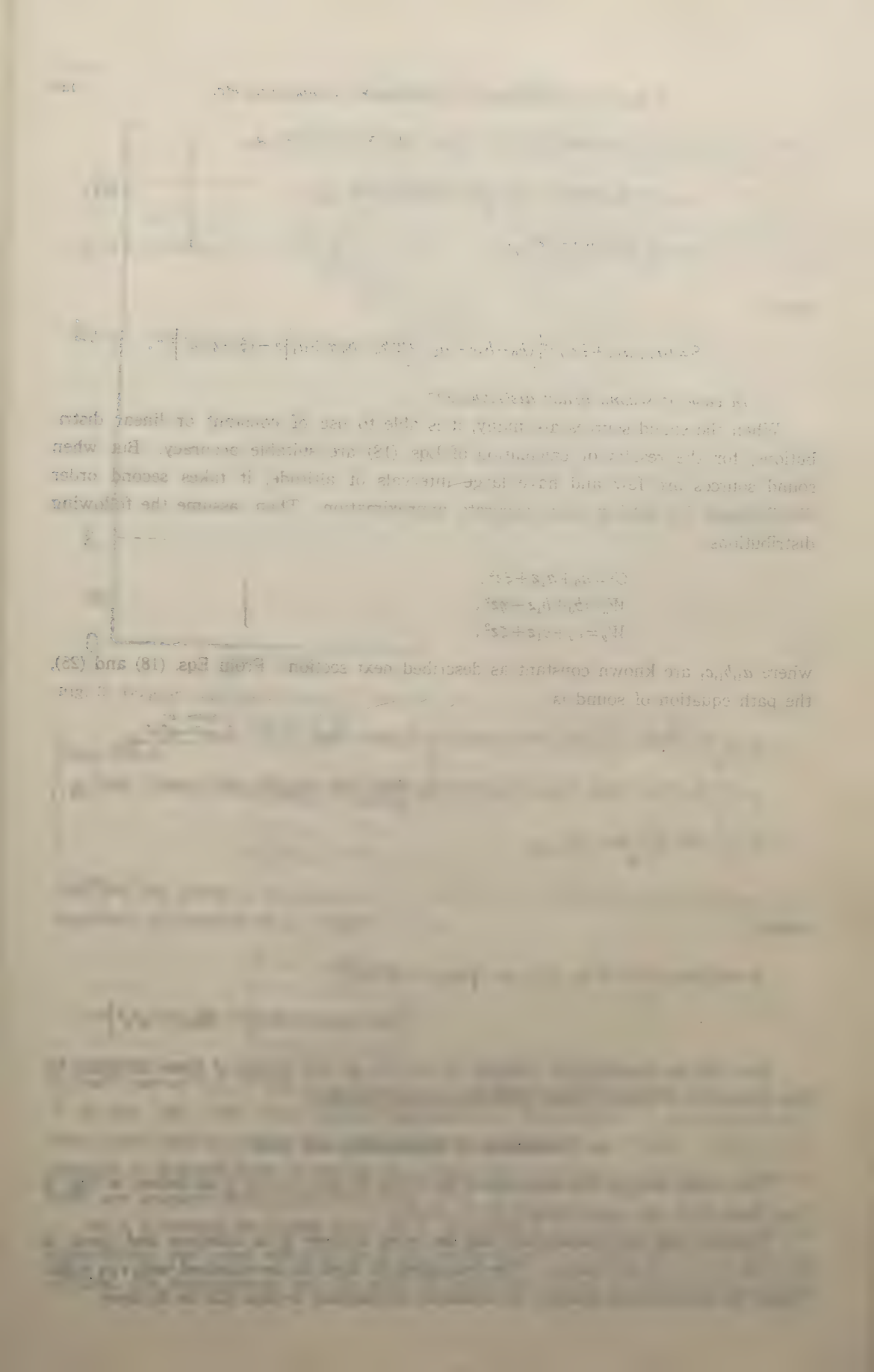

$$\left.\begin{aligned} X&=\int_0^z \frac{(a_0+k_0b_0-b_0^2)+(a_1+k_0\eta-2b_0\eta)z+(\xi-\eta^2)z^2}{S}dz\,,\\ Y&=\int_0^z \frac{(k_0-b_0)c_0+[(k_0-b_0)\xi-c_0\eta]z-\eta\zeta z^2}{S}dz\,,\\ T&=\int_0^z \frac{(k_0-b_0)-\eta z^2}{S}dz\,. \end{aligned}\right\} \qquad (24)$$

where

$$S=(a_0+a_1z+\xi z^2)^{1/2}\left[(k_0-b_0)^2-a_0-\left\{2(k_0-b_0)\eta+a_1\right\}z-(\xi-\eta^2)z^2\right]^{1/2}.$$

c) In case of second order distributions

When the sound sources are many, it is able to use of constant or linear distributions, for the results of calculation of Eqs. (18) are suitable accuracy. But when sound sources are few and have large intervals of altitude, it takes second order distributions, for getting more accurate approximation. Then, assume the following distributions

$$\left.\begin{aligned} C^2&=a_0+a_1z+\xi z^2\,,\\ W_x&=b_0+b_1z+\eta z^2\,,\\ W_y&=c_0+c_1z+\zeta z^2\,, \end{aligned}\right\} \qquad (25)$$

where a_1, b_1, c_1 are known constant as described next section. From Eqs. (18) and (25), the path equation of sound is

$$\left.\begin{aligned} X&=\int_0^z \frac{(a_0+k_0b_0-b_0^2)+(a_1+k_0b_1-2b_0b_1)z+(\xi+k_0\eta-2b_0\eta-b_1^2)z^2-b_1\eta z^3-\eta^2z^4}{S}dz\,,\\ Y&=\int_0^z \frac{(k_0-b_0)c_0+[(k_0-b_0)c_1-b_1c_0]z+[(k_0-b_0)\zeta-c_0\eta-b_1c_1]z^2-(b_1\zeta+c_1\eta)z^3-\eta\zeta z^4}{S}dz\,,\\ T&=\int_0^z \frac{(k_0-b_0)-b_1z-\eta z^2}{S}dz\,, \end{aligned}\right\} \qquad (26)$$

where

$$S=(a_0+a_1z+\xi z^2)^{1/2}\left[(k_0-b_0)^2-a_0-\left\{2(k_0-b_0)b_1+a_1\right\}z+\left\{2(k_0-b_0)\eta+\xi-b_1^2\right\}z^2-2b_1\eta z^3+\eta^2z^4\right]^{1/2}.$$

Eqs. (26) are hyperelliptic integral, so we can get the values of these integrals by the numerical calculus helping with the analog-computer

4. Calculation of temperature and wind

The sound sources are represented by $G_i(X_i, Y_i, Z_i)$, $[i=1, 2\cdots]$ as shown in Fig. 3. The layer S_i is the space deffned by $z_{i-1}\leqq z\leqq z_i$.

Consider that the temperature and the wind in layer S_i is unknown and those in S_{i-1}, S_{i-2}, $\cdots\cdots$, S_1 are known. The quantities in layer S_i are attached with i as suffix. Then, the distributions change, for example, correspond to Eqs. (25) in S_i layer

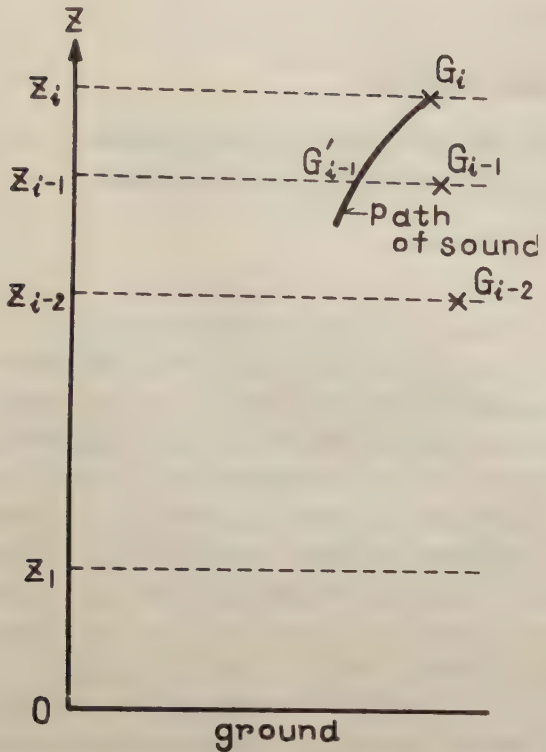

Fig. 3 Diagram showing G's and G'_{i-1} and the path of sound from G_i to O.

$$C^2=a_{0i}=a_{1i}(z-z_{i-1})+\zeta(z-z_{i-1})^2,$$
$$W_x=b_{0i}+b_{1i}(z-z_{i-1})+\eta(z-z_{i-1})^2,$$
$$W_y=c_{0i}+c_{1i}(z-z_{i-1})+\zeta(z-z_{i-1})^2.$$

The following quantities in S_i layer are given by the known value in S_{i-1} layer such as

$$\left.\begin{aligned} a_{0i}&=C^2(z_{i-1}),\\ b_{0i}&=W_x(z_{i-1}),\\ c_{0i}&=W_y(z_{i-1}),\\ k_{0i}&=k_0. \end{aligned}\right\} \quad (27)$$

And $G'_{i-1}(X'_{i-1},Y_{i-1}',Z_{i-1}')$ is the position at the altitude z_{i-1} in the sound path from$G$ to O, as shown in Fig. 3 and T'_{i-1} is the time spent for travel from G'_{i-1} to O.

Now assume the gradients of temperature and wind velocities are continuous at the boundary (z_{i-1}) of S_i and S_{i-1}, in case of 3-c,

$$\left[\frac{\partial_{i-1}}{\partial z}\right]_{z=z_{i-1}}=\left[\frac{\partial_i}{\partial z}\right]_{z=z_{i-1}} \quad (26)$$

then, this is

$$\left.\begin{aligned} a_{1i}&=a_{1(i-1)}+2a_{2(i-1)}\cdot(z_{i-1}-z_{i-2}),\\ b_{1i}&=b_{1(i-1)}+2b_{2(i-1)}\cdot(z_{i-1}-z_{i-2}),\\ c_{1i}&=c_{1(i-1)}+2c_{2(i-1)}\cdot(z_{i-1}-z_{i-2}). \end{aligned}\right\} \quad (29)$$

Eqs. (18) are given as the function of ξ, η and ζ as follows, provided that the lower boundary of integrals is z_{i-1} instead of zero,

$$\left.\begin{aligned} X_i-X'_{i-1}&=X(\xi,\eta),\\ Y_i-Y'_{i-1}&=Y(\xi,\eta,\zeta),\\ z_i-z_{i-1}&=Z,\\ T_i-T'_{i-1}&=T(\xi,\eta,\zeta), \end{aligned}\right\} \quad (30)$$

in each case of 3-a, -b and -c, ξ, η and ζ are detemind simultaneously from X,Y and T of Eqs. (30). The other required quantities for determining the distributions of S_i layer, have been known by Eqs. (27) and (29) with those of S_{i-1} layer. And the temperature is deduced from C^2 by Eq. (3). Thus, the temperature and the wind in S_i layer are uniquely determined with those in S_{i-1} layer.

As it is treated the lowest layer as S_1, in which it is always able to measure for temperature and wind velocity by Radio-zonde between 0 km and about 30 km in altitude, the temperature and the wind in upper layer above S_1 are able to calculate

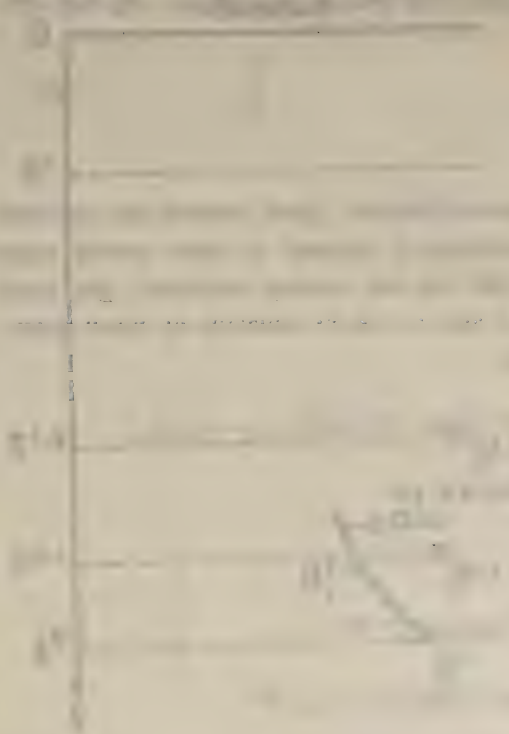

by abovementioned method, successively.

Acknowledgement

The authors wish to express their cordial thanks to Prof. K. Maeda in Kyoto University, and the research menbers of his seminar for valuable discussions.

Reference

Gutenberg B. (1951) Compendium of Met. p. 336.

LETTERS TO THE EDITORS

Ionospheric Radio Wave Scattering in the Electrodynamically Controlled Turbulence

(Received March 1, 1959)

As is well-known, the physical quantity which plays the most important role in the ionospheric radio wave scattering is electron density fluctuations, since they are directly related to the fluctuations in dielectric constant. The most outstanding feature of the problem is that there are fields applied from outside that affects the weakly ionized gas: namely, the electrostatic field $\boldsymbol{E}_0$ and the terrestrial magnetic field $\boldsymbol{H}_0$. We want to know the behavior of electric charges which is drastically controlled by the existing applied electromagnetic fields $\boldsymbol{E}_0$ and $\boldsymbol{H}_0$: therefore, we cannot assume any isotropy on the statistical distributions of variable quantities, such as electron or ion density, electron or ion mass velocity, polarization electric fields and others.

As for what feeds a sizable amount of energy to the ionospheric turbulence in question, it is beyond all surmise: all the same, we can mention some possiblities. One is that the ionospheric Reynolds number being great enough, the air is very liable to initiate an unstable state, thus giving out part of its turbulence energy to electronic and ionic gases through collisions. This is the case in which the onset of turbulence in electronic or ionic gas is brought about by the hydrodynamic turbulence of the air. Another possibility is that any electromagnetic disturbance can influence the behavior of electric charges, such effect being almost independent of the hydrodynamic motion of the air. Thus, the electronic gas can turn into a turbulent state, for example, by some magnetic disturbance. The actual cases are probably between these two extremes: we can name the former the "hydrodynamically controlled turbulence", the latter the "electrodynamic turbulence." We shall show how this electrodynamic turbulence can be studied.

Assuming that $\boldsymbol{E}_0$ and $\boldsymbol{H}_0$ are uniform throughout the medium and utilizing four Maxwell equations and continuity of current, together with the ohm's law expressed as the current density equals the conductivity tensor $[\sigma]$ multiplied by the electric field $(\boldsymbol{E}_0+\boldsymbol{E}_p)$, we have

$$\nabla \cdot \frac{\partial \boldsymbol{E}_p}{\partial t} = -4\pi c^2 \nabla \cdot \{[\sigma](\boldsymbol{E}_0+\boldsymbol{E}_p)\}\,, \tag{1}$$

$$\nabla^2 \boldsymbol{E}_p - \nabla\nabla\cdot\boldsymbol{E}_p = \frac{1}{c^2}\cdot\frac{\partial^2 \boldsymbol{E}_p}{\partial t^2} + 4\pi \frac{\partial}{\partial t}\left\{[\sigma]\left(\boldsymbol{E}_0+\boldsymbol{E}_p\right)\right\}, \tag{2}$$

where $[\sigma] \propto n_e$, as long as we may neglect the existence of negative ions. By this set of equations in which only polarization electric field $\boldsymbol{E}_p$ and electron number density n_e are the variables, we can assess the energy split of the fluctuations n_e under a given

(4)

configuration of $\boldsymbol{E}_0$ and $\boldsymbol{H}_0$. The air molecules can influence the behavior of charges solely through collisions. We define:

$$\overline{\delta n_e \delta n'_e(\boldsymbol{r})} = \int \gamma(\boldsymbol{\kappa}) e^{i\boldsymbol{\kappa}\cdot\boldsymbol{r}} d\boldsymbol{\kappa},$$

$$\overline{E_m E'_n(\boldsymbol{r})} = \int a_{mn}(\boldsymbol{\kappa}) e^{i\boldsymbol{\kappa}\cdot\boldsymbol{r}} d\boldsymbol{\kappa},$$

$$\overline{E_m \delta n'_e(\boldsymbol{r})} = \int S_m(\boldsymbol{\kappa}) e^{i\boldsymbol{\kappa}\cdot\boldsymbol{r}} d\boldsymbol{\kappa},$$

$$\overline{\delta n_e E'_n(\boldsymbol{r})} = \int S'_n(\boldsymbol{\kappa}) e^{i\boldsymbol{\kappa}\cdot\boldsymbol{r}} d\boldsymbol{\kappa},$$

$$\delta n_e = n_e(\boldsymbol{x}, t) - \bar{n}_e, \quad \delta n'_e = n_e(\boldsymbol{x}+\boldsymbol{r}, t) - \bar{n}_e,$$

where the prime indicates the quantities at another point separated by the distance $\boldsymbol{r}$. Integrations in the above formulae are over all $\boldsymbol{\kappa}$ space.

If we assume

i) The state of turbulence remains stationary;

ii) The 4th order correlation can be broken up into combinations of 2nd order correlation, i.e.

$$\overline{\delta n_e \delta n'_e E_m E'_n} = \overline{\delta n_e \delta n'_e} \cdot \overline{E_m E'_n} + \overline{\delta n_e E'_n} \cdot \overline{\delta n'_e E_m} + \overline{\delta n_e E_m} \cdot \overline{\delta n'_e E'_n} \qquad (3)$$

and the 3rd order correlation is negligible when compared with any 2nd or 4th order correlation;

iii) $$\frac{|\delta n_e|}{n_0} \ll 1, \quad \frac{|\boldsymbol{E}_p|}{|\boldsymbol{E}_0|} \ll 1, \qquad (4)$$

then eq. (1) and (2) yield, after some complicated manipulations,

$$-\kappa^2 a_{ij}(\boldsymbol{\kappa}) + \sum_k \kappa_j \kappa_k a_{kj} = \frac{1}{c^2} F\left\{\overline{E'_n \frac{\partial^2 E_{pi}}{\partial t^2}}\right\}, \qquad (5)$$

$$\sum_{i,j=1}^{3} \kappa_i \kappa_j F\left\{\overline{E'_n \frac{\partial^2 E_{pi}}{\partial t^2}}\right\} = -(4\pi)^2 c^4 \sum_{i,j=1}^{3} \kappa_j \kappa_i \sum_{k,l=1}^{3} s_{jk} s_{lm}$$
$$\times \Big[E_{0k} E_{0m} \gamma(\boldsymbol{\kappa}) + E_{0k} n_e S'_m(\boldsymbol{\kappa}) + E_{0m} n_e S_k(\boldsymbol{\kappa})$$
$$+ n_e^2 a_{km}(\boldsymbol{\kappa}) + (2\pi)^3 \int \gamma(\boldsymbol{\kappa}_1) a_{km}(\boldsymbol{\kappa} - \boldsymbol{\kappa}_1) d\boldsymbol{\kappa}_1$$
$$- (2\pi)^3 \int S'_m(\boldsymbol{\kappa}_1) S_k(\boldsymbol{\kappa} - \boldsymbol{\kappa}_1) d\boldsymbol{\kappa}_1 \Big]. \qquad (6)$$

where F stands for the Fourier transfrom and s_{jk} is defined by

$$a_{jk} = s_{jk} n_e, \quad [a] = [s] n_e. \qquad (7)$$

If we could limit the range of our discussions only to the largest irregularity after whose decay distinguishable turbulence starts, then we might be allowed to discard the nonlinear terms (i.e. the integral terms) in eq. (6).

iv) For large irregularity

$$\sum_{k=1}^{3} \kappa_k a_{kj} \simeq 0 \ (j = 1, 2, 3); \qquad (8)$$

v) Eq. (6) reduces to the following type of equation:

$$\sum_{j,l} \kappa_j \kappa_l \Phi_{jl} = 0 ; \tag{9}$$

this Φ_{jl} may be approximated by the general expression for 2nd order correlation tensor which is known in the isotropic case, as,

$$\Phi_{jl} = \Phi(\kappa)(\kappa^2 \delta_{jl} - \kappa_j \kappa_l), \quad (\delta_{jl}: \text{Kronecker's delta});$$

vi) $\kappa^2 \gg (4\pi c)^2 |s_{jk}||s_{lm}| \overline{n_e^2}$ for the ordinary ionospheric irregularity;

vii) We overlook cross terms β_k and β'_m.

All these assumptions result in

$$\begin{cases} \kappa_1^2 \alpha_{11}(\kappa_1, 0.0) = \Lambda_{11} \gamma(\kappa_1, 0, 0), \\ \kappa_2^2 \alpha_{22}(0, \kappa_2, 0) = \Lambda_{22} \gamma(0, \kappa_2, 0), \\ \kappa_3^2 \alpha_{33}(0, 0, \kappa_3) = \Lambda_{33} \gamma(0, 0, \kappa_3), \end{cases} \tag{10}$$

where

$$\Lambda_{jj} = (4\pi c)^2 \sum_{m,k=1}^{3} s_{jk} s_{jm} E_{0k} E_{0m} \tag{11}$$

and 0 wave number means a wave number much smaller than the wave number which contains appreciable amount of energy. To determine $\alpha_{11}(\kappa_1, 0, 0)$, etc., we further assume

viii) Random current flow distribution is established in order to bring the random ohmic losses in the three rectangular directions into equipartition. And the neglect of the Hall current loss results in

$$\sigma_1 \int \alpha_{11}(\boldsymbol{\kappa})\, d\boldsymbol{\kappa} = \sigma_1 \int \alpha_{22}(\boldsymbol{\kappa})\, d\boldsymbol{\kappa} = \sigma_0 \int \alpha_{33}(\boldsymbol{\kappa})\, d\boldsymbol{\kappa} \tag{12}$$

where the contribution to the integrals is mainly made by the energy containing wave number $\boldsymbol{\kappa}_0$; σ_0 and σ_1 are the conductivity parallel and transverse to $\boldsymbol{H}_0$ respectively.

ix) In the ionosphere, the gas by itself seems least likely to produce either hydromagnetic oscillations or electromagnetic waves, so that we may think that electrostatic oscillations are dominant, then α_{11}, α_{22} and α_{33} should be directly given by κ_1, κ_2 and κ_3 respectively.

We know from eq. (5) and (6) and assumptions (v)~(vii), the α_{jl}'s should obey κ^{-3}-law and finally

$$\begin{aligned} &\gamma(\kappa_1, \kappa_2, \kappa_3) \simeq \gamma(\kappa_1, 0, 0) + \gamma(0, \kappa_2, 0) + \gamma(0, 0, \kappa_3) \\ &= \text{Const} \times \left[\frac{\kappa_{01}^3}{\Lambda_{11} \sigma_1 \kappa_1} \frac{1}{\kappa_1} + \frac{\kappa_{02}^3}{\Lambda_{22} \sigma_1 \kappa_2} \frac{1}{\kappa_2} + \frac{\kappa_{03}^3}{\Lambda_{33} \sigma_0 \kappa_3} \frac{1}{\kappa_3} \right] \end{aligned} \tag{13}$$

where Λ_{11}, Λ_{22} and Λ_{33} are given in eq. (11) and $\boldsymbol{\kappa}_0 = (\kappa_{01}, \kappa_{02}, \kappa_{03})$ is the energy-containing wave number. Therefore, when electromagnetic disturbances initially supply the turbulence energy over the same distance, i.e., at the wave number

$$\kappa_{01} \simeq \kappa_{02} \simeq \kappa_{03},$$

v) Eqn. (6) reduces to the form

$$\nabla^2 \phi_0 = 0 .$$

this ϕ_0 may be approximated by the general

$$\phi_0 = \phi_0(x_1, x_2, x_3), \quad i.e. \quad \phi_0 = \phi_0(x_1, x_2)$$

vi) $\varepsilon_0 \gamma (4\pi\varepsilon_0)^{-1} s_{11} \ldots s_{2m} s_{3n}$ for the vacuum

vii) We overlook cross terms γ_α and γ_β

All these assumptions result in

$$\begin{aligned} \varepsilon_0 \gamma_{11}(\varepsilon_1 0,0) &= \lambda_{11}(\varepsilon_1 0,0) \\ \varepsilon_0 \gamma_{22}(0,\varepsilon_2 0) &= \lambda_{22}(0,\varepsilon_2 0) \\ \varepsilon_0 \gamma_{33}(0,0,\varepsilon_3) &= \lambda_{33}(0,0,\varepsilon_3) \end{aligned}$$

where

$$\lambda_{11} = (4\pi\varepsilon_0)^{-1} s_{11} s_{2n} s_{3n}$$

and 0 wave number means a wave number much smaller than the wave number which

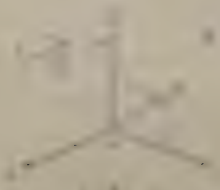

then the ratio

$$(\Lambda_{11}\sigma_1)^{-1}:(\Lambda_{22}\sigma_1)^{-1}:(\Lambda_{33}\sigma_0)^{-1}$$

gives the direct measure for the anisotropic energy partition under the influence of the geomagnetic field and the electric field applied from outside.

[In the case where either $E_0^{\perp}=0$ or $E_0^{//}=0$ (see Fig. 2), the derivation so far carried out is not appropriate, since for such cases we cannot neglect the nonlinear terms in eq. (6).]

We shall give some numerical examples for the case of E-region at 90 km level.

When radio frequency is much higher than electron gyrofrequency, the scattering cross section σ is proportional to $\gamma(\boldsymbol{\kappa})$, i.e.,

$$\sigma \propto \gamma(\boldsymbol{\kappa}),\ \boldsymbol{\kappa}=\boldsymbol{\kappa}_0-\boldsymbol{\kappa}_1 \text{ (See Fig. 3)}$$

By the coordinates shown in Fig. 2, the wave number component κ_3 has quite a small fluctuation intensity. This implies that $\boldsymbol{\kappa}$ should be chosen so that it may have

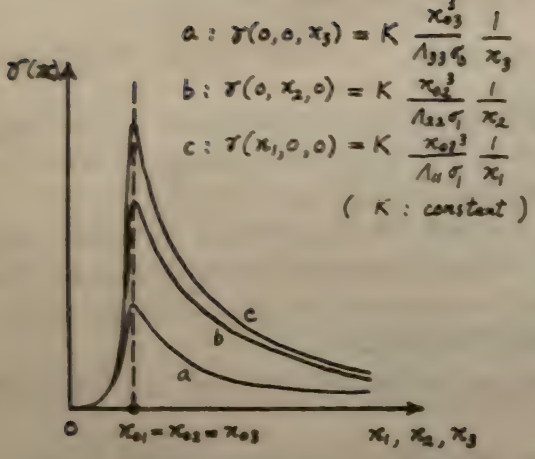

Fig. 1 Split of energy in electron density fluctuations when the intial disturbance is given over the same distance, *viz.* $\kappa_{01}=\kappa_{02}=\kappa_{03}$

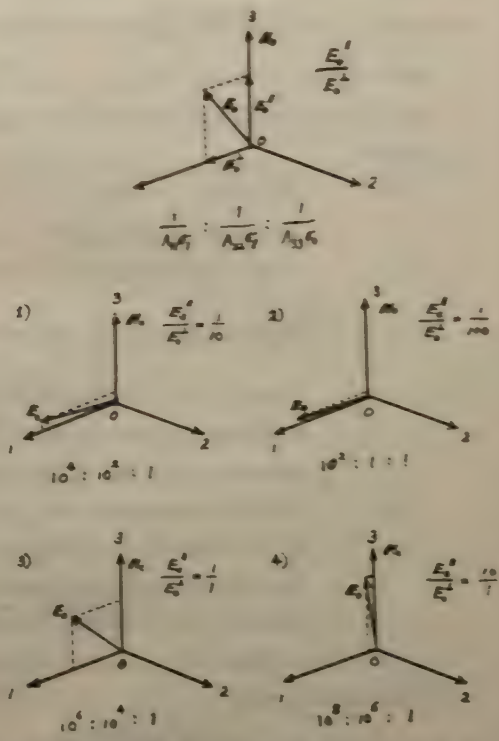

Fig. 2 Numerical examples of anisotropy in the electron density fluctuations in the E-layer (at 90km level)

The ratio $\frac{1}{\Lambda_{11}\sigma_1} : \frac{1}{\Lambda_{22}\sigma_1} : \frac{1}{\Lambda_{33}\sigma_0}$ does not depend on the particular value of $\boldsymbol{E}_0$, but on the angle between the direction of $\boldsymbol{H}_0$ and $\boldsymbol{E}_0$, i.e.

$$\frac{1}{\Lambda_{11}\sigma_1} : \frac{1}{\Lambda_{22}\sigma_1} : \frac{1}{\Lambda_{33}\sigma_0} = 10^8 : 10^4 : \frac{1}{\left(\frac{E_0^{//}}{E_0^{\perp}}\right)^2}.$$

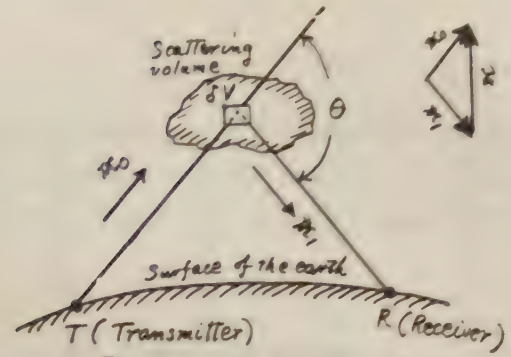

Fig. 3 Scatter propation path

less component of κ_3. Furthermore, because of the existence of the electric field $\boldsymbol{E}_0$, $\boldsymbol{\kappa}$ should be chosen in such a way that $\kappa_1 \perp \kappa_2$. This means that $\boldsymbol{\kappa}$ should be directed perpendicular to $\boldsymbol{H}_0$, and parallel to $\boldsymbol{E}_0$. Then the scatter propagation will be performed with less loss of power and with more efficiency. Thus, according to the direction of $\boldsymbol{\kappa}$ (i.e. choice of the propagation path), the scattered received field will change by 20~50db, so therefore, the study of electrodynamic turbulence is quite important in view of practical use.

By K. MAEDA, S. KATO and T. TSUDA

Department of Electronics, Kyoto University

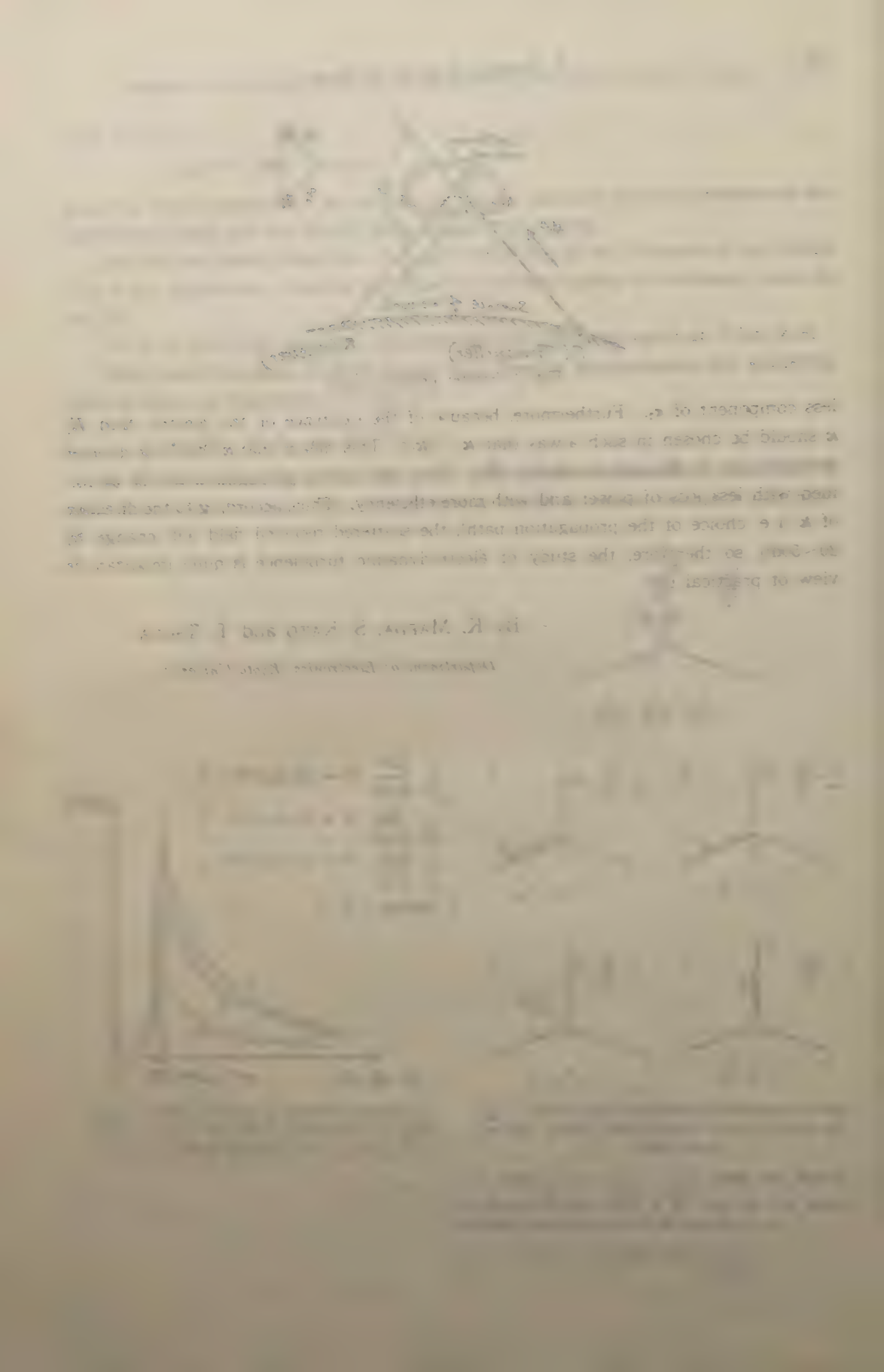

Provisional Report of Observations of Geomagnetic Variations at Aso and Kikai (one of the Amami Islands), during the Solar Eclipse of April 19th, 1958

(Received March 15, 1959)

1. General Description

To investigate the effects on geomagnetic variations due to the solar eclipse of April 19th, 1958, we set up a temporary station at Kikai island in addition to the Aso Magnetic Observatory (one of the IGY stations in Japan). The former is situated at the southern end of annular eclipse zone, and the latter near by the northern end of that zone.

The conditions of the eclipse were as follows:

	Aso	Kikai
Beginning of the eclipse:	$10^h\ 05^m$	$10^h\ 53^m$
Maximum of the eclipse:	$12^h\ 24^m$	$12^h\ 47^m$
Ending of the eclipse:	$14^h\ 43^m$	$14^h\ 40^m$
Degree of the eclipse:	89 %	94.8 %

2. Special Remarks on the Kikai Temporary Station

Geographic position of the Kikai temporary station was as follows:

Latitude: 28°19.0'N
Longitude: 129°57.0'E

We constructed the observational room in a part of the Kikai High School. Magnetic variometers and recorder were set on the concrete floor made of non-magnetic materials, and portable dark room made of vinyl was used, but it showed diurnal variation of the room temperature (its range was about 2°C). It is necessary to correct the temperature effect for Z-values, as the Z-variometer showed the temperature effect, 12.57 mm/°C. But we did not need any temperature-correction for the H- and D-variometer. The sensetivity of each variometer was as follows:

H-variometer: 3.47 mm/
D-variometer: 0.43 mm/
Z-variometer: 2.47 mm/

We used the recording drum which ran 20.5mm/hour.

3. Absolute Measurements

Absolute measurements were made at the playground of the High School, on April 17th, 18th, and 19th. Their mean value was adopted as base values of each component.

Date	Time h	m	H ASO 31590γ + ...	H KIKAI 34211γ + ...	D ASO w5 07'0 + ...	D KIKAI w3 56'1 + ...	Z ASO 34400γ + ...	Z KIKAI 28470γ + ...
18	00	00	101	38	15.2′	10.0′	59	58
	01		84	24	13.9	9.0	58	53
	02		82	20	12.6	7.3	55	46
	03		81	20	11.5	7.1	56	49
	04		93	32	13.4	8.0	55	54
	05		91	32	12.6	7.9	55	54
	06		88	29	12.1	7.4	54	51
	07		83	23	11.9	7.0	54	53
	08		95	36	12.1	7.0	51	53
	09		90	34	10.3	5.9	49	48
	10		73	27	11.2	5.7	35	40
	11		70	32	12.1	6.5	21	34
	12		46	12	17.6	10.9	7	34
	13		52	18	19.1	12.9	12	31
	14		76	36	19.0	13.2	26	36
	15		83	39	19.4	13.2	34	37
	16		74	26	19.1	12.8	33	36
	17		74	21	17.8	12.2	42	36
	18		64	8	15.8	10.4	47	34
	19		60	3	16.5	10.9	45	37
	20		43	−11	16.0	10.4	45	36
	21		53	− 8	16.1	10.4	51	41
	22		56	− 2	13.4	8.3	58	40
	23		60	3	14.5	9.1	57	45
19	00	00	69	11	14.3	8.9	59	48
	01		79	20	13.6	8.5	63	50
	02		80	21	13.4	8.1	61	51
	03		77	19	13.4	8.2	58	49
	04		74	18	14.1	8.6	55	49
	05		81	25	13.8	8.4	55	50
	06		100	39	13.4	8.4	59	52
	07		99	38	13.8	8.4	59	55
	08		74	21	11.0	5.8	55	42
	09	00	76	29	11.4	6.5	41	37
		10	—	30	—	6.2	—	36
		20	80	36	10.3	5.6	39	34
		30	83	40	10.6	5.8	35	33
		40	79	38	11.6	6.6	30	35
		50	83	43	11.5	6.5	27	33
	10	00	83	45	11.8	6.9	24	33
		10	82	48	11.5	6.7	20	29
		20	74	44	13.6	8.1	13	29
		30	76	45	14.3	8.6	9	28
		40	74	46	15·0	9.3	7	26
		50	77	49	15.2	9.2	6	24
	11	00	79	52	15.3	9.2	5	24
		10	84	56	15.6	9.5	2	22
		20	86	58	15.8	9.7	2	23
		30	89	61	16.1	9.7	4	26
		40	97	68	16.1	10.3	7	29
		50	97	68	16.4	10.0	8	28
	12	00	97	68	16.5	10.5	12	30
		10	102	71	16.6	10.1	14	31
		20	106	75	16.5	10.5	17	31
		30	109	78	17.0	11.1	18	32
		40	108	75	17.2	10.9	20	38
		50	105	71	17.3	11.5	22	42
	13	00	108	73	17.4	11.5	23	43
		10	108	71	17.2	11.7	25	42
		20	112	72	17.6	11.6	27	42
		30	112	72	17.7	11.7	30	44
		40	113	74	18.1	11.7	31	44
		50	114	75	18.4	12.4	33	42
	14	00	119	81	18·5	12.0	35	42
		10	119	79	19.1	11.9	35	43
		20	117	79	19.5	13.3	35	47
		30	116	75	19.3	13.0	36	49
		40	116	77	19.2	13.3	36	53

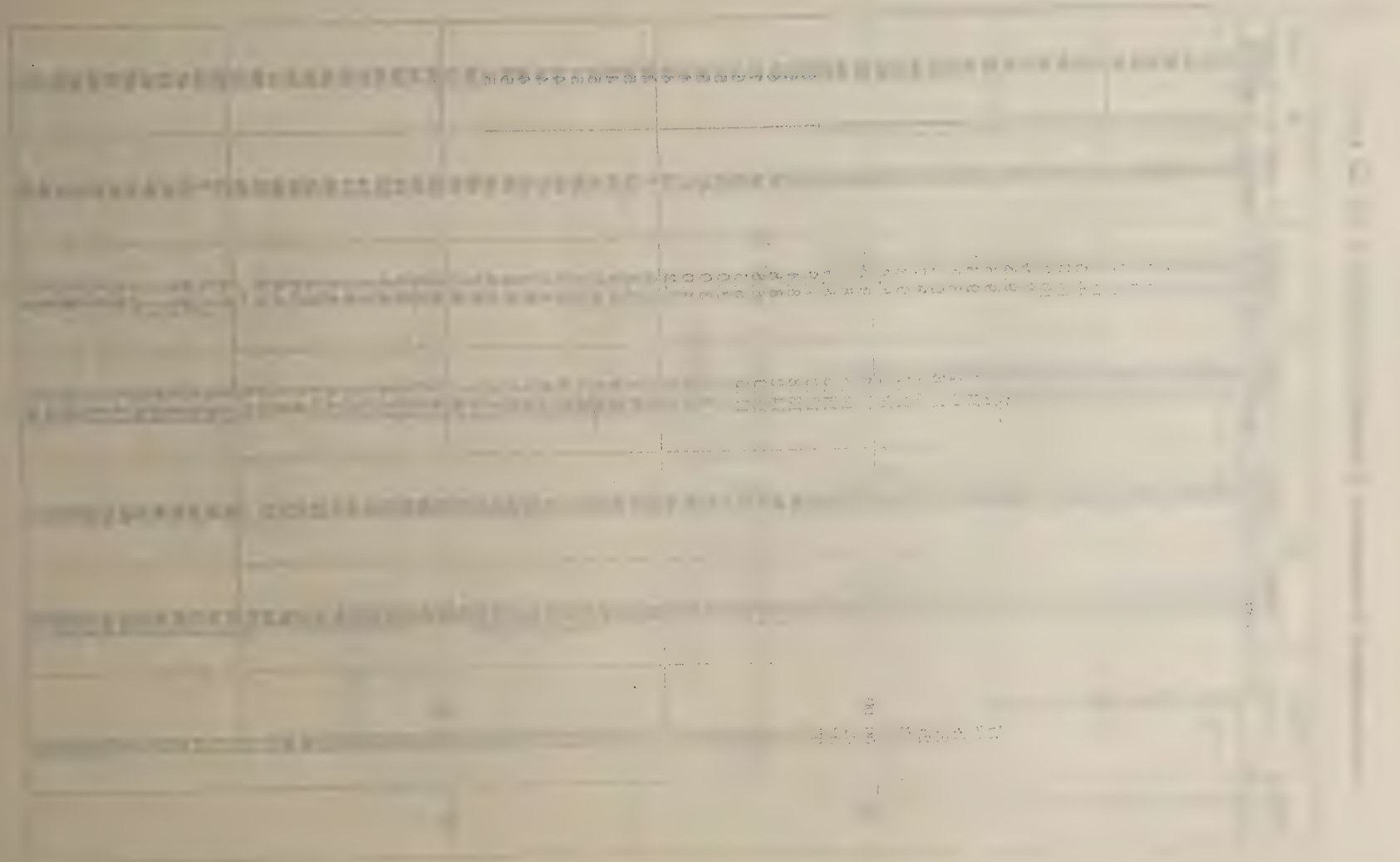

Date	Time h	m	H ASO 31590γ+...	H KIKAI 34211γ+...	D ASO w5°07'0+...	D KIKAI w3°56'1+...	Z ASO 34400γ+...	Z KIKAI 28470γ+...
		50	113	75	19.1	13.5	36	54
	15	00	112	73	18.8	12.8	36	52
		10	112	72	18.0	12.3	37	50
		20	113	71	17.6	11.8	38	49
		30	118	74	17.3	11.6	39	49
		40	119	77	17.1	11.4	40	50
		50	122	77	16.9	11.2	41	50
	16	00	121	75	16.7	11.1	42	51
		10	121	75	16.2	10.5	43	50
		20	120	73	16.0	10.3	44	49
		30	119	70	15.6	10.0	45	49
		40	116	67	15.4	9.6	45	48
		50	113	65	15.2	9.5	45	48
	17	00	111	61	15.2	9.5	45	48
	18		97	48	14.7	9.3	46	53
	19		73	24	14.1	8.8	40	50
	20		81	31	14.6	9.3	47	57
	21		102	50	15.2	9.7	54	64
	22		105	51	14.7	9.3	54	64
	23		97	45	14.2	8.8	53	62
20	00	00	93	41	14.6	9.0	53	63
	01		88	36	14.3	8.8	54	64
	02		87	32	14.5	8.9	54	65
	03		88	36	13.3	7.9	54	62
	04		91	39	13.8	8.4	53	63
	05		101	48	14.2	8.8	56	67
	06		103	48	13.9	8.8	59	70
	07		99	45	11.5	6.5	59	64
	08		83	32	8.1	3.0	58	53
	09		74	29	8.3	3.0	47	50
	10		73	39	9.5	4.0	31	45
	11		78	54	12.3	7.2	13	43
	12		81	62	16.5	10.9	7	48
	13		90	70	19.4	13.9	12	50
	14		92	68	20.0	14.4	16	46
	15		120	86	19.4	14.1	34	55
	16		122	79	16.7	11.0	39	51
	17		119	71	15.0	9.2	42	48
	18		109	59	13.9	8.3	45	48
	19		101	50	14.6	9.2	40	46
	20		102	53	15.1	9.8	45	50
	21		105	55	14.5	9.6	49	51
	22		108	57	14.7	9.2	49	52
	23		99	50	14.7	9.3	49	52
21	00	00	96	48	14.3	8.8	50	53
	01		98	48	14.3	8.8	52	54
	02		102	52	14.5	9.0	54	56
	03		100	50	13.8	8.5	55	58
	04		105	55	13.7	8.4	54	57
	05		104	55	13.5	8.3	54	56
	06		109	59	13.0	8.3	58	59
	07		103	52	11.4	6.2	58	55
	08		105	50	9.0	5.4	56	54
	09		98	53	9.5	4.6	50	47
	10		94	61	10.3	4.9	35	38
	11		102	—	13.0	—	24	35
	12		110	96	15.9	9.4	13	33
	13		118	96	17.6	11.2	8	36
	14		133	99	19.0	12.4	21	41
	15		129	89	18.0	11.6	31	43
	16		126	86	17.2	11.1	40	47
	17		120	78	16.0	10.3	44	48
	18		107	64	14.3	9.0	45	46
	19		105	61	14.5	9.4	43	46
	20		112	69	15.0	9.7	47	51
	21		106	63	15.0	9.7	47	52
	22		119	74	14.3	9.3	50	54
	23		115	71	14.5	9.3	49	54

Date	Time	H		D		Z	
	h m	ASO 31590γ+...	KIKAI 34211γ+...	ASO w5°07'0+...	KIKAI w3°56'1+...	ASO 34400γ+...	KIKAI 28470γ+...
22	00 00	112	69	14.5	9.3		56
	01	113	68	13.8	8.8		57
	02	106	65	14.1	8.9		59
	03	105	63	13.0	8.0		58
	04	104	62	13.4	8.2		59
	05	106	54	13.5	8.4		62
	06	113	71	13.6	8.6		68
	07	105	62	12.1	6.7		66
	08	101	61	10.8	5.2		58
	09	88	57	9.0	3.7		47
	10	87	67	9.7	4.5		39
	11	100	91	12.1	6.6		31
	12	108	108	15.4	10.0		29
	13	118	115	18.3	12.7		30
	14	116	103	19.5	13.8		33
	15	116	93	19.1	13.3		39
	16	117	89	17.4	11.3		44
	17	123	88	16.0	10.0		48
	18	108	70	14.3	8.6		47
	19	97	61	13.9	8.6		48
	20	88	53	15.1	9.7		52
	21	104	67	15.0	9.7		59
	22	110	72	15.0	9.6		61
	23	108	72	15.1	9.5		61

M. Ota, I. Okamoto, M. Yasuhara, S. Fukushima,
and H. Maeda

Aso Magnetic Observatory, Kyoto University

昭和34年3月25日　印刷
昭和34年3月31日　發行
第10卷　第3號

編輯兼
發行者　日本地球電氣磁氣學會
代表者　長谷川万吉

印刷者　京都市南区上鳥羽南戸町63
田中幾治郎

賣捌所　丸善株式會社京都支店
丸善株式會社 東京・大阪・名古屋・仙台・福岡

JOURNAL OF GEOMAGNETISM AND GEOELECTRICITY

Vol. X No. 3

1959

CONTENTS

JOURNAL OF GEOMAGNETISM AND GEOELECTRICITY

Vol. X No. 3

1958

CONTENTS

編輯兼發行者 日本地球電氣電波學會
代表者 長谷川万吉

印刷者 京都市上京区河原町通広小路上ル
田中治郎

印刷所 共立印刷株式会社京都支店

2024-07-01

Box: IA40539219
Old Pallet:
IA405392

Journal of Geomagnetism
and Geoelectricity 1959-
Vol 10 Iss 4

INTERNET ARCHIVE

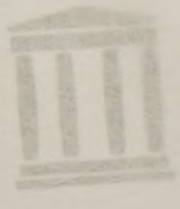

SOCIETY

OF

TERRESTRIAL MAGNETISM AND ELECTRICITY

OF

JAPAN

1959

KYOTO